Tyre models for steady-state vehicle handling analysis

Uil, R.T.

Award date:
2008

Tyre models for steady-state vehicle handling analysis

ing. R.T. Uil

DCT 2007.142

Master's thesis

Coach: Dr. Ir. I.J.M. Besselink (Eindhoven University of Technology / TNO Automotive)

Supervisor: Prof. Dr. H. Nijmeijer (Eindhoven University of Technology)

Members of committee: Dr. Ir. A.J.C. Schmeitz (TNO Automotive)
Dr. Ir. J.A.W. van Dommelen (Eindhoven University of Technology)

Eindhoven University of Technology
Department of Mechanical Engineering
Dynamics and Control Group

Eindhoven, December, 2007

To my late father

Tammo Uil

1950 - 2006

Acknowledgements

This report is the result of my graduation project carried out at the Dynamics and Control group of Eindhoven University of Technology. It has been an eventful period and during my graduation I have been supported by many people.

I would like to express my gratitude to Dr. Ir. Igo Besselink for his coaching, support and critical comments during my research and his knowledge on tyre models.

Special thanks to Prof. Dr. Henk Nijmeijer for his advice and guidance during my study. And I would also like to thank Dr. Ir. Antoine Schmeitz for his guidance during the first months of my graduation project.

Also many thanks to my colleague students for the cooperation and friendship during my study at the university and the many fruitful discussions. And also thanks to my fellow graduation students of the automotive lab for their company during the graduation project.

I would like to thank the members of the Flatplank project, especially Erwin Meinders, for the cooperation and support during the experimental work carried out during my period working as a student assistant.

Finally, I would like to thank my family for their indispensable support during more than eight years of studying. I have appreciated their patience and encouragements very much, also in difficult times.

Abstract

In today's vehicle development and engineering an accurate representation of the tyre force and moment characteristics is of special importance. As the link between the vehicle and the road, the tyre ultimately determines the driving characteristics that can be realised and is an important factor for the ride comfort. Nowadays there are many different tyre models for vehicle handling analysis. One of the most important and widely used tyre handling models is the Magic Formula Tyre model of Pacejka.

Due to the increase in computing power it is possible to develop tyre models that are more complex and capable to deal with various operating conditions. On the basis of the model complexity or model design a classification can be made, such as empirical models, brush and ring models and finite element models. To get more insight in the capabilities of the different tyre models currently available, a comparative study is started in the Dynamics and Control group.

In this study an overview of a selection of existing tyre models available in literature is created. The tyre models selected for this study are; the Magic Formula Tyre model of Pacejka, the TMeasy tyre model of Rill and Hirschberg, the TreadSim tyre model originally developed by Pacejka and extended by researchers of Eindhoven University of Technology and finally the dynamic tyre friction model of Deur based on the LuGre friction model. The objectives are an extensive study of the different tyre models and a comparison of the steady-state force and moment characteristics with measurement data of one reference tyre. The computer models of the Magic Formula and TreadSim were available and models were developed for TMeasy and the model of Deur. The model parameters of the tyre models are determined with an optimisation routine. The fit results of the tyre models are compared and extrapolation qualities of the models are investigated. Finally, based on the knowledge obtained during the study, recommendations for the development of a new improved tyre handling model are given.

From the study of the different tyre models it can be concluded that the Magic Formula Tyre model gives the best approximation of the steady-state tyre characteristics. The physical oriented tyre models (TreadSim and Deur) can not achieve the same accuracy as the semi-empirical based tyre models (Magic Formula and TMeasy).

Advantages of the semi-empirical tyre models are the high accuracy in describing the steady-state tyre characteristics, and fast parameter identification as a result of separate model parameters for describing the force and moment characteristics. Disadvantages are the difficulty of extending the models with new operating conditions (i.e. large increase of model parameters) and the inaccurate extrapolation qualities.

For the physical tyre models the advantages are the smaller number of model parameters necessary for describing the steady-state characteristics. The physical models have better extrapolation qualities and are more suitable for extending with new operating conditions. The disadvantages of these models, are the influence of the model parameters on all force and moment characteristics. Therefore, a more complex parameter identification is necessary and that results in lower computational effort. To increase the computational effort some assumptions are included, which results in larger fit errors of the steady-state characteristics. To improve the fit results of the models, some empirical elements are included.

From the study of the tyre models for vehicle handling analysis, the following recommendations are given. The measurement program used for the parameter identification is insufficient and needs to be extended for investigation of changing operating conditions, such as inflation pressure, velocity and friction.

The current available tyre models can be improved by including dependency on changing operating conditions in the semi-empirical tyre models. The physical tyre models can be more accurate if the poor assumptions of the normal pressure distribution and the contact patch are improved.

In the future the traditional view on tyre modelling will not be sufficient to deal with the high demands. A new improved tyre handling model needs to be capable of dealing with various operating conditions, such as a wide velocity range, accurate camber description, inflation pressure changes, (ambient) temperature influence, tyre wear, higher frequencies for dynamic tyre analysis, etc. A new dynamic tyre model should also be applicable in large fields of application, such as vehicle handling and parking behaviour, ride comfort and noise, and influence on road surface. With these possibilities the tyre handling model can be used in the development of a vehicle, for example for the suspension design, steering-mechanism, safety system design.

Samenvatting

Bij het ontwerpen en ontwikkelen van voertuigen is tegenwoordig een correcte representatie van het bandgedrag van groot belang. De band is de connectie tussen het voertuig en de weg; de band bepaald de uiteindelijke rijeigenschappen van het voertuig en speelt een belangrijke rol in de comforteigenschappen van een voertuig. Tegenwoordig zijn er veel verschillende bandmodellen beschikbaar voor het analyseren van de rijeigenschappen van een voertuig. Een belangrijk en vaak toegepast bandmodel om het voertuiggedrag te analyseren is het Magic Formula bandmodel ontwikkeld door Pacejka.

Door de toename van de rekensnelheid van computers is het mogelijk geworden complexere modellen te ontwikkelen die om kunnen gaan met verschillende bedrijfscondities. Op basis van de complexiteit of het ontwerp van de bandmodellen, kunnen verschillende groepen worden onderscheiden. Voorbeelden hiervan zijn, semi-empirische, borstel en ring modellen en eindige elementen modellen. Om meer inzicht te krijgen in de mogelijkheden van de tegenwoordig beschikbare bandmodellen en de eisen voor een toekomstig bandmodel, is een onderzoek in de Dynamics and Control groep gestart.

In deze studie is een overzicht gemaakt van de verschillende bandmodellen die beschikbaar zijn in de literatuur. Van dit overzicht zijn de volgende bandmodellen geselecteerd voor verder onderzoek: het Magic Formula bandmodel van Pacejka, het TMeasy bandmodel van Rill en Hirschberg, het TreadSim bandmodel oorspronkelijk ontwikkeld door Pacejka en verder uitgebreid door onderzoekers van de Technische Universiteit Eindhoven en als laatste het dynamische wrijvings bandmodel van Deur dat gebaseerd is op het Lugre wrijvingsmodel. De doelstellingen van dit onderzoek zijn het uitvoerig bestuderen van de verschillende bandmodellen en het vergelijken van de stationaire kracht en moment karakteristieken van de verschillende modellen met meetdata van één referentieband. De modellen van de Magic Formula en TreadSim waren reeds beschikbaar en de modellen van TMeasy en Deur zijn gemaakt op basis van de informatie gevonden in de literatuur. De parameters van de bandmodellen zijn bepaald met behulp van numerieke optimalisatie technieken. De fit resultaten van de verschillende modellen zijn met elkaar vergeleken en de extrapolatie kwaliteiten van de modellen zijn onderzocht. Met de opgedane kennis van de verschillende bandmodellen zijn er aanbevelingen gedaan voor de ontwikkeling van een eventueel toekomstig bandmodel voor het beschrijven van het voertuiggedrag.

Uit de vergelijking tussen de verschillende bandmodellen kan worden geconcludeerd dat het Magic Formula bandmodel de beste benadering van de stationaire bandkarakteristieken geeft. De fysische georiënteerde bandmodellen (Treadsim en Deur) behalen niet de nauwkeurigheid van de semi-empirische bandmodellen (Magic Formula en TMeasy).

De voordelen van de semi-empirische bandmodellen zijn de hoge nauwkeurigheid voor het beschrijven van de stationaire bandkarakteristieken en de snelle parameteridentificatie als gevolg van de afzonderlijke model parameters voor het beschrijven van de krachten en momenten. Nadelen zijn de moeilijke uitbreidingsmogelijkheden voor het implementeren van nieuwe bedrijfscondities (d.w.z. grote toename van model parameters) en de onnauwkeurige extrapolatie kwaliteiten.

De voordelen van de fysische bandmodellen zijn het geringe aantal model parameters die nodig zijn voor het beschrijven van de stationaire karakteristieken. Verder hebben fysische modellen beter extrapolatie eigenschappen en zijn eenvoudiger uit te breiden met nieuwe bedrijfscondities. Het grootste nadeel van deze modellen is dat de model parameters invloed hebben op alle kracht en moment karakteristieken. Hierdoor is er een complexere parameter identificatie strategie noodzakelijk en dat resulteert in een langere rekentijd. Om de rekentijd te verkorten zijn er een aantal aannames geïm-

plementeerd, deze aannames resulteren in grotere fitfouten voor de stationaire karakteristieken. Om de fitresultaten van de modellen te verbeteren zijn er weer empirische elementen geïmplementeerd.

Na het bestuderen van de verschillende bandmodellen voor het analyseren van het voertuiggedrag kunnen de volgende aanbevelingen gegeven worden. Het meetprogramma voor het identificeren van de model parameters is onvoldoende en moet worden uitgebreid om veranderende bedrijfscondities te kunnen onderzoeken, zoals bandenspannings-, snelheids- en wrijvingsinvloeden.

De huidige semi-empirische bandmodellen kunnen worden verbeterd door het implementeren van bedrijfsconditie-afhankelijkheid. De huidige fysische bandmodellen worden nauwkeuriger als de slechte aannames ten aanzien van de normaaldruk verdeling en het contactvlak verbeterd worden.

In de toekomst zal de huidige visie omtrent het modelleren van banden niet meer voldoende zijn om te kunnen voldoen aan de hoge eisen. Een toekomstig bandmodel moet in staat zijn om te gaan met verschillende bedrijfscondities, zoals een groot snelheidsbereik, nauwkeurige camber beschrijving, bandenspanningsveranderingen, (omgevings)temperatuur invloeden, banden slijtage, hoge frequentie analyses, enz. Een toekomstig dynamisch bandmodel moet toepasbaar zijn in een groot toepassingsgebied, zoals voertuig weg- en parkeergedrag, comfort gedrag en geluid, en de invloed op het wegdekoppervlak. Hiermee is het mogelijk om het bandmodel te gebruiken voor de ontwikkeling van een voertuig, bijvoorbeeld voor de ontwikkeling van de wielophanging, stuurinrichting en actieve veiligheidssystemen.

Contents

List of Figures

List of Tables

Nomenclature

Symbol	Description	Unit
α	side slip angle	[deg]
α_{ply}	ply steer equivalent slip angle	[deg]
$\bar{y}_\gamma$	average deflection of tread under pure camber slip	[m]
$\bar{y}_y$	average deflection of tread under pure lateral slip	[m]
β	orientation angle of the relative speed	[rad]
Δz	tyre deformation	[m]
Δz_B	average belt deformation	[m]
Δz_F	average tyre flank deformation	[m]
δ	Stribeck exponent	[-]
$\Delta\varphi$	rotation angle	[rad]
$\dot{\psi}$	yaw rate	[rad/s]
γ	wheel camber angle	[deg]
γ_{con}	conicity equivalent camber angle	[deg]
κ	longitudinal wheel sip	[deg]
μ	friction coefficient	[-]
μ_0	static friction coefficient	[-]
μ_{sl}	scale factor to characterise the road condition	[-]
Ω	angular velocity	[rad/s]
ω	wheel angular velocity	[rad/s]
ϕ	empirical scale factor aligning torque	[-]
ψ	yaw angle	[rad]
σ_0	normalised rubber longitudinal lumped stiffness	[1/m]
σ_1	normalised rubber longitudinal lumped damping	[s/m]
σ_2	normalised viscous relative damping	[s/m]
θ	scale factor for different road conditions	[-]
ε	error unit	[%]
ε_γ	coefficient for reduced change of the effective rolling radius caused by camber	[-]
φ	component of the tyre force contribution of a bristle	[N]
ζ	bristle longitudinal position in contact patch	[m]
a	half contact length of the tyre	[m]
a_μ	velocity depended friction coefficient	[s/m]
B	base point of a tread	[-]
B	stiffness factor in Magic Formula	[-]
b	half tyre width	[m]
C	contact centre position	[-]
C	shape factor in Magic Formula	[-]
c_1	pressure distribution shape coefficient, increasing part	[-]
c_2	pressure distribution shape coefficient, decreasing part	[-]
$c_i, i = 1, 2$	pressure distribution shape factor	[-]
$c_{lat,0}$	lateral belt stiffness	[N/m]
c_{px}	longitudinal tread stiffness	[N/m^2]

c_{py}	lateral tread stiffness	[N/m^2]
$c_{vert,0}$	vertical tyre stiffness	[N/m]
c_x	tread longitudinal stiffness	[N/m]
c_{yaw}	belt yaw stiffness	[Nm/rad]
c_z	vertical tyre stiffness	[N/m]
D	peak value in Magic Formula	[-]
dF^0	generalised initial inclination	[N]
dF_x^0	longitudinal initial inclination	[N]
dF_y^0	lateral initial inclination	[N]
E	curvature factor in Magic Formula	[-]
e	tread deflection	[m]
EI_0	belt bending stiffness	[Nm]
F^M	generalised magnitude maximum force	[N]
F^S	generalised magnitude sliding force	[N]
F_C	normalised Coulomb friction	[-]
F_i	force acting on node i	[N]
F_n	normal force	[N]
F_S	normalised Static friction	[-]
F_x	longitudinal tyre force	[N]
F_x^M	magnitude of the maximum longitudinal force	[N]
F_x^S	magnitude of the longitudinal sliding force	[N]
F_y	lateral tyre force	[N]
F_y^M	magnitude of the maximum lateral force	[N]
F_y^S	magnitude of the lateral sliding force	[N]
F_z	vertical tyre load	[N]
$g(v_r)$	Stribeck-type tyre/road sliding friction function	[N]
k	pressure depended friction coefficient	[-]
$K_{x,y,z}$	stiffness coefficients of the static model	[N/m]
L	length of the contact patch	[m]
M_x	overturning moment	[Nm]
M_{zr}	residual torque	[Nm]
M_z	aligning torque	[Nm]
n	pneumatic trail	[m]
$(n/L)_0$	initial value normalised pneumatic trail	[-]
P	pressure distribution over contact area	[N/m^2]
P	the tip of a tread	[-]
p	contact pressure	[N/m^2]
$p(\zeta)$	normalised longitudinal normal pressure distribution	[-]
P_m	normalised maximum value of the pressure distribution	[-]
q	contact force per unit length of circumference	[N]
r_0	unloaded tyre radius	[m]
r_D	dynamic tyre radius	[m]
r_e	effective rolling tyre radius	[m]
r_l, r_r	margins of the trapezoidal pressure distribution	[-]
r_S	static tyre radius	[m]
S	slip point	[-]
s	lateral distortion of the belt	[m]
s	longitudinal slip	[-]
s^M	generalised slip location of maximum force	[]
s^S	generalised slip location sliding force	[-]
s_γ	lateral camber slip	[-]
S_H	horizontal shift in Magic Formula	[-]
S_V	vertical shift in Magic Formula	[-]

s_x	longitudinal slip	[-]
$\hat{s_x}$	normalisation factor longitudinal slip	[-]
s_x^M	longitudinal slip coefficient of the maximum force	[-]
s_x^S	longitudinal slip coefficient of the sliding force	[-]
s_y	lateral slip	[-]
$\hat{s_y}$	normalisation factor lateral slip	[-]
s_y^0	lateral slip coefficient adhesion/sliding	[-]
s_y^M	lateral slip coefficient of the maximum force	[-]
s_y^S	lateral slip coefficient full sliding	[-]
s_y^S	lateral slip coefficient of the sliding force	[-]
t	pneumatic trail	[m]
u	tread deflection in longitudinal direction	[m]
v	vehicle velocity	[m/s]
V_b	velocity of the base point	[m/s]
V_c	velocity of contact centre point C	[m/s]
V_g	sliding speed	[m/s]
v_{rx}	longitudinal relative speed	[m/s]
v_{ry}	lateral relative speed	[m/s]
V_r	wheel linear speed of rolling	[m/s]
v_r	relative velocity between bristle base point and the tip	[m/s]
V_s	wheel slip velocity of slip point S	[m/s]
v_s	Stribeck relative velocity	[m/s]
v_t	average transport velocity	[m/s]
v_x	track velocity	[m/s]
v_y	lateral component of the contact point velocity	[m/s]
v_y^S	lateral sliding velocity	[m/s]
W	width of the tyre contact patch	[m]
x_b	average longitudinal position in the contact patch	[m]
y_b	lateral position in a row of the contact patch	[m]
y_c	tread displacement under influence of a camber angle	[m]
z	horizontal bristle deflection	[m]

Chapter 1

Introduction

1.1 Motivation and background

During the past twenty years, enormous progress has been made in chassis engineering and driveability. Today's vehicles are significantly safer and at the same time more comfortable than cars were in the past. The reasons for this progress can be found in the areas of the various electronic systems and the precise design and tuning by using modern analysis and simulation methods. This results in an increase of product quality and shorter development times. In this context, the significance of modelling and simulation of the tyre behaviour becomes increasingly important. As the link between the vehicle and the road, the tyre ultimately determines the driving characteristics that can be realised and is an important factor for the ride comfort. An overview of the influence of the road, tyres and vehicle on operational characteristics is depicted in figure 1.1. In this figure it can be seen that the tyre affects many different aspects of the vehicle behaviour.

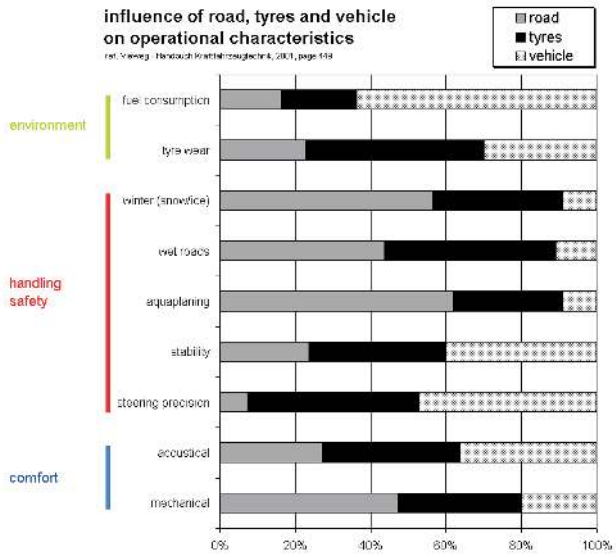

Figure 1.1: Influence of the road, tyre and vehicle on the driving behaviour [6].

Due to the advances in simulation techniques of vehicle development and engineering, the modelling of the tyre is of special importance. Thereby, not only the reliability of quantitative results but also the extension to higher frequency ranges is becoming a necessity. A detailed description of different tyre models and the validation of measurements combined with specific capability tests to show

the range of application of the tyre models are presented in the thesis. One of the most important and widely used tyre handling models is the Magic Formula Tyre model developed by Pacejka. Through his work and the work of other researchers at Delft University of Technology, Volvo, Michelin, TNO Automotive and Eindhoven University of Technology, a number of extensive improvements have been created. Today, the extended Magic Formula is capable of dealing with combined slip, camber, dynamic responses up to about 8 Hz and inflation pressure changes (limited validation). TNO Automotive has developed a software product line based on the Magic Formula Tyre model and carries out measurements for the industry to identify the necessary model parameters. The Magic Formula is also the basis for the dynamic tyre model SWIFT (Short Wavelength Intermediate Frequency Tyre), which describes the high frequency response and is valid up to about 60 to 100 Hz. The main advantages of the Magic Formula Tyre model are its accuracy and its low computational effort. The disadvantages are its empirical background, which makes it difficult to extend the Magic Formula to include other effects like the influence of temperature, speed-dependent effects of tyre-road friction, tyre wear, etc. In addition, the number of parameters required for the formulae is rather large and increases even more if extensions are made.

The Magic Formula Tyre model is introduced in 1987, meanwhile also other researchers have developed tyre models for vehicle handling analyses. Some examples of developed tyre models are the semi-empirical TMeasy tyre model, originally developed for vehicle dynamic calculations of agricultural tractors by professors Rill and Hirschberg. The TreadSim tyre model, a physical tyre model developed originally by Pacejka and later extended by researchers of Eindhoven University of Technology. And the brush type dynamic tyre friction model of Deur based on the LuGre friction model developed by Canudas de Wit and Åström.

A general overview of de inputs and outputs of the analytical tyre models described above, is depicted in figure 1.2. The input variables of a tyre model are defined on the left side, where κ is the

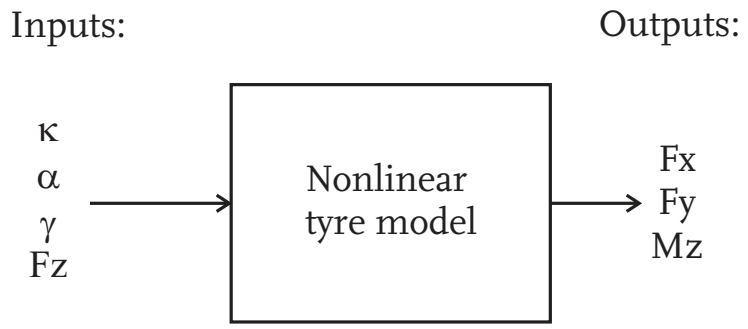

Figure 1.2: Overview of the structure of the analytical tyre models.

longitudinal slip angle, α the lateral slip angle, γ the camber angle and F_z is the vertical load on the tyre. Subsequently, with these input variables and the model parameters of the concerning tyre model, the output variables of tyre model are calculated through a mathematical algorithm. Common outputs of a tyre model are, F_x the longitudinal tyre force, F_y the lateral tyre force and M_z the self-aligning torque.

Nowadays, simulations with physical oriented tyre models are not as fast as with empirical tyre models. However, in the future it is expected that the computational effort becomes less important due to the increase in computing power. It is also expected that the demands on tyre models will increase with respect to the capabilities of the models to deal with various operating conditions and a larger field of application, such as durability, tyre wear, tyre noise, temperature, etc. Therefore a research in the Dynamics and Control Group is started to study different tyre models for use in vehicle dynamics analysis and that are currently available. These tyre models need to be studied in detail and the advantages and disadvantages of the tyre models have to be identified. Finally, a prospective view on tyre modelling in the future should be described.

1.2 Aim and scope

The objectives of this master thesis are to study the selected tyre models, the Magic Formula tyre model, the TMeasy tyre model, the TreadSim tyre model and the dynamic tyre friction model of Deur. The steady-state tyre characteristics of the different tyre models are investigated in comparison with the measurement results. Subsequently, a comparison study between the different tyre models should be carried out. Emphasis in this investigation should be laid on discovering various advantages and disadvantages and study extrapolation qualities for various conditions of the tyre models. Finally, recommendations are given that can be used for developing a new improved tyre handling model to describe the steady-state tyre characteristics.

The aim of this thesis is to make an overview of the selected existing tyre models that are available in literature. The selected tyre models should be studied in detail and compared with each other. Based on the insight obtained by studying the various models, recommendations for an improved tyre handling model are given.

To achieve these objectives, the following activities are defined:

- Literature study with regard to tyre models for vehicle handling analyses.
- Implementation of the studied tyre models in Matlab.
- Familiarisation with the proces of fitting and determining the model parameters out of measurement data.
- Comparison of the various models and investigation of the extrapolation qualities of the models.
- Give recommendations that can be used to develop a new improved tyre handling model.

1.3 Outline of the thesis

First of all the selected tyre models are studied in detail to get more insight in the tyre modelling approach to describe steady-state tyre characteristics. In chapter 2 a short overview of the Magic Formula Tyre model and the fit results is given. Chapter 3 contains the literature of the TMeasy tyre model and the structure of the model created for investigation of the steady-state tyre behaviour. Subsequently, the fit results of the TMeasy model are described. In chapter 4 the TreadSim tyre model is presented. The computer model implementation of TreadSim was already available, this model is reviewed and improvements for the model to produce physical correct tyre behaviour are implemented. The last tyre model, the LuGre dynamic tyre model presented by Deur, is described in chapter 5. The literature of the distributed static model with a non-uniform normal pressure distribution is described. Subsequently, also the structure of the model created for this thesis and the fit results with respect to the measurement data are presented. In chapter 6 a comparison between the different tyre models is presented and some extrapolation qualities of the models are investigated and described. In the last section of chapter 6 a prospective view on tyre modelling in the future is presented. Finally, in chapter 7 the conclusions of this research are presented and recommendations for future research are given.

Chapter 2

The Magic Formula Tyre model

The first tyre model studied in the thesis is the semi-empirical Magic Formula Tyre model. It is a widely used tyre model to calculate steady-state tyre force and moment characteristics for use in vehicle dynamic studies. The development of the model was started in the mid-eighties. In a cooperation between the TU-Delft and Volvo several versions of the tyre model have been developed and these results are presented in the literature of [3], [4] and [29]. In these models the combined slip situation was modelled from a physical view point. In 1993 a purely empirical method, using the Magic Formula based weighting functions is introduced, to describe the tyre horizontal force generation at combined slip [5].
This approach is adopted by Pacejka and TNO and developed further. In the newer version of 'Delft-Tyre' the original description of the aligning torque is altered to adjust a relatively simple physically based combined slip extension. The pneumatic trail is introduced as a basis to calculate this moment about the vertical axis. For a further and more detailed description of the Magic Formula Tyre model a reference is made to the book of Pacejka [28], especially to the sections 4.3.2 and 4.3.3, where a complete listing of the model equations is given. In the next sections a short overview of the model and the fit results will be presented.

2.1 Model description

The general form of the formula that holds for given values of vertical load and camber angle reads:

$$y = D\sin[C\arctan\{(1-E)Bx + E\arctan(Bx)\}] \tag{2.1}$$

with

$$\begin{aligned} Y(X) &= y(x) + S_V & (2.2)\\ x &= X + S_H & (2.3) \end{aligned}$$

where Y is the output variable and is defined as the longitudinal force $F_x = y(\kappa)$ or the lateral force $F_y = y(\alpha)$. X is defined as the input variable and as input the longitudinal slip κ and side slip angle α can be used. The remaining variables of the Magic Formula describe the following coefficients:

B	stiffness factor
C	shape factor
D	peak value
E	curvature factor
S_H	horizontal shift
S_V	vertical shift

The Magic Formula $y(x)$ typically produces a curve that passes through the origin $x = y = 0$, reaches a maximum and subsequently tends to a horizontal asymptote. For given values of the coefficients B,

C, D and E the curve shows an anti-symmetric shape with respect to the origin. To allow the curve to have an offset with respect to the origin, two shifts S_H and S_V have been introduced. A new set of coordinates $Y(X)$ arises as shown in figure 2.1.

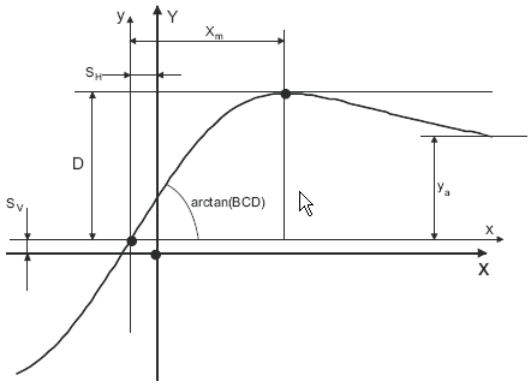

Figure 2.1: Curve produced by the general form of the Magic Formula [28].

The formula (2.1) is capable of producing characteristics that closely match measured curves for the lateral force F_y as a function of the slip angle α and for the longitudinal force F_x as a function of the longitudinal slip κ. Both characteristics have the effect of the vertical load F_z and a camber angle γ included in the parameters.

Figure 2.1 illustrates the meaning of some of the factors by means of a typical side force characteristic. Coefficient D represents the peak value (for $C \geq 1$) and the product BCD corresponds to the slope at the origin ($x = y = 0$). The shape factor C controls the limits of the range of the sine function appearing in (2.1) and thereby determines the shape of the resulting curve. The factor B is left to determine the slope at the origin and is called the stiffness factor. The factor E is introduced to control the curvature at the peak and at the same time the horizontal position of the peak x_m. The offsets S_H and S_V appear to occur when ply-steer and conicity effects and possibly the rolling resistance cause the longitudinal and lateral curves not to pass to the origin. Wheel camber may give rise to a considerable offset of the F_y vs α curves.

The aligning torque M_z can be obtained by multiplying the side force F_y with the pneumatic trail t and adding the usually small (except with camber) residual torque M_{zr}.

$$M_z = t \cdot F_y + M_{zr} \tag{2.4}$$

The pneumatic trail decreases with increasing side slip and is described as:

$$t(\alpha_t) = D_t \cos[C_t \arctan\{B_t\alpha_t = E_t(B_t\alpha_t - \arctan(B_t\alpha_t))\}] \tag{2.5}$$

where

$$\alpha_t = \tan\alpha + S_{Ht} \tag{2.6}$$

The residual torque shows a similar decrease:

$$M_{zr}(\alpha_r) = D_r \cos[\arctan(B_r\alpha_r)] \tag{2.7}$$

where

$$\alpha_r = \tan\alpha + S_{Hf} \tag{2.8}$$

Both the aligning and residual torque are modelled using the Magic Formula, but instead of the sine function, the cosine function is applied to produce a hill-shaped curve, as depicted in figure 2.2. The peaks are shifted sideways. The peak value is defined as D, C is the shape factor determining the level y_a of the horizontal asymptote and the factor B influences the curvature at the peak. Factor E modifies the shape at larger values of slip and influence the location x_0 of the point where the curve intersects the x axis.

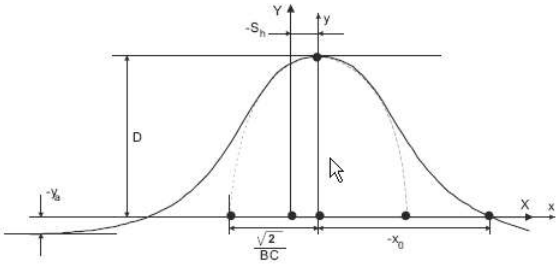

Figure 2.2: Curve produced by the cosine version of the Magic Formula [28].

2.2 Fit program

For this thesis the Magic Formula Tyre model is provided by TNO Automotive to perform an optimisation of the tyre parameters for the reference tyre used in this project. The version of the MF-Tyre model used is v6.02. The Magic Formula Tyre model incorporates many tyre parameters to obtain a good approximation of the tyre behaviour. These parameters can be determined from experimental tyre data. In these tests the forces (F_x, F_y, F_z) and the moments (M_x, M_z) are measured in the measuring hub in the wheel center. Also several other parameters are measured during the tyre tests, for example the slip angle, camber angle, forward velocity, rotational velocity, etc.
To determine the Magic Formula Tyre parameters an optimisation routine is used to minimise the error between the measurement and the Magic Formula Tyre model. In this optimisation routine the following tyre characteristics are optimised:

- Pure longitudinal force fit, pure kappa sweeps
- Pure lateral force fit, pure alpha sweeps
- Pure aligning torque fit, pure alpha sweeps
- Combined longitudinal force fit, combined slip
- Combined lateral force fit, combined slip

All these characteristics are minimised with the error calculation defined as:

$$\varepsilon = \sqrt{\frac{\sum_{i=1}^{N}(Y_{fit} - Y_{meas})^2}{\sum_{i=1}^{N} Y_{meas}^2}} \times 100\% \tag{2.9}$$

where Y_{fit} is the output variable of the Magic Formula Tyre model, Y_{meas} is the output variable of the measurement data and N is the number of measurement points. The results of the optimisation of the Magic Formula Tyre model are depicted in figure 2.3. The optimisation routine of the Magic Formula Tyre model optimises the tyre parameters for pure and combined slip situations and possible with the influence of a camber angle, these measurements conditions are defined in Appendix A table A.2. In the next chapters the different tyre models will be discussed and these tyre models are optimised with the measurement data defined in Appendix A. In table 2.1 the errors of the optimisation of the tyre characteristics with and without a camber angle are presented.

In figure 2.3 the fit results of the optimisation with no camber angle included are depicted. In this figure the fit results and the measurement data for the pure lateral force and aligning torque characteristic are the result of the alpha sweep measurements performed at three vertical loads, namely $F_z = 3000, 5000, 7000$ N. The pure longitudinal characteristic is the result of a straight-line braking experiment, also performed at the three vertical loads defined before. The combined slip characteristic

is the result of a combined braking and cornering experiment. In the figure the results of braking at slip angles of $\alpha = -2, 2, 5, 8$ degree and at a vertical load of $F_z = 5000$ N are depicted.

The overview presented in this figure will also be used for the evaluation of the different tyre models and are discussed in the next chapters.

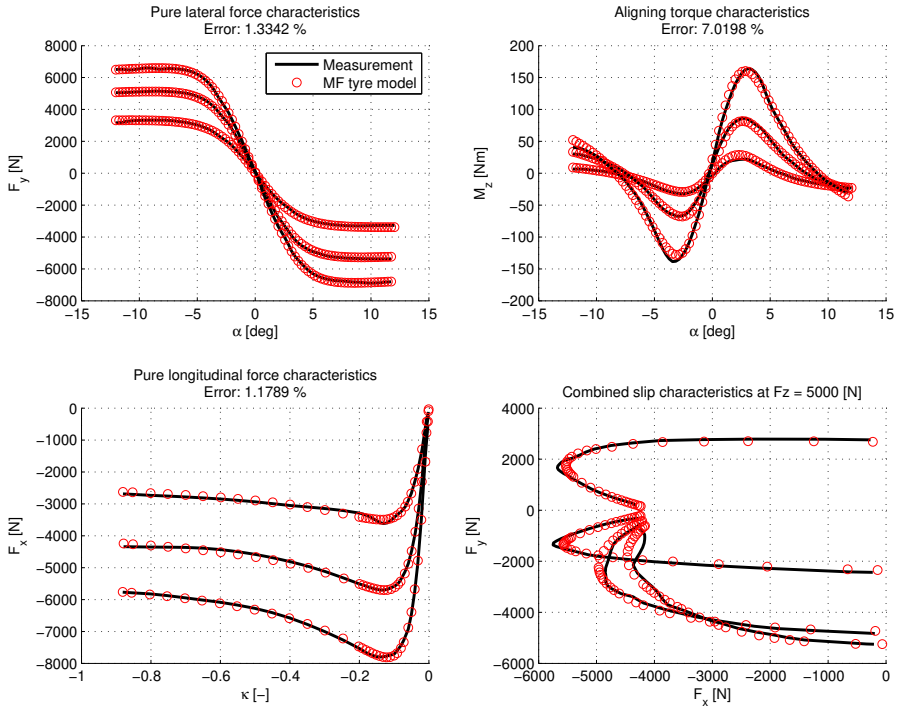

Figure 2.3: General overview of the fit results.

The errors of the fit results of the Magic Formula Tyre model are given in table 2.1.

	ε_{MFtyre} [%]	
	no camber	with camber
pure F_x	1.18	1.74
pure F_y	1.33	1.48
pure M_z	7.02	10.03
combined F_x	2.56	2.63
combined F_y	3.84	4.46
No. fit parameters	63	91

Table 2.1: Errors of the characteristics of the Magic Formula Tyre Model

To investigate the camber influence on the tyre behaviour, the lateral force and aligning torque characteristics are presented in figure 2.4. In this figure the results of the alpha sweep experiment performed at a vertical load of $F_z = 5000$ N and with a camber angle of $\gamma = -5, 0, 5$ degree are depicted.

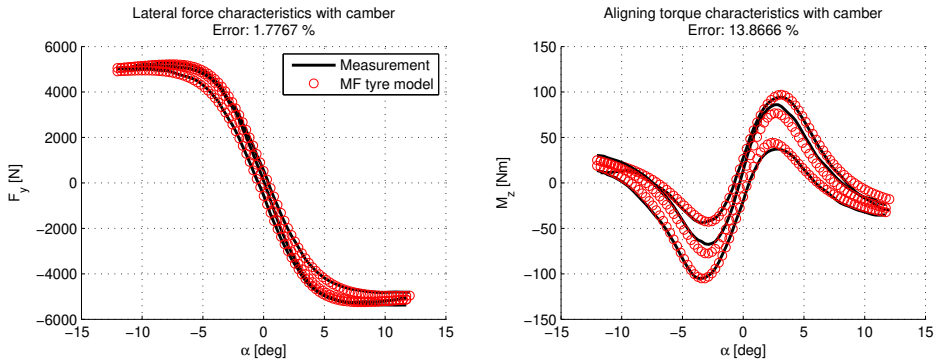

Figure 2.4: Tyre force and moment characteristic with a camber angle.

Chapter 3

The TMeasy tyre model

In this chapter the second tyre model is described, an overview is given of the literature on the TMeasy tyre model and the optimisation of the model parameters out of the measurement data. The TMeasy tyre model belongs to the class of semi-empirical tyre models, where the description of forces and moments relies also on measured and observed force-slip characteristics in contrast to the purely physically based tyre models. The semi-empirical tyre models are characterised by an useful compromise between user-friendliness, model-complexity and efficiency in computation time on the one hand, and precision in representation on the other hand. In the semi-empirical tyre models, the tyre contact area is seen as an even plane and the tyre forces and moments are approximated by appropriate mathematical functions. The functions parameters are set by adaption to measured tyre maps. The semi-empirical tyre model TMeasy has originally been conceived for vehicle dynamic calculations of agricultural tractors and is described in [20]. In the next sections the structure of the TMeasy model created for this thesis will be described.

3.1 Literature of the TMeasy model

3.1.1 Longitudinal and lateral force and slip

For the generation of tyre forces in longitudinal direction, a tyre on a flat bed test rig can be considered. The rim rotates with the angular velocity Ω and the flat bed test runs with the velocity v_x. The distance between the rim center and the flat bed is controlled to the loaded tyre radius r_D corresponding to the wheel load F_z. To illustrate this situation, a picture of a brush model is depicted in figure 3.1.

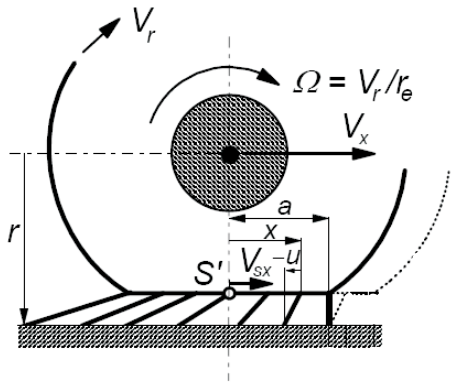

Figure 3.1: Longitudinal slip situation of a brush model [6].

If adhesion between the particle and the track is assumed, then the top of the particle will run with the track velocity v_x and the bottom with the average transport velocity $v_t = r_D\Omega$. Depending on the velocity difference $\Delta v = r_D\Omega - v_x$ the tread particle is deflected in longitudinal direction.

$$u = (r_D\Omega - v_x)t \qquad \text{with} \qquad t = \frac{L}{\Omega r_D} \tag{3.1}$$

where L is defined as the contact length and t is the time a particle spends in the contact patch.

The maximum deflection occurs when the tread particles leaves the contact patch. Particles entering the contact patch are undeformed, whereas the ones leaving have the maximum deflection. This results in a linear force distribution versus the contact length, as depicted in figure 3.2.

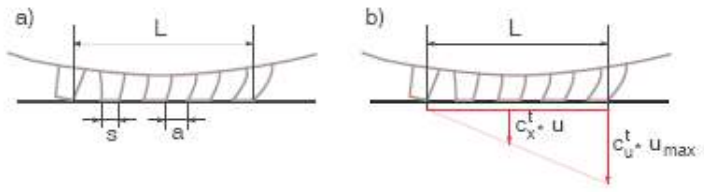

Figure 3.2: Longitudinal force distribution [30].

In this figure c_x^t represents the stiffness of one tread particle in longitudinal direction, s the length of one particle, a the distance between the particles and u_{max} the maximum deflection of a particle. The nondimensional relation between the sliding velocity of the tread particles in longitudinal direction and the average transport velocity form the longitudinal slip.

$$s_x = \frac{-(v_x - r_D\Omega)}{r_D|\Omega|} \tag{3.2}$$

At moderate slip values the particles at the end of the contact patch start sliding and at high slip values only the parts at the beginning of the contact patch will stick to the road. The resulting nonlinear function of the longitudinal force F_x versus the longitudinal slip s_x can be defined by the parameters initial inclination dF_x^0, location s_x^M and magnitude F_x^M of the maximum force, start of full sliding s_x^S and the sliding force F_x^S. The nonlinear function is depicted in figure 3.3.

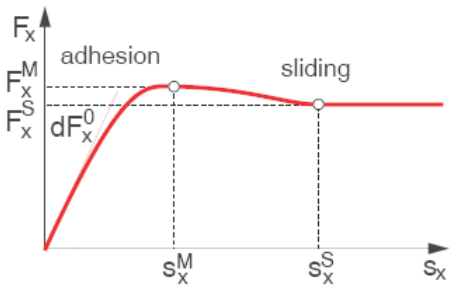

Figure 3.3: Nonlinear curve of the longitudinal force [30].

Similar to the approach of the longitudinal slip, the lateral slip can be defined as.

$$s_y = \frac{-v_y^S}{r_D|\Omega|} \tag{3.3}$$

where v_y^S is the sliding velocity in lateral direction.

As long as the particles stick to the road (small amounts of slip), an almost linear distribution of the forces along the length L of the contact patch appears. At moderate slip values the particles at the end of the contact patch start sliding, and at high slip values only the parts at the beginning of the contact patch stick to the road. The nonlinear characteristic of the lateral force versus the lateral slip can be described by the initial inclination (cornering stiffness) dF_y^0, the location s_y^m and the magnitude F^M of the maximum force, the beginning of full sliding s_y^S, and the magnitude F^S of the sliding force. The lateral force characteristic is depicted in figure 3.4.

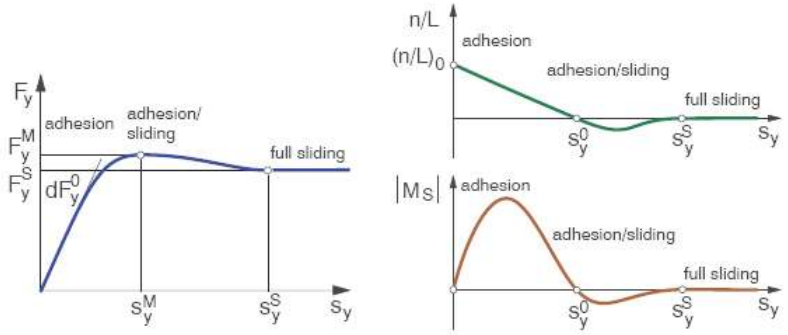

Figure 3.4: Overview of the lateral force and self-aligning curves [30].

The distribution of the lateral forces over the contact patch length also defines the point of application of the resulting lateral force. At small slip angles this point lies behind the center of the contact patch. With increasing slip values it moves forward, sometimes even before the center of the contact patch. At extreme slip values, when practically all particles are sliding, the resulting force is applied at the center of the contact patch. The resulting lateral force F_y with the pneumatic trail n generates the self aligning torque M_z.

$$M_z = -nF_y \tag{3.4}$$

The pneumatic trail has been normalised by the length of the contact patch L. The initial value $(n/L)_0$ and the slip value s_y^0 for the transitional region of adhesion/sliding and the slip value s_y^S for the transitional region of full sliding characterise the aligning torque graph, this is depicted in figure 3.4.

3.1.2 Contact length

To approximate the length of the contact patch L the tyre deformation Δz is split into two parts and is depicted in figure 3.5. The average tyre flank and the belt deformation are defined as Δz_F and Δz_B and for a tyre with full contact to the road the tyre deformation is defined as.

$$\Delta z = \Delta z_F + \Delta z_B = r_0 - r_S \tag{3.5}$$

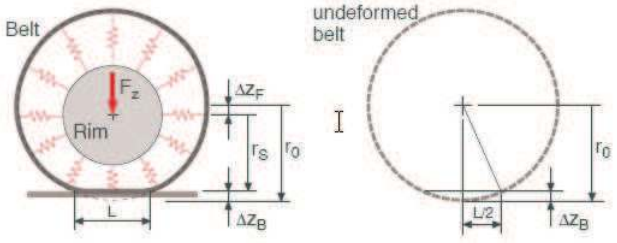

Figure 3.5: Length of contact patch [30].

Assuming that both deflections are equal, this leads to:

$$\Delta z_F \approx \Delta z_B \approx \frac{1}{2}\Delta z \tag{3.6}$$

The belt deflection can be approximated by truncating a circle with the radius of the undeformed tyre r_0 and this results in.

$$(\frac{L}{2})^2 + (r_0 - \Delta z_B)^2 = r_0^2 \tag{3.7}$$

In normal driving conditions the belt deflections are small, $\Delta z_B \ll r_0$. The approximation of the contact length can be simplified to

$$L = \sqrt{8 r_0 \Delta z_B} \qquad \text{with} \qquad \Delta z = 2\Delta z_B = \frac{F_z}{c_z} \tag{3.8}$$

The overall tyre deflection is estimated by the vertical load divided with the vertical stiffness.

3.1.3 Dynamic Rolling Radius

At an angular rotation of $\Delta\varphi$, assuming the tread particles stick to the track, the deflected tyre moves on a distance of x, see figure 3.6. With r_0 as unloaded and $r_S = r_0 - \Delta z$ as loaded or static tyre radius the following equations can be derived.

$$r_0 \sin\Delta\varphi = x \qquad \text{and} \qquad r_0 \cos\Delta\varphi = r_S \tag{3.9}$$

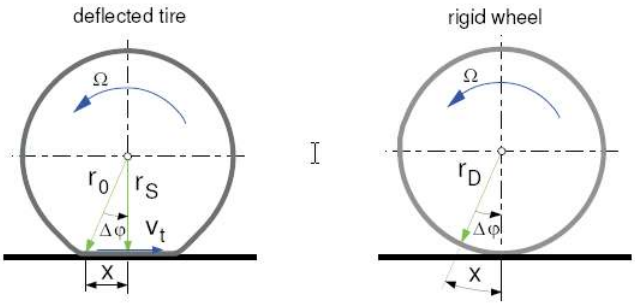

Figure 3.6: Dynamic rolling radius [30].

If the movement of a tyre is compared to the rolling of a rigid wheel, its radius r_D then has to be chosen so, that at an angular rotation of $\Delta\varphi$ the tyre moves the distance.

$$r_0 \sin\Delta\varphi = x = r_D \Delta\varphi \tag{3.10}$$

Subsequently the dynamic tyre radius is defined as

$$r_D = \frac{r_0 \sin\Delta\varphi}{\Delta\varphi} \tag{3.11}$$

At small angular rotations the sine and cosine-functions can be approximated by the first terms of its Taylor-Expansion, this leads to

$$r_D = \frac{r_0\Delta\varphi - \frac{1}{6}\Delta\varphi^3}{\Delta\varphi} = r_0(1 - \frac{1}{6}\Delta\varphi^2) \tag{3.12}$$

and from (3.9) the following relation can be derived

$$\frac{r_S}{r_0} = \cos\Delta\varphi = 1 - \frac{1}{2}\Delta\varphi^2 \quad \text{or} \quad \Delta\varphi^2 = 2(1 - \frac{r_S}{r_0}) \tag{3.13}$$

From (3.12) and (3.13) the dynamic tyre radius can be derived

$$r_D = \frac{2}{3}r_0 + \frac{1}{3}r_S \tag{3.14}$$

The static tyre radius is approximated by

$$r_S = r_0 - \frac{F_z^S}{c_z} \tag{3.15}$$

3.1.4 Generalised tyre characteristics

The TMeasy tyre model is based on an analytical approximation of the steady-state characteristics. The longitudinal force as a function of the longitudinal slip $F_x = F_x(s_x)$ and the lateral force depending on the lateral slip $F_y = F_y(s_y)$ can be defined by their characteristic parameters, the initial inclinations dF_x^0, dF_y^0, the maximal forces F_x^M, F_y^M and the sliding forces F_x^S, F_y^S at the corresponding slip values. During normal driving situations, like acceleration or deceleration in curves, longitudinal s_x and lateral slip s_y appear simultaneously. In the TMeasy tyre model created for this thesis, the analytical approximation of the combined slip situation is used to describe the steady-state tyre characteristic.

Normalisation process

According to [30], the two dimensional tyre characteristic is described by adding vectorally the longitudinal and lateral slip to a generalised slip coefficient.

$$s = \sqrt{\left(\frac{s_x}{\hat{s_x}}\right)^2 + \left(\frac{s_y}{\hat{s_y}}\right)^2} \tag{3.16}$$

The slip coefficients are normalised in order to perform their similar weighting in s. In the literature studied it is not described how these normalisation factors are implemented. The normalisation factors $\hat{s_x}$ and $\hat{s_y}$ are calculated from the location of the maxima s_x^M, s_y^M, the maximum values F_x^M, F_y^M and the initial inclinations dF_x^0, dF_y^0. To realise a normalisation in the model created based on the TMeasy tyre model, the following approximation is implemented.

In figure 3.7a the longitudinal and lateral force at a nominal load of $F_z = 3200$ N are depicted. From these characteristics the intersections of the maximum values and the initial inclinations are determined. The point of intersection is the slip value which is used in the normalisation factors. The second step is to take the maximum values in account to reduce the difference in maximum values of the longitudinal and lateral characteristics. These both values are applied in the normalisation factors defined in (3.17). In figure 3.7b the results of the normalisation process are depicted.

$$\hat{s_x} = \frac{F_x^M}{dF_x^0} \quad \text{and} \quad \hat{s_y} = \frac{F_y^M}{dF_y^0} \tag{3.17}$$

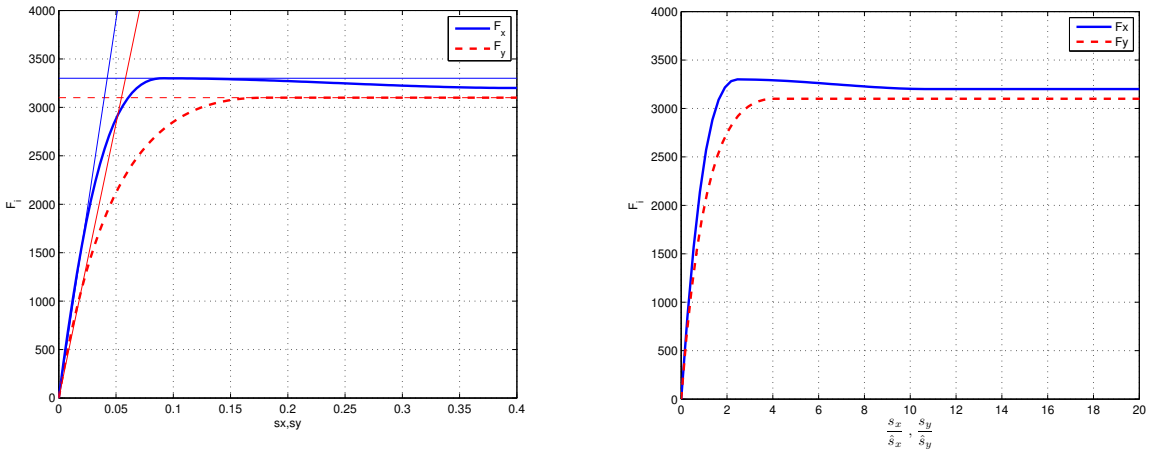

(a) (b)

Figure 3.7: Result of the normalisation.

General slip situation

With the normalisation factors the generalised tyre parameters are calculated with the corresponding values of the longitudinal and lateral tyre parameters.

$$\begin{aligned} dF^0 &= \sqrt{(dF_x^0 \hat{s_x} \cos\varphi)^2 + (dF_y^0 \hat{s_y} \sin\varphi)^2} \\ s^M &= \sqrt{\left(\frac{s_x^M}{\hat{s_x}} \cos\varphi\right)^2 + \left(\frac{s_y^M}{\hat{s_y}} \sin\varphi\right)^2} \\ F^M &= \sqrt{(F_x^M \cos\varphi)^2 + (F_y^M \sin\varphi)^2} \\ s^S &= \sqrt{\left(\frac{s_x^S}{\hat{s_x}} \cos\varphi\right)^2 + \left(\frac{s_y^S}{\hat{s_y}} \sin\varphi\right)^2} \\ F^S &= \sqrt{(F_x^S \cos\varphi)^2 + (F_y^S \sin\varphi)^2} \end{aligned} \tag{3.18}$$

The angular functions

$$\cos\varphi = \frac{s_x/\hat{s}_x}{s} \quad \text{and} \quad \sin\varphi = \frac{s_y/\hat{s}_y}{s} \tag{3.19}$$

grant a smooth transition from the characteristic curve of longitudinal to the curve of lateral forces in the range of $\varphi = 0$ to $\varphi = 90°$.

Subsequently, the characteristic tyre data is used to calculate the generalised force and is described by an analytical function existing of three intervals, a broken rational function, a cubic polynomial and a constant sliding force and defined in (3.20).

$$F(s) = \begin{cases} s^M dF^0 \frac{\sigma}{1+\sigma(\sigma+dF^0\frac{s^M}{F^M}-2)}, & \sigma = \frac{s}{s^M}, \quad 0 \le s \le s^M; \\ F^M - (F^M - F^S)\sigma^2(3-2\sigma), & \sigma = \frac{s-s^M}{s^S-s^M}, \quad s^M < s \le s^S; \\ F^S & s > s^S. \end{cases} \tag{3.20}$$

When defining the curve parameters the condition $dF^0 \ge 2\frac{F^M}{s^M}$ has to be fulfilled, because otherwise the function has a turning point in the interval $0 < s \le s^M$. In figure 3.8 the generalised force curve and the characteristic tyre parameters are depicted. The three intervals of the analytical function and the transition of the generalised curve to the longitudinal and lateral force characteristics can be

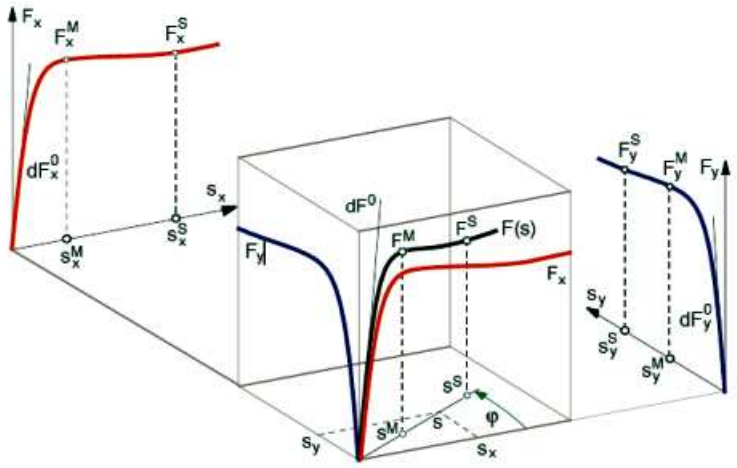

Figure 3.8: Generalised tyre characteristics [30].

recognised. From the generalised force curve and with the angular functions defined in (3.19), the longitudinal and lateral force can be calculated.

$$F_x = F\cos\varphi \tag{3.21}$$

$$F_y = F\sin\varphi \tag{3.22}$$

3.1.5 Wheel load influence

The resistance of a real tyre against deformations has the effect that with increasing wheel load the distribution of pressure over the contact area becomes more and more uneven. According to the literature of the TMeasy tyre model, the tread particles are deflected just as they are transported through the contact area. The pressure peak in the front of the contact area cannot be used, there the tread particles are far away from the adhesion limit because of their small deflection. In the rear of the contact area the pressure drop leads to a reduction of the maximally transmittable friction force. With rising imperfection of the pressure distribution over the contact area, the ability to transmit forces of friction between tyre and road decreases.

In practice, this leads to a degressive influence of the wheel load on the characteristic curves of longitudinal and lateral forces. To add this influence in the TMeasy tyre model the characteristic tyre data for two nominal wheel loads is necessary. For different wheel loads the initial inclinations dF_x^0, dF_y^0, the maximal forces F_x^M, F_y^M and the sliding forces F_x^S, F_y^S are calculated by nonlinear functions

$$F_y^M(F_z) = \frac{F_z}{F_z^N}\left[2F_y^M(F_z^N) - \frac{1}{2}F_y^M(2F_z^N) - \left(F_y^M(F_z^N) - \frac{1}{2}F_y^M(2F_z^N)\right)\frac{F_z}{F_z^N}\right] \tag{3.23}$$

where F_z^N is the nominal load and $2F_z^N$ is double the nominal load. So the parameter $F_y^M(F_z^N)$ is defined as the maximum lateral force at nominal load and $F_y^M(F_z^N)$ is defined as the maximum lateral force at double nominal load.

The location of the maxima s_x^M, s_y^M and the sliding slip values s_x^G, s_y^G are defined as linear functions of the wheel load F_z.

$$s_y^M(F_z) = s_y^M(F_z^N) + \left(s_y^M(2F_z^N) - s_y^M(F_z^N)\right)\left(\frac{F_z}{F_z^N} - 1\right) \tag{3.24}$$

With these wheel load dependent tyre parameters it is possible to fit the tyre model to the measurement characteristics for different wheel loads.

3.1.6 Self-Aligning Torque

According to (3.4) the self-aligning torque M_z is calculated via the pneumatic trail n. The pneumatic trail has been normalised by the length L of the contact area, $n_N = n/L$. In figure 3.9 the development of the pneumatic trail is depicted. Sometimes the pneumatic trail overshoots to negative values before it reaches zero again. In TMeasy this is modelled by introducing the parameter $s_y^0 < s_y^S$.

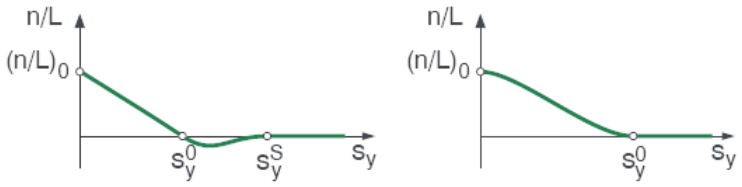

Figure 3.9: Normalised pneumatic trail with and without overshoot [30].

In order to achieve a simple and smooth approximation of the normalised pneumatic trail versus the lateral slip, a linear and a cubic function are overlayed in the section $s_y \leq s_y^0$.

$$\frac{n}{L} = \left(\frac{n}{L}\right)_0 \begin{cases} (1-\omega)(1-s) + \omega\Big(1-(3-2s)s^2\Big) & |s_y| \leq s_y^0 \quad \text{and} \quad s = \frac{|s_y|}{s_y^0}; \\ -(1-\omega)\frac{|s_y|-s_y^0}{s_y^0}\left(\frac{s_y^S-|s_y|}{s_y^S-s_y^0}\right)^2 & s_y^0 \leq |s_y| \leq s_y^S; \\ 0 & |s_y| \geq s_y^S. \end{cases} \tag{3.25}$$

where the factor

$$\omega = \frac{s_y^0}{s_y^S} \tag{3.26}$$

weights the linear and cubic function according to the values of the parameter s_y^0 and s_y^S.

The characteristic curve parameters, which are used for the description of the pneumatic trail, are at first approximation not wheel load dependent. Similar to the description of the characteristic curves of longitudinal and lateral force, here also the parameters for single and double pay load are necessary. The calculation of the parameters of arbitrary wheel loads is done similar to (3.24) by linear inter- or extrapolation.

3.1.7 Camber Influence

Wheel camber γ is defined as the angle between the wheel-centre-plane and the normal to the road, in figure 3.10 the situation for wheel camber is depicted. According to the literature of TMeasy, the inclination angle causes that the tread particles in the contact patch have a lateral velocity which depends on their position ξ and defined as.

$$v_\gamma(\xi) = -\Omega_n \frac{L}{2}\frac{\xi}{L/2} = -\Omega \sin\gamma\xi, \quad -L/2 \leq \xi \leq L/2 \tag{3.27}$$

At the contact point it vanishes whereas at the end of the contact patch it is of the same level as at the beginning, however, pointing into the opposite direction. Assuming that the tread particles stick to the track, the deflection profile is defined as.

$$\dot{y}_\gamma(\xi) = v_\gamma(\xi) \tag{3.28}$$

The time derivative can be transformed to

$$\dot{y}_\gamma(\xi) = \frac{dy_\gamma(\xi)}{d\xi}\frac{d\xi}{dt} = \frac{dy_\gamma(\xi)}{d\xi} r_D|\Omega| \tag{3.29}$$

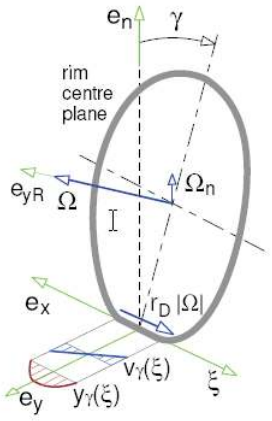

Figure 3.10: Camber angle [30].

where $r_D|\Omega|$ is defined as the average transport velocity. The derivative of (3.28) is defined as

$$\frac{dy_\gamma(\xi)}{d\xi} r_D|\Omega| = -\Omega \sin\gamma \xi \qquad \text{or} \qquad \frac{dy_\gamma(\xi)}{d\xi} = -\frac{\Omega \sin\gamma}{r_D|\Omega|} \frac{L}{2} \frac{\xi}{L/2} \tag{3.30}$$

where $L/2$ is used to achieve dimensionless terms. Subsequently, the camber slip is defined as

$$s_\gamma = \frac{-\Omega \sin\gamma}{r_D|\Omega|} \frac{L}{2} \tag{3.31}$$

With the definition of the camber slip, (3.30) can be simplified to

$$\frac{dy_\gamma(\xi)}{d\xi} = s_\gamma \frac{\xi}{L/2} \tag{3.32}$$

The shape of the lateral displacement profile is obtained by integration of (3.32).

$$y_\gamma = s_\gamma \frac{1}{2} \frac{L}{2} \left(\frac{\xi}{L/2} \right)^2 + C \tag{3.33}$$

To determine the integration constant C, the boundary condition $y(\xi = \frac{1}{2}L) = 0$ is defined. This results in

$$C = -s_\gamma \frac{1}{2} \frac{L}{2} \tag{3.34}$$

Then, the lateral displacement profile can be defined as

$$y_\gamma(\xi) = -s_\gamma \frac{1}{2} \frac{L}{2} \left[1 - \left(\frac{\xi}{L/2} \right)^2 \right] \tag{3.35}$$

For a tyre with pure lateral slip each tread particle in the contact patch has the same lateral velocity and this results in a linear deflection profile. The deflection profiles for pure lateral slip and camber slip are depicted in figure 3.11. The average deflection of the tread particles under pure lateral slip is given by:

$$\bar{y}_y = -s_y \frac{L}{2} \tag{3.36}$$

The average deflection of the tread particles under pure camber slip is obtained from:

$$\bar{y}_\gamma = -s_\gamma \frac{1}{2} \frac{L}{2} \frac{1}{L} \int_{-L/2}^{L/2} \left[1 - \left(\frac{\xi}{L/2} \right)^2 \right] d\xi = -\frac{1}{3} s_\gamma \frac{L}{2} \tag{3.37}$$

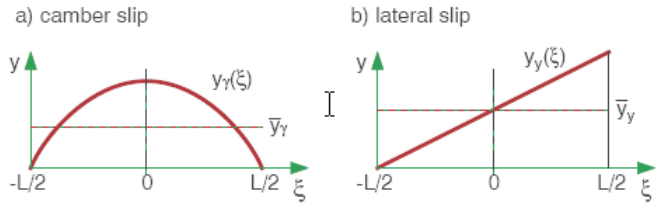

Figure 3.11: Deflection profiles of the tread particles [30].

When both average deflections are compared, the lateral camber slip s_γ can be converted to the equivalent lateral slip s_y^γ with

$$s_y^\gamma = \frac{1}{3} s_\gamma \tag{3.38}$$

In normal driving operation, the camber angle and thus the lateral camber slip are limited to small values. So the lateral camber force can be calculated over the global inclination $dF_y \approx F_y / s_y$

$$F_y^\gamma \approx dF_y s_y^\gamma \tag{3.39}$$

When small slip angles are taken into account and the linearisation of $\sin\gamma \approx \gamma$, this results in

$$\begin{aligned} F_y^\gamma &= dF_y \frac{1}{3} s_\gamma = dF_y \frac{L}{6} \frac{-\Omega \sin\gamma}{r_D |\Omega|} \\ F_y^\gamma &= dF_y \frac{L}{6} \frac{-\Omega}{r_D |\Omega|} \gamma \\ F_y^\gamma &= dF_y \frac{-L}{6 r_D} \gamma \end{aligned} \tag{3.40}$$

where L is the contact length and r_D the dynamic tyre radius. In the created TMeasy tyre model the lateral force is added with the camber force defined in (3.40).

3.2 TMeasy tyre model vs measurement results

The TMeasy tyre model described in the previous sections is based on the literature [20] and [30]. It is known that TMeasy is a commercial product and that the literature only presents the basic idea of the tyre model. Therefore, it is acceptable that some of the approximations made to create the model cause some inaccuracies. It is possible that certain details are not described in the literature and subsequently also not added in the model. The approximations that could cause an inaccuracy are:

- Normalisation factors of the longitudinal and lateral slip coefficients.
- For the calculation of the dynamic tyre radius, the literature describes that some TMeasy parameters are needed to calculate. The calculation of these parameters are not described, so an approximation of the dynamic tyre radius is used.

The model of TMeasy is created according to the general form of the tyre model depicted in figure 1.2. In the next part of this section the TMeasy tyre model created in Matlab is compared with measurement results of the reference tyre described in Appendix A and the accuracy of the optimisation, to give insight in the accuracy of the tyre model with respect to real tyre data.

3.2.1 Fit program

For the validation of the tyre model the measurement data with pure alpha sweeps, pure kappa sweeps and combined slip is used. To calculate the characteristic tyre data of this specific tyre data, an optimisation fit program is written. The fit program minimise the error between the tyre model and

measurement results for the pure longitudinal, lateral and aligning torque characteristics. From this fit program, new characteristic tyre data is calculated which correspond for the reference tyre. The fit parameters for the TMeasy tyre model are:

- Pure longitudinal tyre data at nominal and double vertical load
- Pure lateral tyre data at nominal and double vertical load
- Tyre offset parameters at nominal and double vertical load for the calculation of the aligning torque.

It is chosen to fit the longitudinal, lateral and offset parameters separately, because the fit parameters are also based on pure characteristics. The tyre model is also fitted with the measurements without camber influence. The reason for this is, that the fit parameters of the TMeasy tyre model consist of pure slip parameters, no parameters are included for the camber influence. It can be assumed that during the fit program the accuracy of the fit results are influenced by the camber measurements, because the fit program determines the parameters for pure slip while minimizing pure slip and camber measurements.

The start conditions for the optimisation routine are the characteristic tyre data represented in the paper [20](page 113). With these values the necessary tyre parameters are calculated using the optimisation routine based on the direct search Nelder Mead simplex algorithm. This algorithm is appropriate for unconstrained nonlinear optimisation of a multivariable function. The error calculation used for the parameter identification is the same equation used in (2.9):

$$\varepsilon = \sqrt{\frac{\sum_{i=1}^{N}(Y_{fit} - Y_{meas})^2}{\sum_{i=1}^{N}(Y_{meas})^2}} \times 100\% \tag{3.41}$$

In figure 3.12 an overview of the fit results with respect to the measurement data is presented for the symmetric tyre model. In table 3.1 an overview of the fit errors of the TMeasy tyre model is given.

	ε_{TMeasy} [%]	
	no camber	with camber
pure F_x	1.35	2.03
pure F_y	2.12	2.79
pure M_z	17.20	20.18
combined F_x	7.12	7.36
combined F_y	20.71	20.93
No. fit parameters	26	26

Table 3.1: Errors of the F&M characteristics of the TMeasy Tyre model.

From the fit results it can be concluded that the TMeasy tyre model gives reasonable results for the pure longitudinal and lateral slip characteristics with relatively little model parameters. The tyre model gives a greater error for approximating the aligning torque characteristic. In figure 3.12 an asymmetric tyre behaviour can be recognised in the measurement results of the aligning torque. However, the TMeasy model is symmetric for both positive and negative slip angles.

In the TMeasy tyre model there are no combined slip parameters defined, the combined slip measurements are not used for determining the tyre parameters. However, it is interesting to see if the TMeasy model is capable of approximating the combined slip characteristics with tyre parameters determined of pure slip characteristics. From the combined slip results it can be concluded that the TMeasy tyre model has problems to give a good approximation of the combined slip situation. For all slip angles the model has problems to reach the maximum level of lateral force. For high slip angles it is very clear to see that the peak longitudinal friction coefficients are generally higher than the measurement results. The reason for this could be that the tyre model is described with pure slip tyre

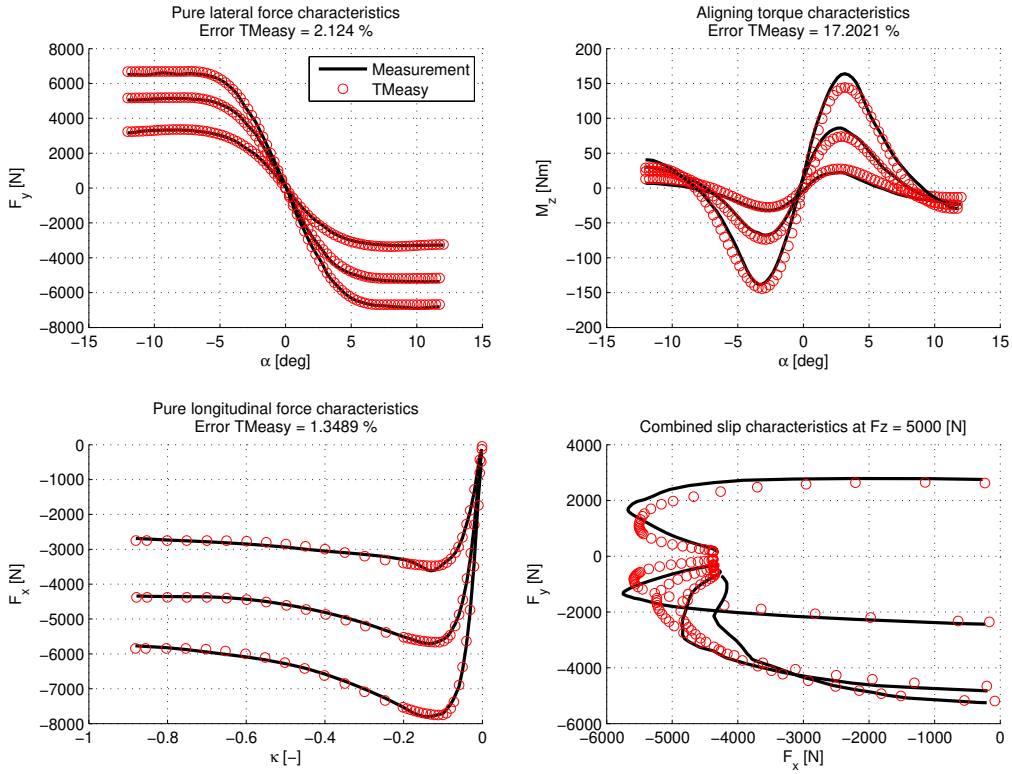

Figure 3.12: Fit results of the TMeasy tyre model.

parameters and these parameters are optimised with respect to the pure slip measurements. Thus, the model gives an approximation of the combined slip situation with pure slip tyre parameters.

The optimised tyre parameters of the TMeasy tyre model for the reference tyre are listed in table 3.2. The fit results of the lateral force and aligning torque characteristic with a camber angle of minus 5 and 5 degrees, are presented in figure 3.13.

3.3 Conclusions of the TMeasy tyre model

After the studying of the literature of the TMeasy tyre model and a comparison study of the model with measurements, it can be concluded that:

- The available literature on the TMeasy tyre model describes only the basic idea of the model. The model created in this thesis is based on this basic idea and it is acceptable that this results in some inaccuracies while describing the tyre force and moment characteristics.
- During the literature study it appears that several parts of the model were not described in detail and some approximations are made to describe these effects.
- In the literature [20] the model is compared with some measurement results. In these results the tyre model shows an asymmetric tyre behaviour, while the model created based on the information found in literature shows a symmetric tyre behaviour for positive and negative slip angles. It is not described which changes are made to include an asymmetric tyre behaviour

Longitudinal force F_x		Lateral force F_y	
F_z	$2 \times F_z$	F_z	$2 \times F_z$
$F_z = 4700$ N $dF_x^0 = 115560$ N $s_x^M = 0.1011$ $F_x^M = 5347$ N $s_x^G = 0.4154$ $F_x^G = 4145$ N	$F_z = 9400$ N $dF_x^0 = 260810$ N $s_x^M = 0.0867$ $F_x^M = 10151$ N $s_x^G = 0.4556$ $F_x^G = 7382$ N	$F_z = 4700$ N $dF_y^0 = 82482$ N $s_y^M = 0.1344$ $F_y^M = 4938$ N $s_y^G = 0.3885$ $F_y^G = 4789$ N	$F_z = 9400$ N $dF_y^0 = 104860$ N $s_y^M = 0.1146$ $F_y^M = 8056$ N $s_y^G = 0.8805$ $F_y^G = 7998$ N
F_z	$2 \times F_z$		
$(n/L)_0 = 0.1842$ $s_y^0 = 0.1316$ $s_y^S = 0.3482$	$(n/L)_0 = 0.2738$ $s_y^0 = 0.1591$ $s_y^0 = 0.2869$		

Table 3.2: optimised tyre parameters of the TMeasy tyre model.

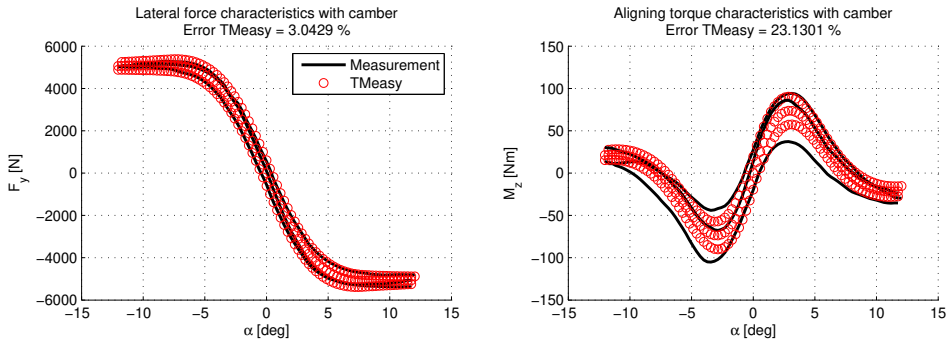

Figure 3.13: Tyre force and moment characteristic with a camber angle.

in the tyre model. To realise asymmetry in the tyre model, an additional slip and camber angle could be defined and added to the tyre model.

- In comparison with the measurement results it can be concluded that the tyre model, with relatively less model parameters, gives a reasonable approximation of the pure longitudinal and lateral tyre force characteristics. Inaccuracy of the tyre model occurs in the aligning torque and combined slip characteristics.

Chapter 4

The TreadSim tyre model

The first physical tyre model investigated in this project is the TreadSim (a tread simulation) tyre model. The original version of TreadSim is developed by Pacejka and described in section 3.3 of Pacejka's book, *Tyre and Vehicle Dynamics* [28]. This model is developed to investigate different aspects of the tyre model which were impossible to include in the analytical brush model. Examples of such complicating features are: Arbitrary pressure distribution, velocity and pressure dependent friction coefficient; anisotropic stiffness properties; combined lateral, longitudinal and camber or turn slip; lateral bending and yaw compliance of the carcass and belt; finite tread width at turn slip or camber.

In the master thesis project of de Hoogh, the TreadSim tyre model of Pacejka is investigated and extended in different directions to be of more use in identifying tyre pressure and velocity relations [21]. In this research the tyre model is extended with anisotropic tread stiffness, a new bristle deflection algorithm, an inverted boat shape pressure distribution and a flexible carcass modelled with elastic beam elements. Furthermore, the algorithm in TreadSim is optimised and this resulted in more accurate fits on measured tyre behaviour, solving of a lateral instability problem and a major reduction of the simulation time. For his investigation also inflation pressure dependency in the vertical tyre and the lateral belt stiffness is included.

The investigation of TreadSim also reveals some weak points. The peak lateral friction coefficient for high vertical loads is generally to high and its dependency on inflation pressure does not match the behaviour found in tyre F&M Measurements. This behaviour is probably caused by the poorly modelled contact patch shape and pressure distribution. Especially for high carcass deformations, thus with high lateral friction at high vertical load, the present carcass model and contact pressure distribution model generates unrealistic contact shapes and pressure distributions. Improvements that could be considered are: Adding mass properties to the carcass model and adapting the carcass deformation routine, transient behaviour or parking/turn slip behaviour and investigate the contact shape representation and pressure distribution.

Before discussing details of the TreadSim tyre model, some remarks can be made concerning the results of the TreadSim model. It turned out that the model realise a carcass deformation of approximately ≈ 0.5 m. It is obvious that such deformations of the carcass are not realistic and this could be the result of an overall to low bending and lateral belt stiffness. In the next sections an overview is given of the TreadSim tyre model studied in the literature presented in [21]. The outputs of the model are examined if the model gives correct data and the model is also compared with the original model of Pacejka to identify the changes made by de Hoogh. Subsequently, the tyre parameters of the model are optimised with respect to the reference tyre described in appendix A and finally the results of the optimization are discussed.

4.1 TreadSim overview

In the model the tyre is assumed to be fitted on a rigid rim and rolling on a flat road with no disturbances. Initially the contact zone is assumed to have a rectangular shape (no carcass deflection) and

positioned symmetrically with respect to the wheel center. The calculation of the forces and moments is based on the time simulation of the deformation history of one tread element while moving through the contact zone. The contact width is divided in several parallel rows of equal length of which a tread element is followed. In figure 4.1 the model with a deflected belt and the tread element that has moved from the leading edge to a certain position in the contact zone is depicted. C is defined as the position of the contact centre with velocity V_c, point S is the slip point with its velocity V_s and $\dot{\psi}$ is the yaw rate. B is the base point of the tread and moves with speed V_b. The tip of the tread is defined as point P. For a more detailed description of the velocities a reference is made to section 2.2 in [28].

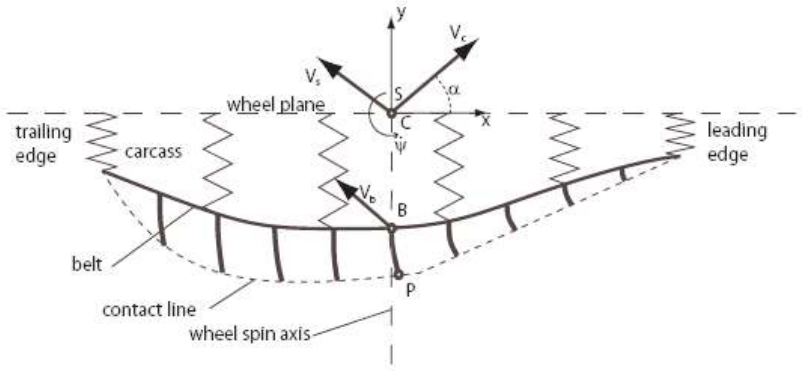

Figure 4.1: TreadSim model with deflected carcass and tread element followed from leading to trailing edge [28].

While moving through the zones the forces acting on the elements are calculated and integrated. After having moved completely through a zone the integration produces the zone forces. These forces act on the belt and the corresponding distortion is calculated. With the updated belt deflection the next passage through the contact rows is performed and the belt deflection calculation is repeated. This iteration procedure is followed until changes in tyre F&M are neglectable between two successive iteration steps. In the next sections the implementation of the TreadSim tyre model is presented and some parts of the model will be described in detail.

4.2 Implementation of the TreadSim tyre model

For the investigation of the steady-state tyre characteristics, the Matlab model created by de Hoogh and presented in [21] is used as the base model for the study of the TreadSim model during the thesis. In figure 4.2 the structure of the TreadSim tyre model is depicted. The input parameters of the model are separated in three categories, namely: state variables, model properties and tyre properties. When all input parameters are defined, the TreadSim model performs a number of iteration steps to calculate the steady-state longitudinal and lateral forces and the aligning moment. The iteration loop continues until the tyre forces and moments between two successive iteration steps differ marginally or the maximum iteration number is reached.

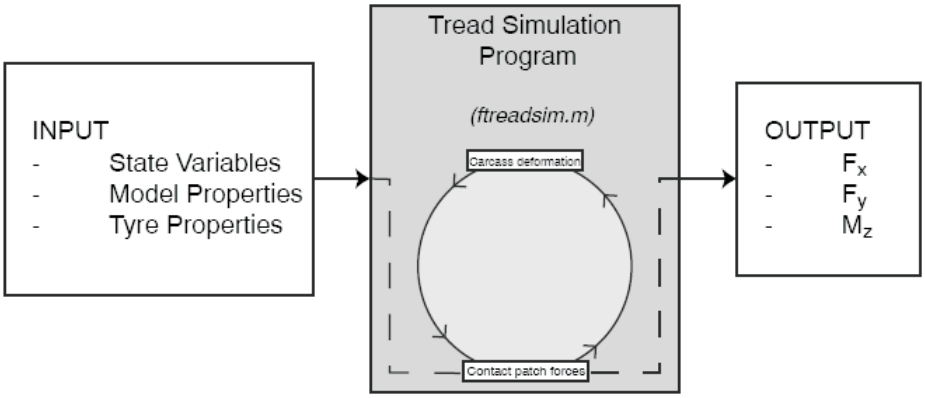

Figure 4.2: Structure of the TreadSim tyre model [21].

The state variables contains:

α	lateral slip angle [deg]
γ	camber angle [deg]
κ	longitudinal slip [-]
F_z	vertical load [N]
V_c	velocity of point C [m/s]
$\frac{1}{R}$	curvature [1/m]
p_{infl}	inflation pressure [bar]

Table 4.1: The state variables.

Before the simulation starts the user selects the number of rows in the contact patch, the number of bristles in a row, the number of beam elements in the tyre circumference and the total number of iterations. By choosing the number of bristles and elements it is possible to make the TreadSim model fast to be used in vehicle simulations or accurate for optimization of the tyre parameters by selecting a low or high number of bristles and elements respectively. The model is able to produce a schematic presentation of the bristle deformations in the contact patch, to activate this feature the parameter *picture* will be set to one. All these variables belong to the model properties.

Model properties:

n_{row}	number of rows in the contact patch
$n_{bristle}$	number of bristles in one row
$n_{beamelem}$	number of beam elements in the tyre circumference
i_{itend}	maximum number of carcass deflections iterations
$picture$	if picture is 1, contact patch deformations picture is created

Table 4.2: The model properties.

Although TreadSim is a physical tyre model, the tyre properties need to be determined from a tyre measurement data set. These measurements are used for all the tyre models in the thesis and described in appendix A. The optimization of these tyre parameters are described in the section where

the optimization routine is discussed. In the next sections the calculation of the forces and moments and the optimization of the tyre parameters are described in detail.

4.3 TreadSim model described in detail

In figure 4.3 the deflected element at the end of two successive time steps is depicted. When the element is sliding, the sliding speed vector $\mathbf{V}_g$, that has a direction opposite to the friction force vector $\mathbf{q}$, is directed opposite to the deflection vector $\mathbf{e}$.

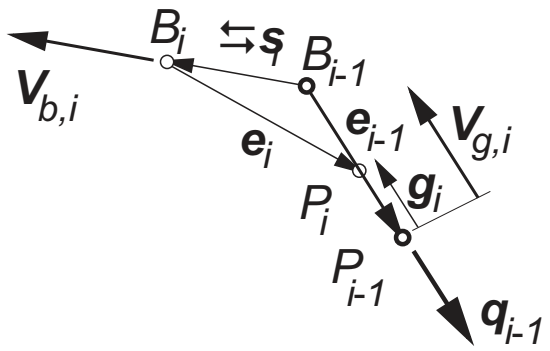

Figure 4.3: Tread element with deflection $\mathbf{e}$ in two successive positions $i-1$ and i [28].

The contact length is divided into n intervals. Over each time step Δt the base point B moves over an interval length towards the rear. With given length:

$$\Delta x = \frac{2a}{n} \tag{4.1}$$

and the linear speed of rolling $V_r = r_e\Omega$, the time step Δt is obtained:

$$\Delta t = \frac{\Delta x}{V_r} \tag{4.2}$$

With the velocity vector $\mathbf{V}_b$ of point B (the connection point of carcass and bristle), the displacement vector $\Delta\mathbf{s}$ of this point over the time step becomes:

$$\Delta\mathbf{s} = \mathbf{V}_b\Delta t \tag{4.3}$$

The base point B moves along the peripheral line or a line parallel to this line. With the known lateral coordinate y_b of this line of base points with respect to the wheel centre plane, the local slope $\partial y_b/\partial x$ can be determined. Then, with the slip velocity $\mathbf{V}_s$ of the slip point S, the yaw rate of the line of intersection $\dot{\psi}$ and the rolling speed V_r, the components of $\mathbf{V}_b$ can be found. The velocity of point B may be considered as the sliding velocity of this point with respect to the ground and (2.55),(2.56) of Pacejka's book [28] are used for its determination. With the average x position $x_b = x + 0.5\Delta x$, the velocity equations are defined as:

$$V_{bx} = V_{sx} + y_{b0}(\dot{\psi} + \Omega\sin\gamma) - \theta_{con,x}(y)V_r + \theta_{\gamma x}(y)y_{b0}\Omega\sin\gamma \tag{4.4}$$

and

$$V_{by} = V_{sy} - x_b\dot{\psi} - \frac{\partial y_b}{\partial x_b}V_r \tag{4.5}$$

with the slip and roll velocities

$$V_{sx} = -V_{cx}\kappa, \quad V_r = r_e\Omega = V_{cx} - V_{sx}, \quad V_{sy} = V_{cx}\tan\alpha \tag{4.6}$$

The θ's are expressed in terms of the camber angle and of equivalent camber and slip angles γ_{con} and α_{ply} to account for conicity and ply-steer and defined as.

$$\theta_{con,x}(y) = -\frac{y}{r_e}(1-\varepsilon_{\gamma x})\gamma_{con} \tag{4.7}$$

$$\theta_{\gamma x}(y) = -\varepsilon_{\gamma x} \tag{4.8}$$

4.3.1 Carcass modelling

In the project of de Hoogh an evaluation of the original iteration process is performed and it turned out that the iteration process shows an instability for certain combinations of vertical load, belt yaw and belt bending stiffness. It was concluded by de Hoogh that the instability was the result of the used method in TreadSim to evaluate the belt deformation. The belt deformation is determined with a second order polynomial and the lateral force F_y is a linear function of the magnitude of this polynomial. When the model is evaluated with a high vertical load and thus a long contact length, the polynomial produces a slope of the belt deformation pattern $\partial y_b/\partial x$ at $x_b = a$ greater than $\tan\alpha$, which is physically not expected [21].

De Hoogh has chosen to improve the belt deformation with elastic beam elements. Carcass stiffness shows to have a large influence on the lateral tyre behaviour and the stiffness of the belt is largely influenced by the inflation pressure. Therefore, to improve the carcass compliance a lateral belt deformation model that exists of elastic beam elements was introduced and depicted in figure 4.4a.

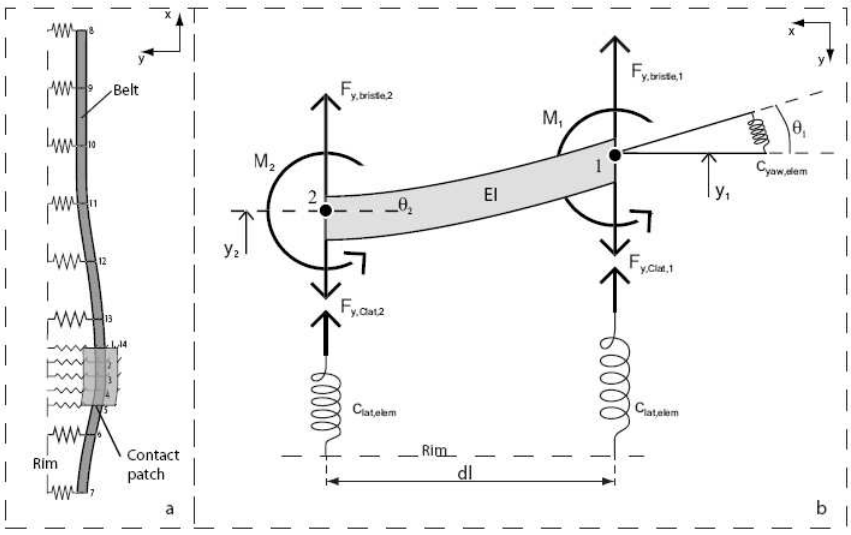

Figure 4.4: Belt deformation model (a); Beam element (b) [21].

In the model, the carcass and belt are only compliant in lateral direction; consequently the longitudinal carcass/belt compliance is neglected. The lateral carcass compliance is modelled with springs and the belt is represented by two-dimensional beam (finite) elements. One element is enlarged and depicted in figure 4.4b and rotated 90 degrees anticlockwise. All elements have bending stiffness EI and are connected to the rim with lateral stiffness $c_{lat,elem}$ and torsional stiffness $c_{yaw,elem}$. The belt consist of two types of elements differing in length dl. The first type is defined in the contact length

between the bristles in a row, consequently the number of type 1 elements equals the number of bristles in one row minus one ($n_{elem,type1} = n_{bristle} - 1$) and has length dl_1. The second type of element with length dl_2 is used in the circumference of the belt not in contact with the ground. The number of type 2 elements equals the total number of beam elements minus the number of element of type 1 ($n_{elem,type2} = n_{beamelem} - n_{elem,type1}$). Preferably the length of a type 2 element, dl_2, is taken greater than the length dl_1 to keep TreadSim's computational effort low with this carcass modelling approach. The stiffness of one element is defined as.

$$\underline{C}_{elem} = \frac{EI}{dl^3}\begin{pmatrix} 12 & 6dl & -12 & 6dl \\ 6dl & 4dl^2 & -6dl & 2dl^2 \\ -12 & -6dl & 12 & -6dl \\ 6dl & 2dl^2 & -6dl & 4dl^2 \end{pmatrix} + \begin{pmatrix} c_{lat,elem} & 0 & 0 & 0 \\ 0 & c_{yaw,elem} & 0 & 0 \\ 0 & 0 & c_{lat,elem} & 0 \\ 0 & 0 & 0 & c_{yaw,elem} \end{pmatrix} \tag{4.9}$$

with

$$c_{lat,elem} = \frac{c_{lat}dl}{2} \quad \text{and} \quad c_{yaw,elem} = \frac{c_{yaw}dl}{2} \tag{4.10}$$

Using $\underline{C}_{elem}$ and $dl1$, $dl2$ substituted for dl depending on the element type, a complete stiffness matrix $\underline{C}_{belt}$ is built representing the stiffness of the entire belt.

$$\mathbf{F} = \underline{C}_{belt}\mathbf{s} \tag{4.11}$$

with the vector **F** containing the applied forces F_i and moments M_i on the nodes, and vector **s** the lateral displacements s_i and rotations θ_i of the nodes.

Besides the effect of inflation pressure on the vertical stiffness of the tyre, there is also an influence of inflation pressure on the lateral belt stiffness (c_{lat}) and bending stiffness (EI) of the belt. The implementation of this inflation pressure dependency applied by de Hoogh is removed from the model, while not a clear definition of the derivation of these relations is given in the report of de Hoogh. Both the lateral and bending stiffness significantly influence the lateral behaviour of the tyre, especially the cornering stiffness and its peak value are very sensitive for the relation between inflation pressure and belt stiffness. Therefore the exact relation should be studied in more detail or should be validated for passenger car tyres for more accurate lateral tyre behaviour.

With the lateral forces generated in the contact patch the distortion of the belt is obtained. The force F_i acting on node i is the sum of the corresponding y-component of the deformation forces from bristles with number i.

$$F_i = \sum_{j=i}^{j=n_{row}} F_{y,brislte,i,j} \tag{4.12}$$

No bristles are 'attached' to the nodes outside the contact patch ($i > n_{bristle}$) and consequently no lateral force is applied on these nodes. The moments M_i acting on the belt are zero at all times. When all deformation forces in the contact patch are generated, **F** can be obtained. Together with the inverted stiffness matrix, the updated distortion of the belt **s** is calculated. The lateral displacement y_b of the belt at the contact centre is attributed to camber and subsequently the updated belt deformation is used by de Hoogh to derive the new carcass velocity.

$$y_{b_i} = y_{b_0} + s_i + \frac{(a^2 - x^2)}{2r_e}(1 - \varepsilon_{\gamma y})(\gamma_{con} + \sin\gamma) \tag{4.13}$$

with y_{b_0} the initial lateral position of the row and s_i the lateral belt deformation. The adoption of camber and conicity in the lateral coordinate of point B_i is similar to the original implementation of

Pacejka. The new belt slope $\left(\frac{\partial_{y_b}}{\partial_{x_b}}\right)$ is derived by de Hoogh from (4.13).

$$\frac{\partial_{y_b}}{\partial_{x_b}} = -\tan(\theta_i) - \frac{x_b}{r_e}\sin\gamma + \theta_y(x_b, y_b) \tag{4.14}$$

where

$$\theta_y(x_b, y_b) = -\varepsilon_{\gamma y}\frac{x_b}{r_e}\sin\gamma + (1-\varepsilon_{\gamma y})\frac{x_b}{r_e}\gamma_{con} + \alpha_{ply} \tag{4.15}$$

4.3.2 Element deformation

With the displacement vector $\Delta\mathbf{s}$, defined in (4.3), the change in deflection $\mathbf{e}$ over one time step can be derived. By keeping the directions of motion of points B and P constant during the time step, an approximate expression for the new deflection is obtained. After the base point B has moved according to the vector $\Delta\mathbf{s}$, the deflection becomes:

$$\mathbf{e}_i = \mathbf{a}_i + \mathbf{g}_i \quad \text{with} \quad \mathbf{a}_i = \mathbf{e}_{i-1} - \Delta\mathbf{s} \tag{4.16}$$

In this equation the vector $\mathbf{a}_i$ is introduced as the displacement of point B over one time step plus the deformation vector $\mathbf{e}_{i-1}$. This vector is equal to the deformation vector $\mathbf{e}_i$ if sliding does not occur, else the difference between $\mathbf{e}_i$ and $\mathbf{a}_i$ is equal to the sliding distance $\mathbf{g}_i$. The sliding vector $\mathbf{g}_i$ of point P is pointing in the direction of the deflection force $\mathbf{q}_{a,i}/\|\mathbf{q}_{a,i}\|$, calculated with stiffness of the tread elements $\underline{C}_p$:

$$\mathbf{q}_{a,i} = \underline{C}_p\mathbf{a}_i \quad \text{and} \quad \underline{C}_p = \begin{pmatrix} c_{px} & 0 \\ 0 & c_{py} \end{pmatrix} \tag{4.17}$$

It is checked if the element starts to slide or adheres to the ground. Adhesion occurs when the deformation force is equal or smaller compared to the maximum friction force, defined as the contact pressure (p_i) multiplied with the friction coefficient (μ_i) of the element with the road:

$$\|\underline{C}_p\mathbf{a}_i\| \leq \mu_i p_i \tag{4.18}$$

In case of adhesion the sliding distance is $g_i = 0$ and from (4.16),(4.17) it follows that the force per unit length becomes:

$$\mathbf{e}_i = \mathbf{a}_i \quad \text{results in} \quad \mathbf{q}_i = \underline{C}_p\mathbf{e}_i \tag{4.19}$$

Sliding starts when the deflection force is larger than the friction force:

$$\|\underline{C}_p\mathbf{a}_i\| \geq \mu_i p_i \tag{4.20}$$

The element start to slide until it satisfies the force equilibrium:

$$\|\underline{C}_p(\mathbf{e}_i)\| = \|\underline{C}_p\left(\mathbf{a}_i + c\frac{\mathbf{q}_{a,i}}{\|\mathbf{q}_{a,i}\|}\right)\| = \mu_i p_i \tag{4.21}$$

Where c is the multiplier of the direction vector $\frac{\mathbf{q}_{a,i}}{\|\mathbf{q}_{a,i}\|}$ and solved from this equation.

$$c = c_{px}^2 a_{ix}^2 + c_{py}^2 a_{iy}^2 - \mu_i^2 p_i^2 \tag{4.22}$$

The new deflection vector $\mathbf{e}_i$ and element deformation force $\mathbf{q}_i$ read:

$$\mathbf{e}_i = \mathbf{a}_i + c\frac{\mathbf{q}_{a,i}}{\|\mathbf{q}_{a,i}\|} \quad \text{and} \quad \mathbf{q}_i = \underline{C}_p\mathbf{e}_i \tag{4.23}$$

The total force by row is calculated as:

$$F_{y,row} = \sum \int_{-a}^{a} q(x)dx \tag{4.24}$$

And resulting from that the total lateral force, is the sum of the forces by row:

$$F_y = \sum F_{y,row} \tag{4.25}$$

4.3.3 Friction coefficient

The friction law used in the TreadSim tyre model is the Savkoor friction law. This friction model is fit on experiments done with tread rubber friction on abrasive paper subjected to different contact pressures and velocities. Initially, only the velocity depended friction law was used. To add pressure dependency the friction law is extended with the pressure dependency of the Savkoor friction law.

$$\mu_d(\upsilon) = \left(\frac{p}{p_0}\right)^{-k} \frac{\mu_0}{1 + a_\mu ||V_b||} \tag{4.26}$$

with p_0 the reference contact pressure and k, μ_0 and a_μ constants. For the determination of the friction coefficient, the sliding velocity of the tip of the element over the ground is necessary (sliding point P). However, this velocity is not available at this stage of the calculation. Through iterations it could be possible to determine the sliding speed at the position considered. Instead, an approximation for this velocity, the velocity of the base point B, is used to determine the current value of the friction coefficient.

4.3.4 Contact patch and normal pressure distribution

The contact patch shape is approximated with a rectangular shape that changes size with tyre vertical deflection. The tyre deflection itself depends on the applied vertical load, the inflation pressure and the forward velocity and is determined with empirical relations.

$$\delta = \frac{F_z}{c_{vert}} \qquad c_{vert} = c_{vert,0} \frac{p_{infl}}{p_{infl,0}} (1 + 2.4 \cdot 10^{-3}(V_c - 16.67)) \tag{4.27}$$

The contact length is a function of the unloaded tyre radius r_0, the vertical load F_z and the vertical stiffness c_{vert} and is adopted with the empirical formula from the work of Besselink [6], and shows to be a good approximation to obtain the contact length through the tyre deflection for a wide range of tyre sizes.

$$a = 0.35 r_0 \left(\frac{\delta}{r_0} + 2.25\sqrt{\frac{\delta}{r_0}}\right) \tag{4.28}$$

The result of this formula, a, equals half of the contact length. Half the tread width b is obtained by taking 90% of the section width defined in the tyre dimensions.

In the TreadSim tyre model, created by de Hoogh, a normal pressure distribution model with an 'inverted-boat' shape in the longitudinal direction and uniform in the lateral direction is used to predict the maximum allowable total shear stresses of a brush element. This method is originally created by Sjahdanulirwan and Yang [31]. The shape of the pressure distribution is adjustable by two factors, so a different increasing and decreasing pressure zone can be recognised. By setting the two shape factors to zero an uniform pressure distribution is created. The algorithm for calculating the pressure distribution is described below. The constant pressure in the constant pressure zone yields

$$P_{max} = \frac{F_z}{2b2a(1 - \frac{c_1}{2} - \frac{c_2}{3})} \tag{4.29}$$

with c_1 and c_2 the relative increasing pressure zone length and decreasing pressure zone length respectively. The pressure distribution over the contact is area is defined as:

$$P = \begin{cases} P_{max}\{\frac{x}{2ac_1}\} & 0 \le x \le 2ac_1, \\ P_{max} & 2ac_1 \le x \le (2a - 2ac_2), \\ P_{max}\{1 - \frac{(x-2a+2ac_2)^2}{(2ac_2)^2}\} & (2a - 2ac_2) \le x \le 2a \end{cases} \tag{4.30}$$

with the x-axis in length direction of the contact path ant the y-axis perpendicular to the length direction in the contact plane.

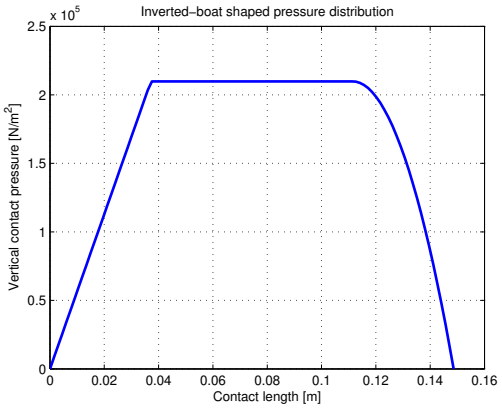

Figure 4.5: Contact pressure distribution over contact area at $F_z = 5000$ N.

In figure 4.5 a calculated pressure distribution at a vertical load of F_z=5000 N and with shape factors of $c1$=$c2$=0.25 is depicted. In comparison with the pressure distribution that actually occurs under a tyre, this is a poor approximation of the real behaviour. Through knowledge obtained from FEM-models, it is also known that the normal pressure distribution has some peak pressures at both sides of the contact area. An example of a normal pressure distribution realised by a FEM-model is depicted in Appendix B.

Another example of a different approach to predict the pressure distribution is the normal stress distribution developed by M. Gipser and it is implemented in the semi-physical tyre model, called BRIT model (Brush and Ring Tyre model) [18]. In Appendix B the principles of this normal stress distribution are further described. It should be further investigated how a more realistic normal pressure distribution can be implemented in the TreadSim tyre model. It is recommended to extend the investigations of contact patches of tyres at Eindhoven University of Technology and develop a model to describe the normal pressure distribution.

4.3.5 Camber thrust

When a tyre experience a camber angle and is loaded against the road, the tread base in the contact patch shows a lateral displacement. The centerline of the exterior follows an elliptical orbit at camber angle γ. When a part of the tread comes into contact with the road, the tread shows a shift in lateral direction, this is depicted in figure 4.6. In the recent TreadSim tyre model of de Hoogh the lateral displacement is modelled by:

$$y_c = r_0 sin\gamma \cdot sin\left(\frac{x_i}{r_0} + \frac{\pi}{2}\right) \tag{4.31}$$

In the thesis of de Hoogh [21], the derivation of this displacement is not described. Subsequently, in the literature of Pacejka [28] it is studied how this behaviour is interpreted and the following equation describes the tread displacement under influence of a camber angle:

$$y_c = \frac{1 - \varepsilon_\gamma}{2r_e}(a^2 - x^2)sin\gamma \tag{4.32}$$

Where r_e is the effective rolling radius, ε_γ is the coefficient for reduced change of the effective rolling radius caused by camber, a is half the contact length, x is the longitudinal position of the tip of a brush element and γ is the camber angle. This equation corresponds with the deflection profile of the TMeasy tyre model, see (3.35).

Both approaches are compared to each other to investigate the lateral displacement over the contact length caused by a camber angle. The results of both equations are depicted in figure 4.7. From this

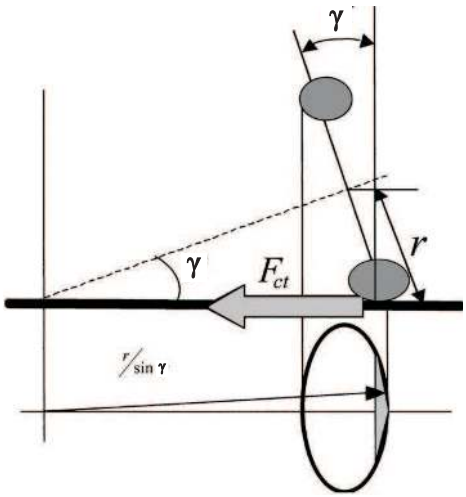

Figure 4.6: Camber thrust model [22].

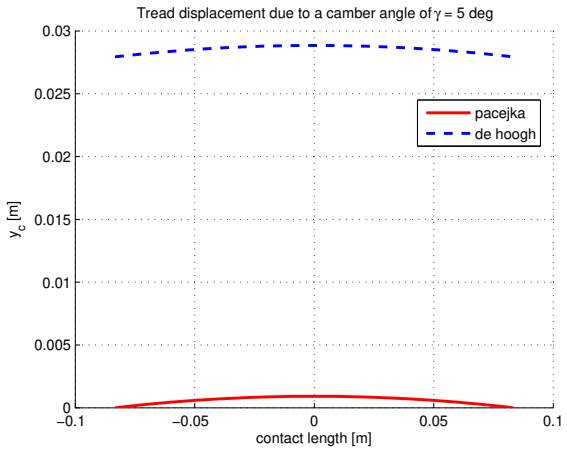

Figure 4.7: Lateral tread displacement under influence of a camber angle.

figure it can be concluded that the equation derived by de Hoogh does not give a good approximation of the tread behaviour under influence of a camber angle. The influence of the camber angle on the lateral tread displacement is very large in the approach of de Hoogh, the tread displacement is approximately 0.03 m in compliance with a half contact length of approximately 0.1 m. In the updated TreadSim tyre model, an adapted approach of the equation of Pacejka is used instead of that from de Hoogh. In addition the influence of conicity is implemented as an equivalent camber angle.

4.4 Fit results of the TreadSim tyre model

After the study of the TreadSim tyre model and the algorithm created by de Hoogh, some alterations are made to improve the model. These alterations results in physical correct data produced by the model. In a previous section it was already described that the TreadSim model requires a number of input parameters. The state variables and model properties are introduced in that section. In this section the optimisation of the tyre properties is discussed. Although TreadSim is a physical tyre model, the tyre properties have to be determined from a tyre measurement data set. An optimisation

routine, the direct search Nelder Mead simplex algorithm, is used that minimises the error between the measurements and the force and moment characteristics described by TreadSim.

4.4.1 Optimisation routine

In the optimisation routine the difference between the measured F&M data of an arbitrary tyre and TreadSim output is minimised for pure longitudinal and pure lateral measurement data with the influence of a camber angle. The following objective function is considered:

- Minimise $f(x)$ = difference between the measured and TreadSim F&M data with the error calculation defined as:

$$f(x) = 100\% \cdot \sqrt{\frac{1}{n}\sum_{i=1}^{n} \begin{pmatrix} \lambda_{F_x}\left(\frac{F_{x,treadsim}-F_{x,measurement}}{\max(|F_{x,measurement}|)}\right)^2 + \\ \lambda_{F_y}\left(\frac{F_{y,treadsim}-F_{y,measurement}}{\max(|F_{y,measurement}|)}\right)^2 + \\ \lambda_{M_z}\left(\frac{M_{z,treadsim}-M_{z,measurement}}{\max(|M_{z,measurement}|)}\right)^2 \end{pmatrix}} \tag{4.33}$$

with n the number of measured values of F_x, F_y and M_z forces in the kappa and alpha sweeps. The weighting factors λ_{F_x}, λ_{F_y} and λ_{M_z} are introduced to emphasise one of the three tyre characteristics when optimizing the tyre parameters. In the optimisation the weighting factors are set to one. This objective function is used in the optimisation instead of the error calculation defined in (2.9) and (3.41), while in TreadSim the forces and moments are calculated for a single slip value. When the slip angle reach the value zero, dividing by zero occurs and this is avoided by using the error calculation defined above.

With this optimisation routine the tyre parameters are optimised for the reference tyre, described in appendix A. After the optimisation the forces and moments are calculated with the optimised tyre properties. To give a good comparison with the other tyre models, the tyre forces and moments characteristics are compared with the measurement data and now the error calculation of (2.9) is used. In the overview of figure 4.8 the results of the F&M fit of the TreadSim tyre model are depicted. The tyre characteristics of the pure slip measurements (longitudinal, lateral and aligning torque) are depicted for three vertical loads ($F_z = 3000, 5000, 7000$ N). The combined slip characteristic is the result of the measurements of combined braking and cornering at different slip angles ($\alpha = -2, 2, 5, 8$ deg). The errors of the slip characteristics of the TreadSim tyre model for the optimisation with and without a camber angle are presented in table 4.3. From the results it can be concluded that the

	$\varepsilon_{TreadSim}$ [%]	
	no camber	with camber
pure F_x	4.46	5.26
pure F_y	4.50	5.38
pure M_z	25.29	26.23
combined F_x	6.33	5.99
combined F_y	12.12	16.02
No. parameters	14	14

Table 4.3: Errors of the F&M characteristics of the TreadSim Tyre model.

TreadSim tyre model gives a reasonable fit of the F&M measurement data. The longitudinal force characteristic shows that TreadSim has problems to give a good approximation of the peak longitudinal force and for higher vertical loads the model has a moderate approximation of the longitudinal force for a locked wheel. Overall it gives a lower longitudinal friction coefficient for the different vertical loads. The lateral force characteristics gives a reasonable approximation of the F&M fit. For higher vertical loads some problems occur, the TreadSim tyre model is not able to fit the maximum friction level. TreadSim generates a peak lateral friction coefficient that is generally higher than the measured

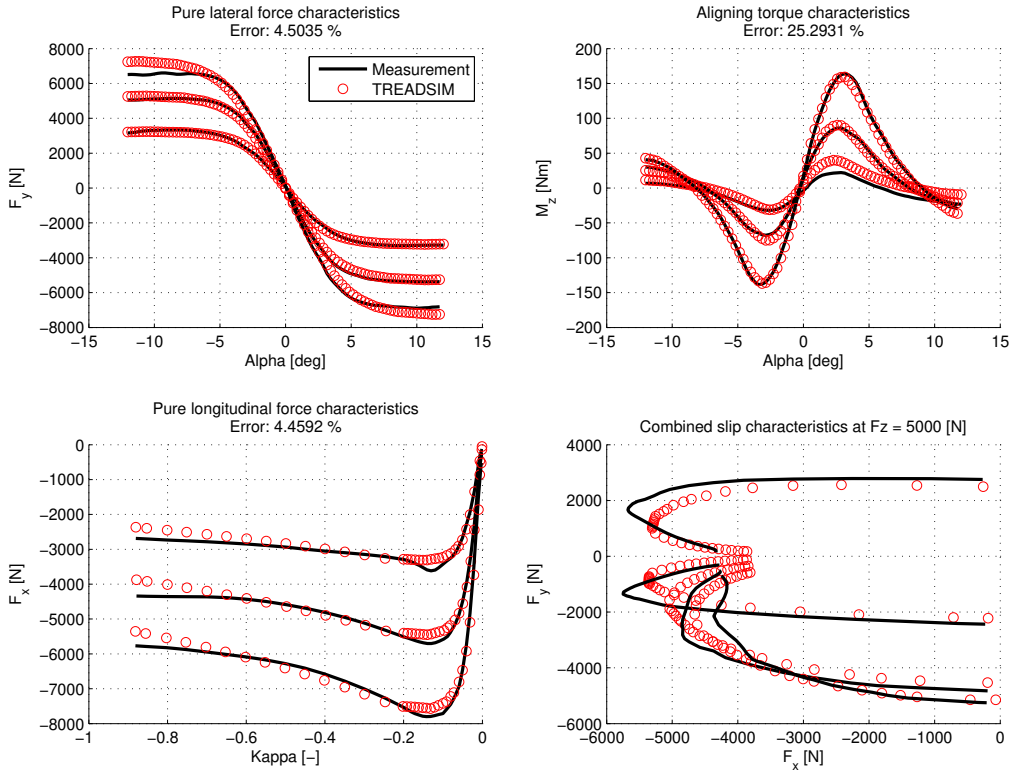

Figure 4.8: F&M fit results of the TreadSim tyre model.

peak friction. Also for higher vertical loads the TreadSim model shows a cornering stiffness $C_{F\alpha}$ that is slightly too low. For the aligning torque characteristics the TreadSim model shows a deviation in the characteristic at a low vertical load. For higher vertical loads the approximation of the aligning torque characteristic is more accurate. The measurement data shows an asymmetric peak aligning moment for positive and negative slip angles, this behaviour is also recognised in the TreadSim model. The combined slip characteristics reveals once more one af the shortcomings of the TreadSim model, that it has problems to fit the maximum friction levels at higher vertical loads.

The optimised tyre parameters of the TreadSim model for the reference tyre are listed in table 4.4. The fit results of the lateral force and aligning torque characteristic with a camber angle of minus 5 and 5 degrees are presented in figure 4.9.

4.5 Conclusions of the TreadSim tyre model

From the study of the TreadSim tyre model and the comparison of the fit results with the measurements, it can be concluded that:

- The updated version of the TreadSim tyre model created by de Hoogh is available at the university and is used in this thesis. The structure of the model is investigated and it is studied if the outcome of the model is physically correct. The outcome of the model reveals that the tyre properties shows unrealistic values, especially the overall too low bending and lateral belt stiffness and the resulting large magnitude of the lateral carcass deformation. To improve the

	x	Tyre parameters
Friction law	μ_0 $[-]$	1.2034
	a_μ $[s/m]$	0.0412
	k $[-]$	0.0824
Stiffness coefficients	c_{px} $[N/m^2]$	$2.9559 \cdot 10^7$
	c_{py} $[N/m^2]$	$2.8728 \cdot 10^7$
Pressure distribution	c_1 $[-]$	0.0360
	c_2 $[-]$	0.2546
Carcass parameters	$c_{vert,0}$ $[N/m]$	135989
	c_{yaw} $[Nm/rad]$	2452
	EI_0 $[Nm]$	1278
	$c_{lat,0}$ $[N/m]$	82666
Tyre properties	α_{ply} $[deg]$	-0.0664
	γ_{con} $[deg]$	-0.9094
	ε_γ $[-]$	0.5606

Table 4.4: Optimised tyre parameters of the TreadSim tyre model.

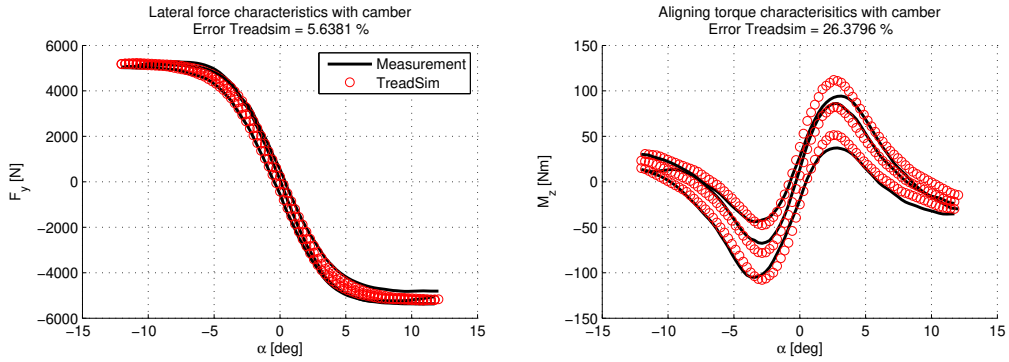

Figure 4.9: Tyre force and moment characteristic with a camber angle.

model, the original model of Pacejka is studied and some adaptations are implemented in the current model, particularly in the deformation of a tread through the contact patch.

- From the fit results it can be concluded that for high vertical loads the TreadSim model has problems to give a good approximation of the measurement results. TreadSim generates a peak friction coefficient that is generally higher than the measured peak friction. This could be the result of the poorly modelled contact patch shape and the unrealistic normal pressure distribution.

- From the longitudinal force characteristic it can be concluded that in the higher slip region the slope of the locked wheel force is steeper than the measurement data. Therefore, the model has problems to reach the maximum level of longitudinal force. From the combined slip situation it can be concluded that the TreadSim model has an overall to low longitudinal peak friction coefficient in comparison with the measurement data.

- Improvements that could be considered to improve the TreadSim tyre model are the improvement of the contact shape deformation, also under the influence of a camber angle. Other improvements that should be studied are the normal pressure distribution and the possibility to derive the pressure distribution from a FEM model.

Chapter 5

Dynamic tyre friction model

The second physical tyre model studied in the thesis, is the dynamic brush model based on the LuGre friction model of Canudas de Wit and Åström [7]. The LuGre friction model is known for describing special cases of friction situations and was developed as a joint cooperation between the Department of Automatic Control at Lund University (Sweden) and Laboratoire d'Automatique de Grenoble (France). The model describes a dynamic force phenomenon that arises when frictional surfaces are sliding on each other. Subsequently, there have been several investigations to make the LuGre dynamic friction model suitable for the tyre-road contact problem. In the formulation for tyres the LuGre model assumes the frictional surface to consist of bristles, with movements described by differential equations. An extension of the LuGre tyre model is proposed by Deur [10], [14] and [16]. The model describes the dynamics of longitudinal and lateral tyre friction forces, as well as the self aligning torque dynamics. In this chapter the distributed tyre friction model is described, for investigation of the steady-state tyre behaviour. In the next sections the basic idea behind the LuGre dynamic friction model is described and following several extensions of the LuGre model are studied and described. Finally, an optimisation routine is created and the steady-state dynamic tyre friction model is validated with respect to experimental data.

5.1 Basic idea behind the LuGre friction model

Most of the existing model-based friction compensation schemes use classical friction models, such as Coulomb and viscous friction. The classical friction models are described by static maps between velocity and friction force. Typical examples are different combinations of Coulomb friction, viscous friction and the Stribeck effect. However, these models explain no hysteretic behaviour when studying friction for nonstationary velocities, and no variations in the break-away force with the experimental condition, and not small displacements that occur at the contact interface during stiction. Canudas de Wit proposed a new dynamic friction model that combines the stiction behaviour, that is the Dahl effect, with arbitrary steady-state friction characteristics which can include the Stribeck effect [7]. Stribeck observed that for low velocities, the friction force is decreasing continuously with increasing velocities. The Dahl model is a dynamic model describing the spring-like behaviour during stiction. This model is essentially Coulomb friction with a lag in the change of friction force when the direction of motion is changed. A further explanation of the different friction effects is described in appendix C.

The friction model proposed by Canudas de Wit is visualised as two rigid bodies that make contact through elastic bristles. When a tangential force is applied, the bristles will deflect like springs which give rise to the friction force, see figure 5.1. For simplicity the bristles on the lower part are shown as being rigid. If the force is sufficiently large some of the bristles deflect so much that they will slip. This phenomenon is highly random due to the irregular forms of the surfaces. The friction model is also based on the average behaviour of the bristles. The average deflection of the bristles is denoted by

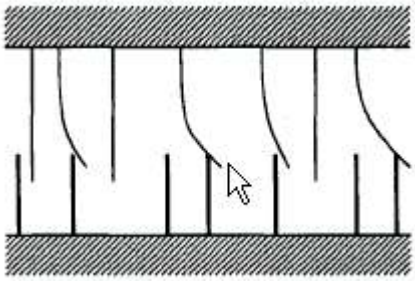

Figure 5.1: The friction interface between two surfaces is thought of as a contact between bristles [8].

z and is modelled by

$$\frac{dz}{dt} = v_r - \frac{|v_r|}{g(v_r)}z \tag{5.1}$$

where v_r is the relative velocity between the two surfaces. The first term gives a deflection that is proportional to the integral of the relative velocity. The second term claims that the deflection z approaches the value

$$z_{ss} = \frac{v_r}{|v_r|}g(v_r) = g(v_r)\text{sgn}(v_r) \tag{5.2}$$

in steady state, that means that v_r is constant. The function $g(v_r)$ is positive and depends on many factors such as material properties, lubrication, temperature. It need not be symmetrical, direction dependent behaviour can therefore be captured. For typical bearing friction, $g(v_r)$ will decrease monotonically from $g(0)$ when v_r increases. This corresponds to the Stribeck effect. The friction force generated from the bending of the bristles is described as

$$F = \sigma_0 z + \sigma_1 \frac{dz}{dt} \tag{5.3}$$

where σ_0 is the stiffness and σ_1 a damping coefficient. A term proportional to the relative velocity could be added to the friction the friction force to account for viscous friction so that

$$F = \sigma_0 z + \sigma_1 \frac{dz}{dt} + \sigma_2 v_r \tag{5.4}$$

The model defined in (5.1) and (5.4) is characterised by the function g and the parameters σ_0, σ_1 and σ_2. A parameterisation of g that has been proposed to describe the Stribeck effect is

$$g(v_r) = F_C + (F_S - F_C)e^{-(v_r/v_s)^\delta} \tag{5.5}$$

where F_C is the Coulomb friction level, F_S is the level of the stiction force, v_s is the Stribeck velocity and δ is the Stribeck exponent. With the description from above the model is characterised by six parameters σ_0, σ_1, σ_2, F_C, F_S and v_s. For a steady-state motion the relation between velocity and friction force is given by

$$\begin{aligned} F_{ss}(v_r) &= \sigma_0 g(v_r)\text{sgn}(v_r) + \sigma_2 v_r \\ &= F_C\text{sgn}(v_r) + (F_S - F_C)e^{-(v_r/v_s)^\delta}\text{sgn}(v_r) + \sigma_2 v_r \end{aligned} \tag{5.6}$$

When the velocity is not constant, the dynamics of the model will be important and give rise to different phenomena. In [7] also the dynamic model behaviour is investigated, such as the presliding displacement, frictional lag and stick-slip motion. However, the emphasise in these thesis is on the steady-state tyre behaviour and therefore these results will not be discussed further.

Canudas de Wit has proposed a new dynamic friction model that is simple yet captures most friction phenomena. The model can describe arbitrary steady-state friction characteristics. It supports hysteretic behaviour due to frictional lag, spring-like behaviour in stiction and gives a varying break-away force depending on the rate of change of the applied force. All these phenomena are unified into a first-order nonlinear differential equation. The model can readily be used in simulations of systems with friction [7]. In the next sections the development of a dynamic tyre friction model based on the LuGre friction model is described.

5.2 Dynamic tyre friction model development

In the research of Canadus de Wit a dynamic friction force model for tyre-road interaction for ground vehicles is proposed [8]. The model is based on the LuGre friction model, which is described in section 5.1. The dynamic LuGre friction model is able to accurately capture velocity and road-surface dependence of the tyre friction force. Deur proposed a modification of the LuGre dynamic tyre model [10]. According to Deur the LuGre dynamic tyre model has a more compact mathematical form compared to the original brush model of van Zanten [32]. Therefore, the LuGre model is suitable for its transformation to a simpler lumped model form. In the next sections the dynamic tyre model of Deur and the extensions to a 3D dynamic tyre model will be described.

The friction force in the tyre-road interface is the main mechanism for converting wheel angular acceleration (due to the motor torque) to forward acceleration (longitudinal force). Therefore, the study of friction force characteristics has a great share in the automotive industry. A common assumption in most of the tyre friction models is that the normalised tyre friction

$$\mu = \frac{F}{F_n} = \frac{\text{Friction force}}{\text{Normal force}} \tag{5.7}$$

is a nonlinear function of the normalised relative velocity between the road and the tyre (slip coefficient s) with a distinct maximum. The friction coefficient μ depends also on the velocity of the vehicle and road surface conditions, among other factors. The development of friction force at the tyre-road interface is very much a dynamic phenomenon. In other words, the friction force does not reach steady-state instantaneously, but rather exhibits significant transients behaviour which may differ significantly from its steady-state value.

At first the LuGre friction model is applied for longitudinal motion of the vehicle. In further research the model is also extended for combined longitudinal and lateral motion and to investigate the aligning torque behaviour. In this section, first the model describing longitudinal motion is presented and subsequently also the model extended for combined longitudinal and lateral motion is presented.

5.2.1 Distributed tyre model for longitudinal motion

The longitudinal tyre force F_x is usually described as a static function of the longitudinal slip s which is usually defined as

$$s = \begin{cases} \frac{v - r\omega}{v} & \text{for} \quad r\omega \leq v \neq 0 \quad \text{(braking)} \\ \frac{r\omega - v}{r\omega} & \text{for} \quad v \leq r\omega \neq 0 \quad \text{(traction)} \end{cases} \tag{5.8}$$

where v is the vehicle velocity, ω the wheel angular velocity and r is the effective tyre radius at free rolling. In figure 5.2 a representation of the tyre brush model with the several parameters is depicted.

Dynamic models can be formulated as a lumped or distributed models. Distributed models assume the existence of an area of contact (or patch) between the tyre and the road. This patch represents the projection of the part of the tyre that is in contact with the road. It is assumed that the tyre-road contact is realised through a lot of tiny, massless and elastic elements (so-called bristles) attached to a circular belt. The contact patch has a rectangular form with the length L. In the paper describing this model [10] a uniform normal pressure distribution is assumed. If the relative v_r velocity between the bristle point attached to the belt and the tip which adheres to the ground

$$v_r = r\omega - v \tag{5.9}$$

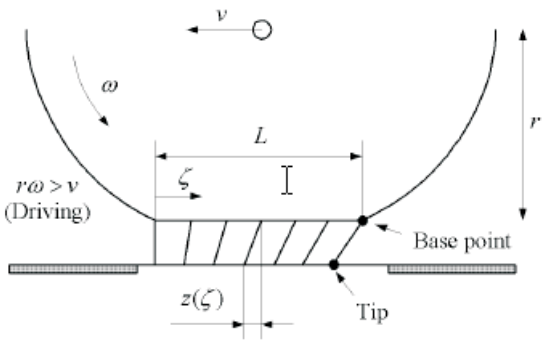

Figure 5.2: Tyre brush model [10].

is different from zero (slip s>0), the bristles are deformed producing the tyre longitudinal force F_x.

Friction transferred from a base point to the road can be described for pure longitudinal motion by an equivalent mechanical model shown in figure 5.3a. The model consist of a mass-less spring

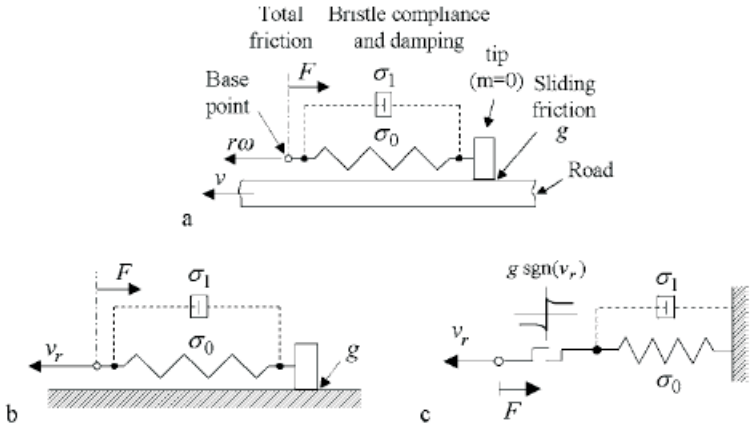

Figure 5.3: Mechanical model of bristle friction in wheel coordinate system (a), road coordinate system (b) or equivalently as shown in (c) [16].

with the stiffness coefficient σ_0, which accounts for the bristle compliance effect, and a mass-less tip-road friction element with a static friction characteristic g. The equivalent model in the road coordinate system is depicted in figure 5.3b. This model can be seen as a dynamic friction model, with an internal state which corresponds to the spring deflection. In case of full tyre-road adhesion the bristles will deflect over a linear tire-road contact line. Outside the low-slip region, tips of some bristles will slide over the road. In such a sliding regime, the tip moves with respect to the wheel axis with the same speed $r\omega$ as the base point (under steady-state conditions). The initial tip-road contact point (at ζ=0) continues to move with the wheel center speed v. The tip transfers the sliding friction $g(v_r)$ to the road. The bristle deflection becomes constant in case of a uniform divided normal pressure distribution.

The traditional way of describing the bristle friction equivalent model shown in figure 5.3b and c, is to separately describe the friction behaviour for the adhesion (stick) region and the sliding region. The bristle deflection process in the adhesion region is usually described by the linear stress-strain curve. To give more insight in the different friction effects and to implement friction models in simulation models, an overview of different static and dynamic friction effects is added in appendix C. The LuGre friction model is an extension of the Dahl model with the Stribeck effect, see (5.1) and (5.4), as proposed by Canudas de Wit [7] and described in the section above.

According to the LuGre dynamic friction model, the bristle deflection process at the position ζ of the contact patch ($0 \leq \zeta \leq L$) and at the time t can be described for pure longitudinal motion (α=0) by the following first-order nonlinear differential equation [8]:

$$\frac{dz(\zeta,t)}{dt} = v_r(t) - \frac{\sigma_0|v_r(t)|}{g(v_r(t))}z(\zeta,t) \tag{5.10}$$

The differential of the deflection variable z, as a function of two independent variables ζ and t, is given by:

$$dz(\zeta,t) = \frac{\partial z(\zeta,t)}{\partial \zeta}d\zeta + \frac{\partial z(\zeta,t)}{\partial t}dt \tag{5.11}$$

In the report of Deur *et al.* [13] the longitudinal tyre dynamics are described, and if the brush model kinematic relations are taken into account, the differential equation becomes:

$$\frac{\partial z(\zeta,t)}{\partial t} = \frac{dz(\zeta,t)}{dt} - \frac{\partial z(\zeta,t)}{\partial \zeta}\frac{d\zeta}{dt} = v_r - r|\omega|\frac{\partial z(\zeta,t)}{\partial \zeta} \tag{5.12}$$

Inserting (5.10) into (5.12) yields the final partial differential equation of the LuGre tyre friction model:

$$\frac{\partial z(\zeta,t)}{\partial t} = v_r - \frac{\sigma_0|v_r|}{g(v_r)}z - r|\omega|\frac{\partial z(\zeta,t)}{\partial \zeta} \tag{5.13}$$

$$F_x(t) = \frac{1}{L}\int_0^L \left[\sigma_0 z(\zeta,t) + \sigma_1\frac{\partial z(\zeta,t)}{\partial t} + \sigma_2 v_r\right] d\zeta \tag{5.14}$$

where σ_1 and σ_2 are the bristle damping coefficient and the friction viscous coefficient, respectively. The deflection saturation is implicity included in (5.13) through the term proportional to the deflection variable z, which accounts for the bristle plastic deformation effect. Compared to the originally proposed LuGre tyre model by Canudas de Wit and Tsiotras [8], the model proposed by Deur [13] differs from that model that the damping term in the model output (5.14) is modified in the way that the partial deflection derivative is used. According to Deur, in this model the standard derivative from [8] is used, the damping term would damp tyre force oscillations not only in time, but also in space. It appears to be unrealistic and would result in a damping-dependent steady-state curve, which would be highly sensitive to variations of the vehicle-wheel speed [10].

For the steady-state behaviour of the LuGre dynamic tyre model, the left side of (5.13) equals zero. This leads to a first-order, ordinary differential equation, with the following solution as derived in [8] and [13]:

$$z(\zeta) = \mathrm{sgn}(v_r)\frac{g(v_r)}{\sigma_0}\left(1 - e^{-\zeta/\mathrm{Z}}\right) \tag{5.15}$$

with the constant Z defined as:

$$\mathrm{Z} = \left|\frac{r\omega}{v_r}\right|\frac{g(v_r)}{\sigma_0} \tag{5.16}$$

In (5.15) the exponential steady-state deflection distribution for the LuGre model is shown, which according to Deur is of a more natural form than the saturated linear form of the original brush model. However, in the literature of Deur [10] this is not validated with any kind of experiment that the bristle deflection is of an exponential shape.

The first-order differential equation (5.15) is inserted into (5.14) and the integral equation is derived by Deur and leads to the following final expression for the steady-state longitudinal tyre force:

$$F_x = \mathrm{sgn}(v_r)g(v_r)\left[1 - \frac{\mathrm{Z}}{L}\left(1 - e^{-L/\mathrm{Z}}\right)\right] + \sigma_2 v_r \tag{5.17}$$

According to Deur the final expression of the steady-state longitudinal force (5.17) is of a more simpler form than the corresponding equation of the original LuGre tyre model defined by Canudas de Wit and Tsiotras [8]. In figure 5.4 the result of the LuGre dynamic tyre model proposed by Deur is presented. This force-slip curve is realised with the parameters defined in the paper of Deur [10].

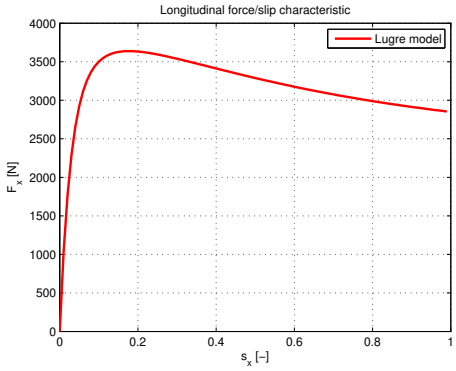

Figure 5.4: Longitudinal force-slip curve for the LuGre tyre model (braking).

5.3 Extension of the LuGre tyre model for combined longitudinal and lateral motion

In further research of Deur, the dynamic tyre friction model based on the LuGre friction model is extended for combined longitudinal and lateral motion, and calculation of the self aligning torque [14]. The extended model is derived for both uniform and non-uniform normal pressure distributions along the longitudinal (x)-axis. In this section the extended model with non-uniform normal pressure distribution is presented. Along the lateral (y)-axis, the uniform normal pressure distribution is assumed. The dynamic tyre model for longitudinal motion and uniform normal pressure distribution is already derived in section 5.2. For the complete derivation of the corresponding static model with asymmetric trapezoidal normal pressure distribution, a reference is made to [14, 15, 16].

Static tyre models are usually expressed in a single, dimensionless longitudinal slip parameter s. For the combined slip situation the longitudinal slip definition of (5.8) is extended with the slip angle α and defined as:

$$s = \begin{cases} \frac{v\cos\alpha - r\omega}{v\cos\alpha} & \text{for} \quad r\omega \leq v\cos\alpha \neq 0 \quad \text{(braking)} \\ \frac{r\omega - v\cos\alpha}{r\omega} & \text{for} \quad v\cos\alpha \leq r\omega \neq 0 \quad \text{(traction)} \end{cases} \tag{5.18}$$

where r is the effective tyre radius at free rolling. In figure 5.5 the brush model for combined longitudinal and lateral motion is depicted.

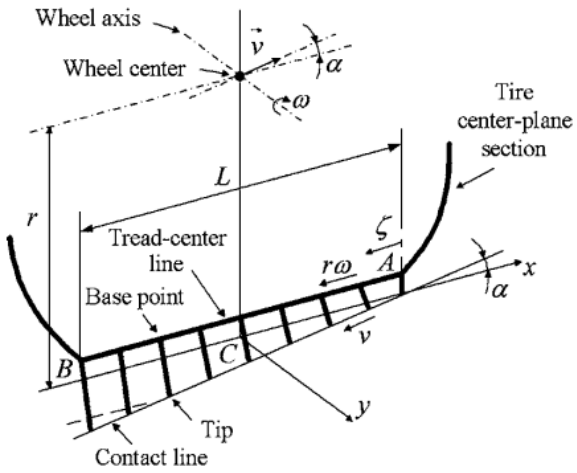

Figure 5.5: Brush model of a tyre for combined longitudinal and lateral motion [14].

The longitudinal, lateral and absolute values of the relative speed between a bristle base point and the corresponding tip-road contact point are given by the following equations:

$$v_{rx} = r\omega - v\cos\alpha \tag{5.19}$$
$$v_{ry} = v\sin\alpha \tag{5.20}$$
$$v_r = \sqrt{v_{rx}^2 + v_{ry}^2} \tag{5.21}$$

When $v_{rx} \geq 0$, corresponds with the driving situation and braking is determined when $v_{rx} < 0$. In reality, the relative speeds v_{rx}, v_{ry} and v_r vary along the contact length due to turning, camber and deflection variation effects. That means that the relative speeds should be extended with longitudinal bristle position (ζ)-dependent terms. However, these effects are neglected in order to obtain a simple (analytical) tyre model.

In the case of combined longitudinal and lateral motion, the bristles are deflected in both the longitudinal (x) and lateral (y) directions. Thus, (5.13) is transferred into two equations for these two directions and presented by the following vector equation:

$$\frac{\partial z_{x,y}(\zeta,t)}{\partial t} = v_{rx,y} - \frac{\sigma_{0x,y}|v_{rx,y}|}{g_{x,y}(v_r, v_{rx,y})} z_{x,y}(\zeta,t) - r|\omega|\frac{\partial z_{x,y}(\zeta,t)}{\partial \zeta} \tag{5.22}$$

where subscripts x, y represents the corresponding direction. Due to the anisotropic nature of the tyre, different longitudinal and lateral stiffness coefficients σ_{0x} and σ_{0y} are used. The longitudinal and lateral components $g_{x,y}$ of the tyre-road sliding friction force g are positive according to the LuGre model structure [7, 13] and defined as:

$$g_{x,y}(v_r, v_{rx,y}) = \left|\frac{v_{rx,y}}{v_r}\right| g(v_r) \tag{5.23}$$

Inserting (5.23) into (5.22) and rearranging the last equation, leads to the final deflection equations for combined longitudinal and lateral motion:

$$\frac{\partial z_{x,y}(\zeta,t)}{\partial t} = v_{rx,y} - \frac{\sigma_{0x,y}|v_r|}{g(v_r)} z_{x,y}(\zeta,t) - r|\omega|\frac{\partial z_{x,y}(\zeta,t)}{\partial \zeta} \tag{5.24}$$

According to the output equation of the LuGre friction model (5.4), the longitudinal and lateral components of the tyre force contribution of a bristle at the position ζ in the tyre central plane (defined per unit area of the contact patch) can be expressed as [10, 13]:

$$\varphi_{x,y}(\zeta,t) = \frac{1}{LW}\left[\sigma_{0x,y} z_{x,y}(\zeta,t) + \sigma_{1_{(x,y)}}\frac{\partial z_{x,y}(\zeta,t)}{\partial t} + \sigma_2 v_{rx,y}\right] \tag{5.25}$$

where σ_1 is the damping coefficient and σ_2 is the viscous friction coefficient, L is the length and W is the width of the contact patch. The total longitudinal and lateral components of the tyre friction force is derived by Deur by integrating the bristle force contributions over the contact patch area:

$$\begin{aligned} F_{x,y}(t) &= \int_{-W/2}^{W/2}\int_0^L \varphi_{x,y}(\zeta,t)d\zeta dy = W\int_0^L \varphi_{x,y}(\zeta,t)d\zeta \\ &= \frac{1}{L}\int_0^L \left[\sigma_{0x,y} z_{x,y}(\zeta,t) + \sigma_{1(x,y)}\frac{\partial z_{x,y}(\zeta,t)}{\partial t} + \sigma_2 v_{rx,y}\right] d\zeta \end{aligned} \tag{5.26}$$

Accordingly, the self aligning torque M_z for the basic case of zero residual torque and pure cornering is calculated as:

$$M_z = W\int_0^L \varphi_y(t)\left(\frac{L}{2} - \zeta\right) d\zeta \tag{5.27}$$

The dynamic tyre model derived by Deur and given by (5.24), (5.26) and (5.27) has an analytical solution for the steady-state case. For the steady-state operation, the term $\partial z_{x,y}(\zeta,t)/\partial t$ in (5.24) equals zero. According to this, the partial differential equation is transformed into the ordinary differential equation in the space variable ζ, defined as:

$$z_{x,y}(\zeta) = \mathrm{sgn}(v_{v_{rx,y}}) \left| \frac{v_{rx,y}}{v_r} \right| \frac{g(v_r)}{\sigma_{0x,y}} \left(1 - e^{-\zeta/\mathrm{Z}_{x,y}}\right) \tag{5.28}$$

with

$$\mathrm{Z}_{x,y} = \left| \frac{r\omega}{v_r} \right| \frac{g(v_r)}{\sigma_{0x,y}} \tag{5.29}$$

Instead of the uniform longitudinal normal pressure distribution, a more realistic non-uniform pressure distribution can be used to obtain a more accurate tyre friction model. The longitudinal normal pressure distribution $p(\zeta)$ is described by an asymmetric trapezoidal function depicted in figure 5.6.

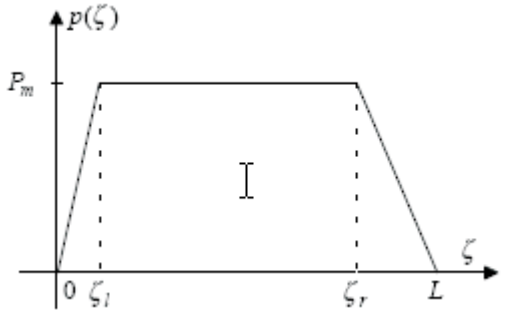

Figure 5.6: Asymmetric trapezoidal normal pressure distribution.

The maximum pressure value P_m relates to the normal force F_z as:

$$P_m = \frac{2}{1 + r_r - r_l}\bar{p} = \frac{1}{WL}\frac{2}{1 + r_r - r_l}F_z \tag{5.30}$$

with the relative left and right margins of the trapezoidal distributions defined as:

$$r_{l,r} = \frac{\zeta_{l,r}}{L} \tag{5.31}$$

A method to implement a non-uniform normal pressure distribution in the LuGre dynamic tyre friction model can be realised by scaling the output equation (5.25) with the factor F_z/F_{z0}, which corresponds to the case of scaling both the function g and the stiffness coefficient σ_0 in the state equation (5.22) with unchanged the output equation. In the dynamic tyre friction model, this method is used to include the normal pressure distribution.

$$\varphi_{x,y}(\zeta,t) = \frac{p(\zeta)}{F_{z0}} \left[\sigma_{0x,y} z_{x,y}(\zeta,t) + \sigma_{1_{(x,y)}} \frac{\partial z_{x,y}(\zeta,t)}{\partial t} + \sigma_2 v_{rx,y} \right] \tag{5.32}$$

The distributed dynamic tyre friction model of Deur with a non-uniform normal pressure distribution is defined by (5.22), (5.26), (5.27) and (5.32). The corresponding static model with asymmetric trapezoidal normal pressure distribution is derived by Deur and presented in [15]. The integral equations (5.26) and (5.27) are solved on the intervals $[0,\zeta_l]$, $[\zeta_l,\zeta_r]$ and $[\zeta_r,L]$. The following final expressions of the static model for non-uniform normal pressure distribution are defined as:

$$F_{x,y} = \frac{v_{rx,y}}{|v_r|} g(v_r) \left\{ 1 - \frac{2}{1+r_r-r_l} \rho_{x,y} \left[\frac{\rho_{x,y}}{r_l} (1 - e^{-r_l/\rho_{x,y}}) - \frac{\rho_{x,y}}{1-r_r} (e^{-r_r/\rho_{x,y}} - e^{-1/\rho_{x,y}}) \right] \right\} + \sigma_2 v_{rx,y} \tag{5.33}$$

$$M_z = \frac{v_{ry}}{|v_r|} g(v_r) \frac{L}{2} \left\{ 1 - K_v \frac{2}{1+r_r-r_l} \rho_y^2 \left[\frac{4\rho_y - 1}{r_l} - \frac{4\rho_y + 2r_l - 1}{r_l} e^{-r_l/\rho_y} - \frac{4\rho_y + 2r_r - 1}{1-r_r} e^{-r_r/\rho_y} + \frac{4\rho_y + 1}{1-r_r} e^{-1/\rho_y} \right] \right\} + \frac{L}{2}(1 - K_v)\sigma_2 v_{ry} \tag{5.34}$$

with

$$K_v = \frac{2}{L^2} \int_0^L \zeta \bar{p}(\zeta) d\zeta = \frac{2}{3} \frac{1 + r_r + r_r^2 - r_l^2}{1 + r_r - r_l} = \bar{p}_m \frac{1 + r_r + r_r^2 - r_l^2}{3} \tag{5.35}$$

$$\rho_{x,y} = \frac{\mathrm{Z}_{x,y}}{L} = \frac{1}{L} \left| \frac{r\omega}{v_r} \right| \frac{g(v_r)}{\sigma_{0x,y}} \tag{5.36}$$

The stiffness coefficients for the static model are found to be:

$$K_{x,y} = \frac{1}{2} L \sigma_{0x,y} K_\nu \tag{5.37}$$

$$K_z = \frac{1}{6} L^2 \sigma_{0y} \frac{r_r^3 + r_l^2 - r_l^3}{1 + r_r - r_l} \tag{5.38}$$

5.3.1 Structure of the LuGre model used in this thesis

For the investigation of the steady-state tyre behaviour of the LuGre dynamic tyre friction model, a model is created based on the literature of Deur and described in the previous sections. The structure of the model is based on the overview depicted in figure 1.2. The input variables of the LuGre tyre model are the lateral slip angle α, the longitudinal slip s, the forward velocity v and the vertical load on the tyre F_z. From the slip quantities the angular velocity of the wheel is determined for the braking and driving situation as:

Braking:

$$\omega = \frac{-(v \cos\alpha) \cdot (s-1)}{r_0} \tag{5.39}$$

Driving:

$$\omega = \frac{-v \cos\alpha}{r_0 (s-1)} \tag{5.40}$$

In these equations the free rolling radius r_0 is used instead of the effective rolling radius, this approach is also used in the other tyre models described in this thesis.

The dynamic tyre friction model is tested by Deur if it can provide accurate description of the tyre characteristics. In order to further enhance the model accuracy, some physical and empirical model extensions are proposed by Deur.

The parameters of the friction curve $g(v_r)$, see (5.5), depends on the motion directions. For the two-dimensional $(x-y)$ motion of a friction element, the parameters are made linearly dependent on the orientation angle β of the relative speed (slip) vector $\vec{v_r}$:

$$\beta = \arctan(|v_{ry}/v_{rx}|) \tag{5.41}$$

The parameters of the original sliding friction function, see (5.23) are defined for pure longitudinal motion:

$$g_{x0}(v_r) = F_C + (F_S - F_C) e^{-|v_r/v_s|^\delta} \tag{5.42}$$

The corresponding friction function for pure lateral motion is expressed as:

$$g_{y0}(v_r) = G_y g_{x0}(v_r) \tag{5.43}$$

Resulting, the sliding friction function for combined longitudinal and lateral motion is defined as:

$$g(v_r) = \left(1 + \frac{G_y - 1}{\pi/2}\beta\right) g_{x0}(v_r) = \left(1 + \frac{G_y - 1}{\pi/2}\beta\right) \left[F_C + (F_S - F_C)e^{-|v_r/v_s|^\delta}\right] \tag{5.44}$$

The introduction of the modal parameter G_y provides independent tuning of high-slip (sliding) and low-slip (adhesion) parts of pure braking/cornering tyre curves.

The model is validated with respect to the Magic Formula Tyre model by Deur. It turned out that the prediction error of the self aligning torque was larger than the corresponding error of prediction of the longitudinal and lateral force curves [16]. Therefore, an empirical extension of the model is introduced by Deur to improve the self aligning torque accuracy. According to Deur the accuracy of the self-aligning torque static curves can be increased by using a slip-dependent right margin of the trapezoidal normal pressure distribution $r_r(\alpha)$. The curve $r_r(\alpha)$ can be interpolated by using a curve based on the "Magic Formula" form of Pacejka and is defined as:

$$r_r(\alpha) = D\sin(C\arctan((1-E)B|\alpha| + E\arctan(B|\alpha|))) + S_v(F_z) \tag{5.45}$$

The aligning torque model is validated by Deur and introduction of the variable margin r_r improves the shape of the curves and the accuracy of the peak value. However, the accuracy of the self aligning torque model is still significantly lower than the accuracy of the force model. The LuGre tyre model parameter identification is based on experimental results. However, in these results no proportional relation between M_z and F_z is included. Therefore, it is proposed by Deur to scale the self aligning torque relation (5.27) by an empirical factor ϕ with a dependency on the normal force F_z included.

The change of road condition (dry asphalt, wet asphalt, snow, ice) influences the parameters F_C and F_S of the sliding friction function $g(v_r)$, see (5.5). The road condition is characterised by a single parameter μ_{sl} which scales the nominal sliding friction function $g_0(v_r)$ valid for dry asphalt conditions [8]. Typical values of the road condition coefficient μ_{sl} are 1.0, 0.6, 0.2, 0.1, for dry asphalt, wet asphalt, snow, and ice, respectively.

The low-slip (adhesion) parts of the tyre curves are not influenced by the friction coefficients F_C and F_S, this can be seen in (5.37). According to Deur experimental results have shown that the low-slip slope of the $F_x(s)$ curve and the $F_y(\alpha)$ curve depends on the road condition. In order to include this effect in the LuGre model, the stiffness coefficients $\sigma_{0x,y}$ are made linearly dependent on the road condition.

$$\sigma_{0x,y}(\mu_{sl}) = \mu_{sl}\sigma_{0x,y} \tag{5.46}$$

Experiments of the road condition dependency with the static model [16] shows that the road condition should be introduced in the model by scaling the total tyre friction functions $F_{x,y}$ and M_z by the road condition coefficient μ_{sl}, rather than scaling the sliding friction function $g(v_r)$ only.

According to Deur the low-slip slope of the $F_x(s)$ curve depends on the tyre road condition up to a certain sliding friction coefficient which is equal to approximately 0.3. That means that the slope is different for dry asphalt and ice/snow conditions, but not for dry and wet asphalt. In this case, the following saturated road condition-dependence of the tyre stiffness coefficients is more appropriate than the linear dependence.

$$\sigma_{0x,y}(\mu_{sl}) = \left(1 - e^{-\mu_{sl}/0.3}\right)\sigma_{0x,y} \tag{5.47}$$

The distributed dynamic tyre model created for this thesis is extended with the defined physical and empirical extensions. The final static model defined in (5.33), (5.34) with the extensions included, results in:

$$\begin{aligned} F_{x,y} &= \mu_{sl} \cdot F_{x,y} \\ M_z &= \mu_{sl} \cdot M_z \\ M_z &= \phi \cdot M_z \end{aligned} \tag{5.48}$$

5.4 Optimisation of the tyre parameters

In this section an optimisation routine is described that minimise the error between the dynamic tyre friction model and the measurement results of the reference tyre. This measurement data is also used to validate the other tyre models in this thesis, see appendix A. Deur introduced a set of tyre parameters that are highly dependent on different tyre-road conditions and have a dependency on the normal force. The set of tyre parameters are defined in the appendix of [16]. The tyre parameters defined by Deur are presented in table 5.1.

Tyre parameters:

$\sigma_{0x} = p.kx1 \cdot F_z$	longitudinal stiffness coefficient [N/m]
$\sigma_{0y} = p.ky1 \cdot F_z^2 + p.ky2 \cdot F_z + p.ky3$	lateral stiffness coefficient [N/m]
$\mu_c = p.muc1 \cdot F_z + p.muc2$	Coulomb friction force [N]
$\mu_s = p.mus1 \cdot F_z + p.mus2$	Stribeck friction force [N]
$G_y = p.gy1 \cdot F_z^2 + p.gy2 \cdot F_z + p.gy3$	model parameter [-]
$L = p.pl1 + p.pl2 \cdot \sqrt{F_z}$	length contact patch [m]
$v_s = p.vs$	stribeck velocity [m/s]
$\delta = p.delta$	stribeck parameter [-]
$\sigma_2 = p.sigma2$	viscous friction coefficient [Ns/m]
$r_l = p.rl$	left margin trapezoidal pressure distribution [-]
$B = p.B$	magic formula parameter [-]
$C = p.C$	magic formula parameter [-]
$D = p.D$	magic formula parameter [-]
$E = p.E$	magic formula parameter [-]
$S_v = p.sv1 \cdot F_z p.sv2$	vertical shift parameter magic formula [-]
$\phi = p.ph1 \cdot F_z^2 + p.ph2 \cdot F_z + p.ph3$	empirical scale factor aligning torque [-]
$\alpha_{\text{ply}} = p.alphaply$	plysteer equivalent slip angle [deg]

Table 5.1: Tyre parameters for the LuGre tyre friction model.

The tyre parameters are determined with a numerical optimisation routine, the direct search Nelder Mead simplex algorithm, with respect to the measurement data. The difference between the measured F&M data of the reference tyre and the LuGre tyre model output is minimised for pure longitudinal and lateral measurement data and also for combined slip measurements with three different vertical tyre loads. In the tyre model of LuGre no camber angle is defined, so the measurements performed with negative and positive camber angles are neglected in this optimisation routine.

The LuGre tyre model is minimised with the following error calculation:

$$\varepsilon = \sqrt{\frac{1}{n}\sum_{i=1}^{n}\left(\begin{array}{l}\lambda_{F_x}\left(\frac{F_{x,lugre}^2 - F_{x,measurement}^2}{F_{x,measurement}^2}\right) + \\ \lambda_{F_y}\left(\frac{F_{y,lugre}^2 - F_{y,measurement}^2}{F_{y,measurement}^2}\right) + \\ \lambda_{M_z}\left(\frac{M_{z,lugre}^2 - M_{z,measurement}^2}{M_{z,measurement}^2}\right)\end{array}\right)} \times 100\% \tag{5.49}$$

with n the number of calculated errors using the least square method of the F_x, F_y and M_z characteristics. The weighting factors λ_{F_x}, λ_{F_y} and λ_{M_z} are introduced to emphasise one of the three tyre characteristics when optimizing the tyre parameters. In the optimisation performed in this section and presented below, the weighting factors are set to one. This error calculation is used, while the tyre parameters are influenced by all the tyre characteristics. No tyre parameters are defined for pure slip

or the combined slip situation. In figure 5.7 an overview of the results of the force and moment characteristics of the LuGre tyre model is depicted. The errors depicted in this overview and in table 5.2 are calculated with the error calculation of (2.9) to give a good comparison with the other tyre models studied. The errors of the slip characteristics of the LuGre Tyre model from figure 5.7, are presented

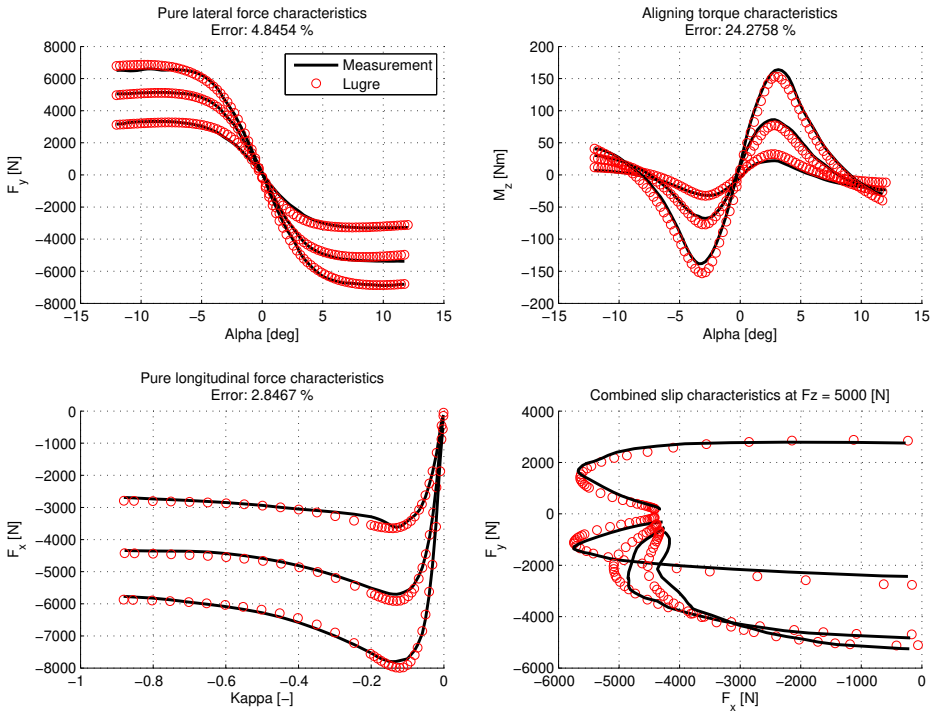

Figure 5.7: F&M fit results of the LuGre tyre model.

in table 5.2. With the optimisation routine the tyre parameters for the reference tyre are determined.

	ε_{LuGre} [%]	
	with camber	no camber
pure F_x	-	2.85
pure F_y	-	4.85
pure M_z	-	24.28
combined F_x	-	3.84
combined F_y	-	8.58
No. parameters	-	26

Table 5.2: Errors of the F&M characteristics of the LuGre Tyre model.

In table 5.3 the results of the optimisation are presented.

The results from figure 5.7 shows that the optimised LuGre tyre model with the non-uniform normal pressure distribution and interpolated tyre parameters, predicts quite similar pure braking and cornering tyre static curves as the measurement results. For the highest vertical load of $F_z = 7000$ N the LuGre tyre model shows a disagreement in the lateral force curve with respect to the measurement result. This phenomenon is also recognised by Deur and it should primarily be a consequence of certain inaccuracy of straight-line interpolation of the optimised coefficient of the level of stiction

Results of the optimised tyre parameters:

σ_{0x}	$= 2.303F_z \cdot 10^5$
σ_{0y}	$= (-0.165F_z^2 + 2.3157F_z + 1.9979) \cdot 10^5$
μ_c	$= -0.0226F_z + 0.9905$
μ_s	$= -0.0599F_z + 2.2884$
G_y	$= 0.0043F_z^2 - 0.0242F_z + 0.9208$
L	$= 0.156 + 0.050\sqrt{F_z}$
v_s	$= 2.5933$
δ	$= 0.9325$
σ_2	$= 0$
r_l	$= 0.1564$
B	$= 12.6552$
C	$= -8.7877$
D	$= 0.0305$
E	$= 0.5581$
S_v	$= -0.0054F_z + 0.7062$
ϕ	$= 0.0232F_z^2 + 0.0213F_z + 0.6917$
α_{ply}	$= 0.0015$

Table 5.3: Values optimised tyre parameters LuGre tyre model.

force $\mu_S(F_z)$ [16]. The longitudinal force curve shows a slight too high maximum force for the highest vertical load. The aligning torque curve shows good fit results with respect to the measurements. It should be noticed that the aligning torque relation, see (5.34), is scaled by an empirical factor ϕ, which is optimised as a function of the normal force F_z. The right margin of the trapezoidal pressure distribution $r_r(\alpha)$ is optimised for different normal forces and with an slip angle dependency. The "magic" formula, see (5.45), is used for this purpose. The results with this optimised functions included shows a good improvement of the shape of the curves and the accuracy of the peak values in comparison with the results of the LuGre dynamic tyre friction model without the empirical dependency [16].

In the combined slip characteristic, the combined longitudinal and lateral force curve is depicted for a vertical load of F_z = 5000 N. From the combined curve it can be concluded that the LuGre tyre model at high slip angles has some problems to give a good approximation of the maximum friction levels. The LuGre tyre model shows a slightly higher friction level at these slip angles.

Overall it can be concluded that the LuGre tyre friction model as proposed by Deur shows promising results for the steady-state tyre behaviour. However, an important note on this is, that there are still tyre parameters needed that are numerical optimised with respect to measurement data. Especially, to give a good approximation of the aligning torque curves empirical scale factors are needed to reach a certain accuracy. So physical tyre models gives, till a certain level, a good approximation of the steady state tyre behaviour. However, to reach the same level of accuracy of the empirical tyre models nowadays, physical tyre models also need some empirical defined tyre parameters that are optimised with respect to the measurement data.

In the more recent research of Deur several tyre effects are investigated which have a large influence on the tyre behaviour. These effects, such as camber, turn-slip, conicity, ply-steer, etc., are also implemented in the LuGre dynamic tyre friction model and presented in the literature [11], [12] and [17]. These extensions are not implemented in the model created for this thesis.

5.5 Conclusions of the dynamic tyre friction model

In this chapter the second physical tyre model, the dynamic tyre friction model, is studied and described. First the basic principle of the LuGre friction model is treated. Subsequently, the implementation of the LuGre friction model in a dynamic tyre model, as proposed by Deur, is described. The

model that describes combined longitudinal and lateral motion is created based on the documentation found in the literature. With this model an parameter identification is carried out and a comparison study with the measurement results of the reference tyre is performed. From these results, the following conclusions can be drawn.

- The model validation has shown that the LuGre tyre model with an asymmetric non-uniform normal pressure distribution over the tyre/road contact patch shows reasonable accurate static behaviour of the longitudinal and lateral tyre forces.
- To give a better approximation of the self aligning torque behaviour, this relation is scaled by an empirical factor and the right-margin of the trapezoidal pressure distribution is described with an equation based on the "magic" formula.
- The tyre parameters need a normal force dependency to give a good approximation of the measurement results for different vertical loads.
- Overall the dynamic tyre friction model based on the LuGre friction model gives promising results for the steady-state tyre behavior. However, physical tyre models still need tyre parameters that are optimised with respect to measurements to reach the same level of accuracy of empirical tyre models. Only the number of model parameters needed for the optimisation are smaller than for instance the number of parameters of the Magic Formula Tyre model.
- In the more recent research the LuGre tyre model is extended with important tyre effects, such as camber, turn-slip, conicity, ply-steer and more. However, these extensions are not implemented in the model created for this thesis. The implementation of these effects should be studied and the influence on the tyre characteristics described by the dynamic tyre friction model should be investigated.

Chapter 6

Comparison and extrapolation qualities of the tyre models

In the previous chapters the tyre models studied during this thesis are described. In this chapter the tyre models are compared based on the fit results and the extrapolating qualities of the tyre models are investigated. The extrapolation qualities are analysed by adjusting the forward velocity and the friction levels. For these two situations no measurement data is available and a relative comparison between the results of the different tyre models is carried out. The comparison is not only based on the results of the tyre models, also on information found in literature. In the last section a prospective view on tyre modelling in the future is described.

6.1 Comparison of the tyre models based on the fit results

In this first section of the comparison, the different tyre models are compared based on the fit results presented in the previous chapters. In table 6.1 an overview of the fit errors of the different tyre models is shown. The tyre models which include a camber dependency, are optimised with and without a camber angle. When the fit errors of the tyre models are compared, it can be concluded that the Magic

No camber	ε_{MFtyre} [%]	ε_{TMeasy} [%]	$\varepsilon_{TreadSim}$ [%]	ε_{LuGre} [%]
pure F_x	1.18	1.35	4.46	2.85
pure F_y	1.33	2.12	4.50	4.85
pure M_z	7.02	17.20	25.29	24.28
combined F_x	2.56	7.12	6.33	3.84
combined F_y	3.84	20.71	12.12	8.58
No. parameters	63	26	14	26
With camber	ε_{MFtyre} [%]	ε_{TMeasy} [%]	$\varepsilon_{TreadSim}$ [%]	ε_{LuGre} [%]
pure F_x	1.74	2.03	5.26	-
pure F_y	1.48	2.79	5.38	-
pure M_z	10.03	20.18	26.23	-
combined F_x	2.63	7.36	5.99	-
combined F_y	4.46	20.94	16.02	-
No. parameters	91	26	14	-

Table 6.1: Errors of the optimisation results of the tyre models

Formula tyre model gives the best approximation of the steady-state tyre characteristics. To achieve this accuracy the Magic Formula has around twice the amount of tyre parameters defined to calculate

the steady-state tyre characteristics. To extend the Magic Formula with additional effects that influence the tyre behaviour, such as inflation pressure, velocity, temperature, surface friction dependency, the amount of tyre parameters will increase. The advantages of the Magic Formula are its accuracy and its low computational effort.

The second model that has a semi-empirical background, is the TMeasy tyre model. The mathematical function to calculate the forces is divided in three intervals and is defined by the characteristic parameters, to describe the longitudinal and lateral characteristics. From the fit results it can be concluded that the TMeasy model gives a reasonable approximation of the longitudinal and lateral force characteristic. However, the error of the aligning torque characteristic is greater and the TMeasy model has problems to give a good approximation of the combined slip characteristic. The maximum longitudinal force is generally too high for large slip angles. For smaller slip angles the model has problems to reach the maximum level of lateral force. This could be caused by the fact that the tyre parameters are defined as pure slip parameters and with these pure slip parameters the combined slip situation is described.

When the physical tyre models are considered it can be concluded that overall these models have larger fit errors with respect to the Magic Formula Tyre model. For the TreadSim tyre model it can be concluded that for higher vertical loads the model shows a lateral force characteristic where the cornering stiffness and the peak lateral friction coefficient differ from the measurement results. This could be the result of the poor approximation of the contact patch shape and the unrealistic normal pressure distribution. For the longitudinal force characteristic the slope of the locked wheel curve is steeper than the measurement data. The model has also problems to reach the maximum level of longitudinal force. From the combined slip situation it can be concluded that the TreadSim model has an overall to low peak longitudinal and lateral friction coefficient in comparison with the measurement data. It turned out that the model of de Hoogh realised a carcass deformation of approximately 0.5 m. Deformations of the carcass with this magnitude are not realistic and could be the result of an overall too low bending and lateral belt stiffness. In the optimisation routine the constraints of these both stiffnesses are adjusted, resulting in a carcass deformation of approximately 0.03 m and is a more realistic carcass deformation.

From the fit results of the LuGre dynamic tyre friction model, it can be concluded that the model gives a reasonable approximation of the steady-state tyre characteristics. The lateral force characteristic shows that, for high vertical loads, the LuGre model has problems to give an accurate approximation of the measurement data. The peak lateral friction coefficient is too high at these vertical loads. The cornering stiffness differs at low vertical loads with respect to the measurement data. The longitudinal force characteristic of the LuGre model is quite accurate. To give a good approximation of the aligning torque behaviour, an empirical scale factor for the aligning torque is introduced to improve the relation between the vertical load and the aligning torque. The accuracy of the aligning torque characteristic is increased by using a slip-dependent right margin of the trapezoidal normal pressure distribution. This curve is interpolated by using a "magic" formula based equation. The introduction of the variable margin improves the shape of the curves and the accuracy of the peak value. Furthermore, the tyre parameters need a normal force dependency to give a good approximation of the measurement results for different vertical loads. The combined slip approximation is more accurate than the results of the TreadSim tyre model.

Camber behaviour

In the lower part of table 6.1 the errors of the optimisation with camber influence included are presented. In the LuGre tyre model used for this thesis no camber behaviour is modelled. Therefore, no optimisation with respect to the camber measurements with the LuGre model is performed. From the fit errors with the camber measurements included, it can be concluded that overall the fit errors of the different tyre models show an increase for the pure slip characteristics. The optimised tyre parameters are adjusted to give an approximation of the camber behaviour, as a result the accuracy of the pure slip characteristic will decrease. From the fit results it can be concluded that the Magic Formula Tyre model again shows the smallest error for the pure and combined slip characteristics in comparison with the TMeasy and TreadSim tyre model.

In the previous chapters an overview of the camber behaviour on the lateral force and aligning torque characteristics for the different tyre models are presented. The approximation of the Magic Formula lateral steady-state characteristic is quite accurate for a camber angle of minus 5 and 5 degrees. The fit errors of the other two models are considerably larger in comparison with the measurement data. The TMeasy model shows a reasonable approximation, for both a positive and negative camber angle the peak lateral tyre force is slightly too high. The TreadSim tyre model has the largest fit errors in describing the camber behaviour. The cornering stiffness and the steady-state lateral force differs with respect to the measurement data.

From the aligning torque characteristics it can be concluded that the different tyre models has problems to give an accurate approximation of the camber behaviour on the self aligning torque curves. The fit error of the Magic Formula Tyre models is considerably smaller than the other tyre models. The only comment on the results is that the Magic Formula show a small deviation in the peak value of the aligning torque with respect to the measurement results. The TMeasy tyre model has a more inaccurate approximation of the aligning torque behaviour. The tyre model has problems to reach the same level of maximum torque for positive and negative camber angles. The measurements show a strong asymmetric behaviour, which is not recognised for the TMeasy tyre model. The TreadSim tyre model has also problems to give an accurate approximation of the maximum aligning torque levels.

6.2 Behaviour at different forward velocities

The next situation studied for this thesis, is a changing forward velocity for the different tyre models. In practice it is common that tyres are measured at one forward velocity, generally at a velocity of 60 km/h. Subsequently, the tyre parameters of the tyre models are optimised with respect to the measurements performed at this velocity. However, it is unknown if the tyre models optimised at this velocity gives a good approximation of the tyre behaviour at different velocities. This is an important matter when the tyre models are applied in full vehicle simulations to investigate the vehicle handling behaviour. In simulations with full vehicle models an alteration of the velocity will occur and thus it is important that tyre models gives an accurate description of the tyre forces in these situations. In the literature there is hardly any information available of the tyre behaviour at different velocities. To get more insight in the tyre behaviour in this situation, measurement data obtained from the TNO Tyre Test Trailer at different velocities is provided by TNO Automotive and measurement results at different velocities are found in the literature of Guo *et al.* [19]. In figures 6.1 and 6.2 the measurement results at different velocities from TNO are presented.

In figure 6.1 braking at 3 and 60 km/h is depicted, during this measurement the tyre was under a slip angle of minus two degrees. It is unknown under what conditions the measurements are performed, so the results should be interpreted with some caution, however it gives an indication of the tyre behaviour at different velocities. From the results it can be concluded that the peak longitudinal force will increase when the tyre is braked under a low velocity. The measurement data also shows that the slope of the locked wheel longitudinal force is straighter at lower velocities. The longitudinal slip stiffness of the measurement at 3 km/h is lower with respect to the measurement at 60 km/h.

The measurements performed by TNO Automotive contain also pure alpha sweep measurements at four different velocities. In figure 6.2 the results of these measurements for the lateral force and aligning torque characteristics are depicted. From these results it can be concluded that the maximum sliding lateral force shows a small increase at a descreasing velocity. For larger slip angles, the lateral force curve at high speeds shows a more decreasing tendency than that at low speeds. A decreasing velocity has no influence on the cornering stiffness. When the measurement results are observed, the characteristic at 3 km/h shows a wobbling behaviour in the cornering stiffness. This behaviour could be caused by a relaxation effect of the alpha sweep. The forward velocity of the tyre is very low and the velocity of the slip-angle sweep is unknown, thus it could be that the velocity of the slip-angle sweep is larger than the forward velocity and results in that relaxation effect that causes a wobbling in the cornering stiffness.

From the measured aligning torque characteristics it can be concluded that there is a slight increase in torque for an increasing velocity. There is no alteration of the aligning stiffness at lower velocities,

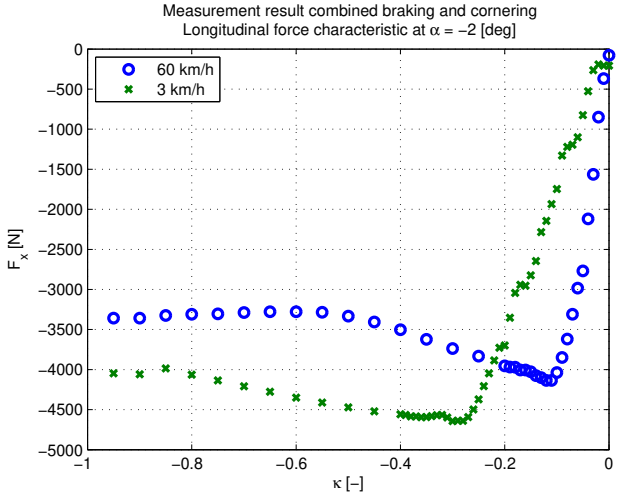

Figure 6.1: Measurement result of braking at different velocities.

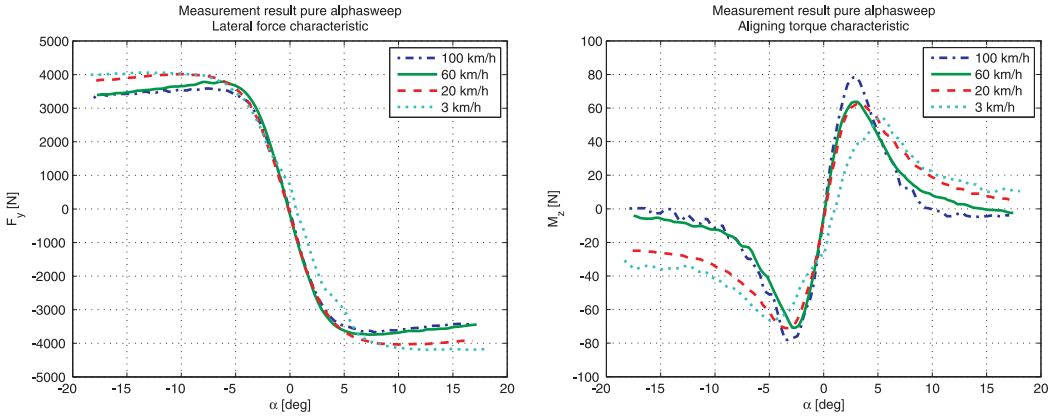

(a) (b)

Figure 6.2: Measurement results of alphasweeps performed at different velocities.

the strange wobble at 3 km/h can also be recognised in the aligning torque curve. At high speeds the aligning torque curve becomes negative at large slip angles as opposed to a positive aligning torque at low speeds.

With respect to the available measurement data and information found in literature, the tyre behaviour of the models at different velocities can be evaluated. In the two semi-empirical tyre models, the Magic Formula and TMeasy, no dependency of the forward velocity is included. This means that, if the tyre model parameters are derived according to merely one single speed, significant differences may occur for vehicle dynamic simulations. The optimised tyre parameters with this pre-defined velocity are not entirely valid for a situation where the vehicle is driving with a different velocity. So measurements performed with different velocities are needed to describe the influence of this effect for these models. The results of the semi-empirical tyre models will be shown, however, this will result in similar tyre characteristics at different velocities. In the figures 6.3,6.4 and 6.5 an overview of the influence of different velocities $V_x = 5, 20, 60, 100$ [km/h] on the tyre characteristics for pure kappa and alpha sweeps is depicted. In this overview the vertical load on the tyre is $F_z = 5000$ [N].

A disadvantage of the semi-empirical tyre models as a result of the missing velocity dependency, is if the models are applied in full vehicle models for vehicle handling analysis. In vehicle dynamic simulations with a changing velocity the output of the tyre forces and moments will not change and

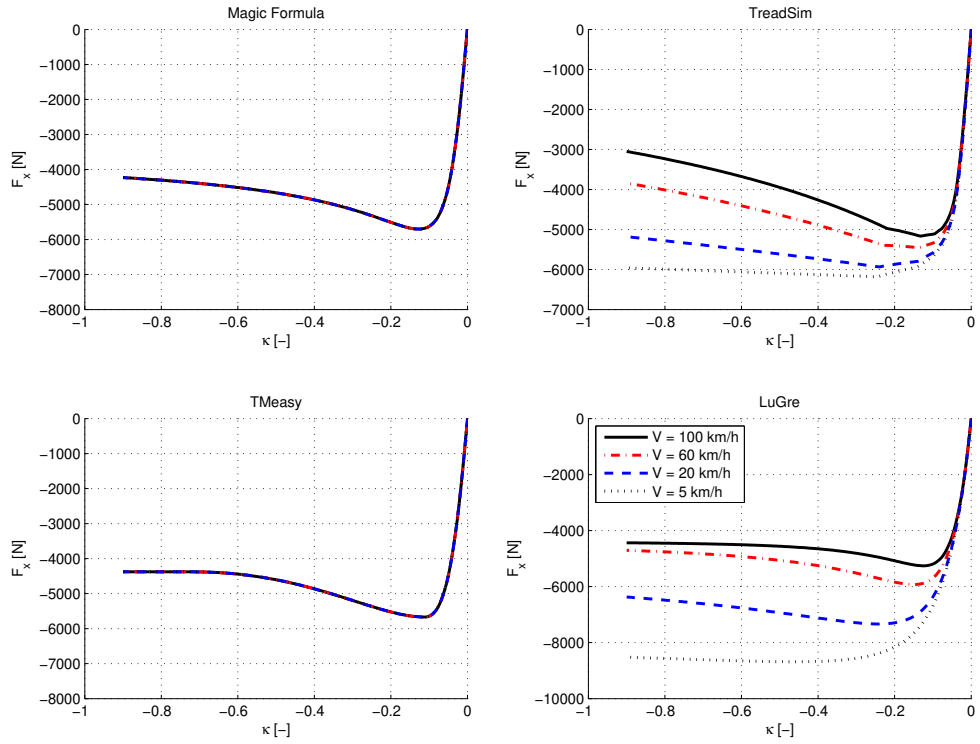

Figure 6.3: Tyre longitudinal force characteristic for different velocities.

significant differences may occur in these situations.

For the physical tyre models it is clear to see that the variation in the velocity has the largest influence on the longitudinal tyre force characteristic. For a decreasing velocity the longitudinal sliding friction coefficient increases for the tyre models. The LuGre tyre model shows the largest increase in longitudinal sliding friction coefficient and also the maximum peak value of the longitudinal force shows a large increase for driving with a low velocity. The TreadSim tyre model shows approximately the same level of peak longitudinal force for different velocities. For very low velocities the slope of the locked wheel longitudinal force curve becomes straight, there is almost no decrease of the longitudinal force for braking in the situation of a low forward velocity.

In comparison with the tyre behaviour observed from the measurement data of TNO the following conclusions can be drawn. The increase in longitudinal force of the LuGre tyre model in comparison with the measured curves is very large. The increase in longitudinal force produced by the TreadSim tyre model is more in proportion with the measurement data. From the measured curves it seems to be that the longitudinal tyre stiffness decreases for a lower velocity, to give a good conclusion on this behaviour more measurements at different velocities need to be performed.

From the measured lateral tyre force curves it can be concluded that there is a small increase in maximum lateral force and for low velocities there is no decrease in lateral tyre force for an increasing lateral slip angle. The results of the physical tyre models correspond with this observed tyre behaviour. However, the LuGre tyre model shows an increase in lateral tyre forces that is larger than the observed tyre behaviour in the measurements. The lateral tyre behaviour of the TreadSim tyre model corresponds better with the observed behaviour. From the measurements it can be concluded that a decreasing velocity has no influence on the cornering stiffness. Corresponding with the longitudinal characteristics, the physical tyre models do not show an alteration in stiffness with a changing velocity.

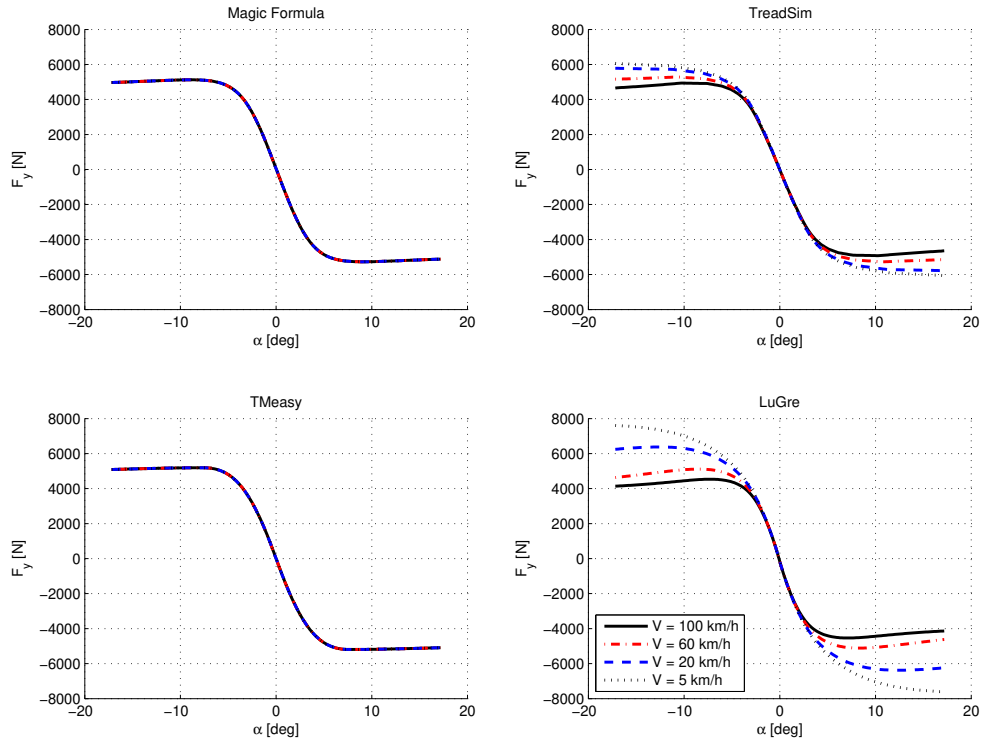

Figure 6.4: Tyre lateral force characteristic for different velocities.

From the measured aligning torque characteristics it can be concluded that there is a small increase in torque for increasing velocity. The opposite behaviour can be observed in the results of the physical tyre models. In the characteristics of the physical tyre models it can be seen that a decreasing velocity causes a small increase in the aligning torque. For changing velocity there is no alteration in the aligning stiffness of the physical tyre models, this behaviour is also observed in the measurements.

In a study of K. Guo *et al.* [19] the influence of the velocity on the tyre behaviour is also investigated. An important conclusion of that investigation is, that the speed dependences are mainly due to friction as a function of the sliding speed. The phenomena that the saturated lateral force increased at large slip angles at very low travelling speeds and decreased at high speeds arise because the friction coefficient is a function of the sliding speed with a peak value at low sliding speeds. The reason that the alignment moment varies with the travelling speed at large slip angles is that the friction coefficient is distributed unevenly over the contact patch [19].

It can be concluded that the physical tyre models give a reasonable description of the tyre behaviour at changing velocities. There is not a lot of measurement data at different velocities available, thus it is difficult to give an accurate statement of the behaviour shown by the tyre models. However, with the measurement data presented here, the tyre behaviour of the TreadSim tyre model corresponds quite well with the observed tyre behaviour. The influence of the velocity on the tyre behaviour of the LuGre tyre model seems to be too large in comparison to the measurement results.

6.3 Tyre behaviour for different friction levels

The last situation investigated in this chapter is the study of the tyre behaviour for different friction levels. The tyre models are studied for three different situations, namely friction levels approximately

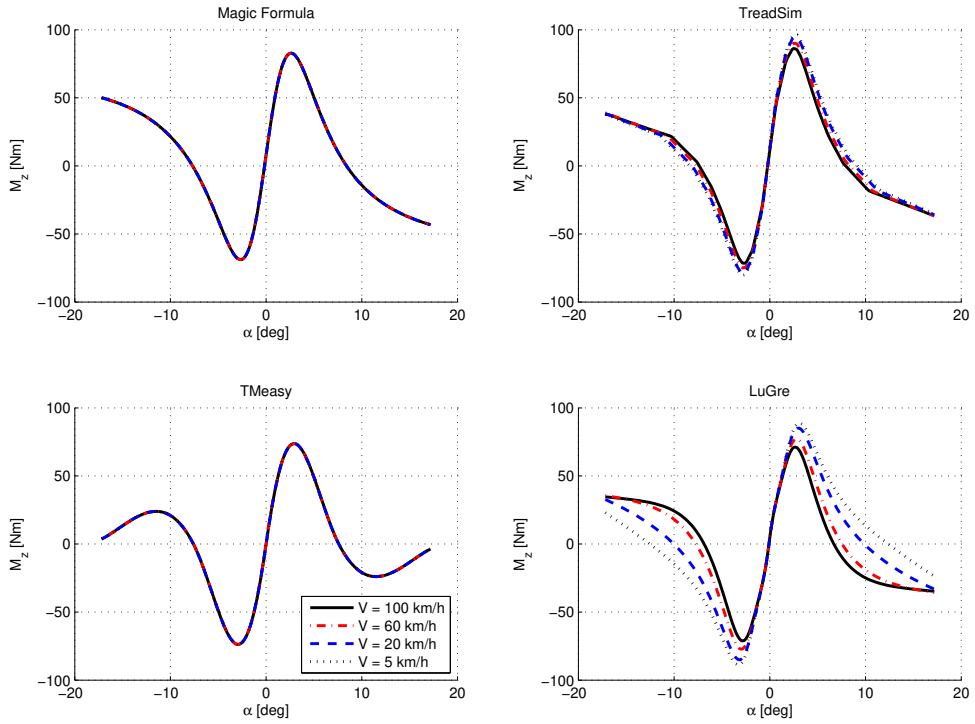

Figure 6.5: Tyre aligning torque characteristic for different velocities.

corresponding with dry asphalt, wet asphalt and snow. The friction levels chosen for these situations are $\mu = 0.2, 0.6, 1.0$. The vertical load on the tyre for these three situation corresponds with $F_z = 5000$ [N]. The tyre parameters optimised with the measurement data are used. For the investigation of the tyre behaviour for different friction levels, the friction coefficient is adjusted in the tyre models.

In the tyre models the influence of the friction coefficient on the tyre behaviour are modelled in different ways. For the different tyre models, these methods will be described. In the Magic Formula Tyre model the friction coefficient is described as:

$$\mu_y = (p_{Dy1} + p_{Dy2} df_z) \cdot (1 - p_{Dy3}\gamma^2) \cdot \lambda_{\mu y} \qquad (> 0) \tag{6.1}$$

where p_{Dy1} is the lateral friction coefficient. The other two coefficients p_{Dy2}, p_{Dy3} are dependent of the friction on the load and camber respectively. Subsequently, a friction scaling coefficient $\lambda_{\mu y}$ is introduced influencing the variable D of the magic formula, see figure 2.1. Thus, the friction scaling coefficient has influence on the peak value of the lateral force. The same method is applied to adjust the longitudinal force characteristic.

The tyre characteristics of the TMeasy tyre model are valid for one specific tyre road combination only. If the coefficient of friction is changed an adaption of the tyre parameters of the given model is proposed. In the TMeasy tyre model the maximum and the sliding force are influenced by a changing friction scaling coefficient. The tyre parameters are scaled as:

$$s^M \rightarrow \frac{\mu_L}{\mu_0} s^M \quad , F^M \rightarrow \frac{\mu_L}{\mu_0} F^M \quad , s^S \rightarrow \frac{\mu_L}{\mu_0} s^S \quad , F^S \rightarrow \frac{\mu_L}{\mu_0} F^S \tag{6.2}$$

where the fraction $\frac{\mu_L}{\mu_0}$ corresponds with the scaling coefficient for different friction levels.

In the TreadSim tyre model the velocity depended empirical formulation for the friction of rubber

compounds, known as the Savkoor friction law, is applied and defined as:

$$\mu_d(\upsilon) = \left(\frac{p}{p_0}\right)^{-k} \frac{\mu_0}{1 + a_\mu ||V_b||} \tag{6.3}$$

where p_0 is the reference contact pressure, k the pressure exponential factor, μ_0 the starting friction coefficient (assumed to be equal to the static friction coefficient), a_μ the speed parameter and V_b the sliding velocity of the base point of the tread. This friction model is fit on experiments done with tread rubber friction on abrasive paper subjected to different contact pressures and velocities. For the study of the influence of different friction levels on the tyre characteristics, the static friction coefficient μ_0 is adjusted with the scaling coefficients.

In the LuGre tyre model the road condition is characterised by a single scaling parameters μ_{sl} and this parameter influences the parameters μ_C and μ_S of the sliding friction function $g(v_r)$, see (5.23). These parameters are defined as the Coulomb friction force and the Stribeck friction force respectively. According to Deur, experiments has shown that the low-slip slope of the longitudinal and lateral tyre force depends on the road condition [33]. In the model of Deur the friction scaling coefficients are included as scaling parameters of the stiffness coefficients $\sigma_{0,x,y}$. Deur also concluded that the road condition should be introduced by scaling the total tyre friction functions $F_{x,y}$ and M_z by the friction scaling coefficients, rather than scaling the sliding friction function $g(v_r)$ only [16]. In other experiments it has been shown that the low-slip slope of the longitudinal force curve depends on the tyre road condition only up to a certain sliding friction coefficient which is equal to approximately $\mu_{sl} \approx 0.3$. The slope is different for dry asphalt compared to driving on snow, but not for driving on wet asphalt. Therefore, the following saturated road condition dependence of the tyre stiffness coefficients is proposed:

$$\sigma_{0x,y}(\mu_{sl}) = \left(1 - e^{-\mu_{sl}/0.3}\right) \sigma_{0x,y} \tag{6.4}$$

For the tyre models studied in this thesis, the implementation of the road condition dependency is described. It can be seen that different approaches are used to implement this effect. In the next overview the results of the tyre behavior for different friction levels are presented. In figure 6.6 the longitudinal and lateral tyre characteristics for the friction level corresponding with a snow surface (μ = 0.2) are depicted. In this figure it is clear to see that the tyre models show distinguish friction behaviour with respect to each other. The LuGre tyre model shows a clear dependency on changing friction levels. In both the longitudinal and lateral force characteristic it is clear to see that the longitudinal and cornering stiffness and the magnitude of the maximum force has a strong dependency on changing friction levels. This behaviour is not recognised in the other three tyre models (Magic Formula, TMeasy, TreadSim). These tyre models have a dependency on the friction level included, the tyre characteristics are scaled with a friction scale coefficient and that results in an alteration of the maximum forces. However, the friction level has not influence on the longitudinal and cornering stiffness, this seems mot an adequate representation of the real tyre behaviour.

In December 2002 a three year during European project was started called VERTEC. This project is defined as the Vehicle, Road, Tyre and Electronic Control Systems Interaction: Increasing vehicle active safety by means of a fully integrated model for behaviour prediction in potentially dangerous situations. This project is a cooperation of 10 partners based on experts in the field of road, vehicle, tyre and electronic dynamic vehicle control. In the literature of [24] an overview of the VERTEC project is given. An activity in this program was the friction prediction of tyres in presence of water, ice, snow and slush on pavement. Therefore, a lot of measurements on different surfaces with different test facilities are performed, such as the Nokian Friction measurement vehicle (NFMV), VTI Test vehicle BV12 (BV12) and the VTI Tyre test facility (TTF) and the MTS flat track (flat track) of Pirelli. The results of the tyre tests in this project are presented in [23]. In figure 6.7 the results of the different test facilities performed with a summer tyre of Pirelli, the Pirelli P7 205/60R15V, are depicted.

From these results it can be concluded that the three tyre models, Magic Formula, TMeasy and TreadSim, have a tyre behaviour that is different with respect to the results shown by the VERTEC project. This is due to the fact that the characteristics of these models are scaled with a parameter that

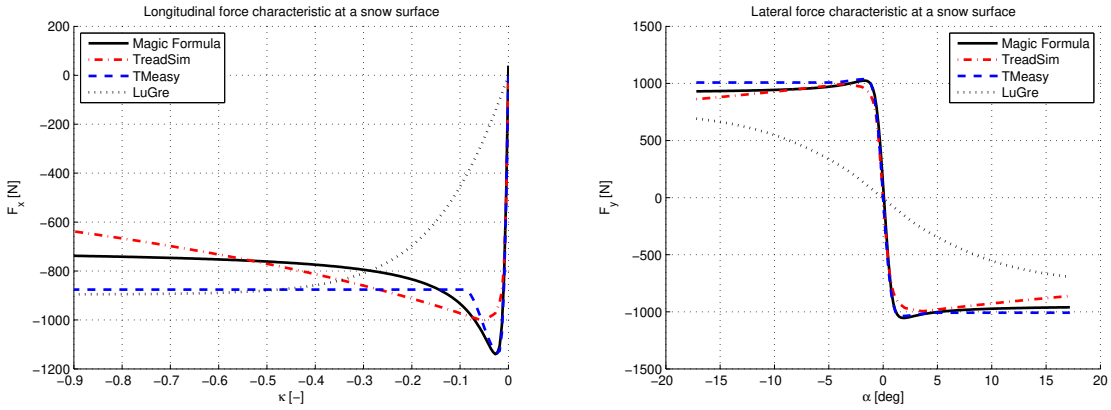

(a) (b)

Figure 6.6: Tyre force characteristics on friction level $\mu = 0.2$.

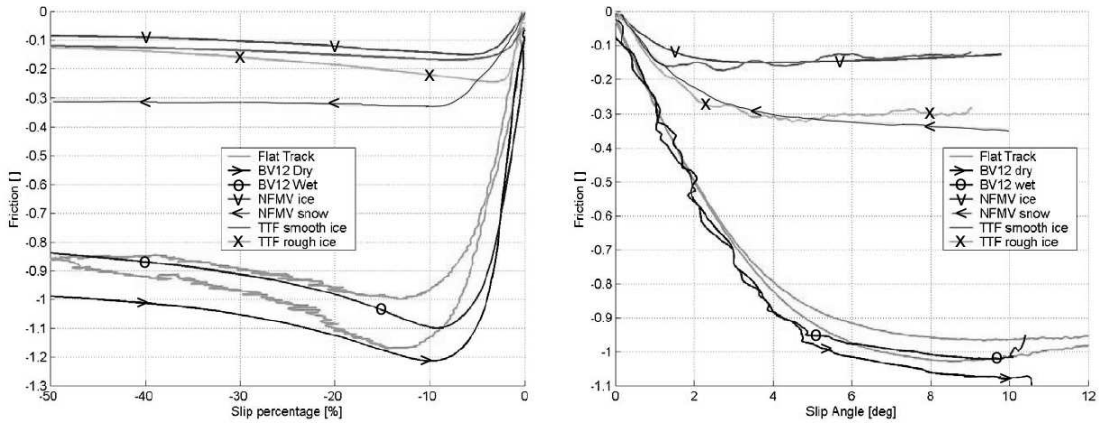

(a) (b)

Figure 6.7: VERTEC test results at different surfaces [23].

should represent the friction coefficient. However, it can be seen that during braking and cornering on snow and ice, the stiffnesses and magnitudes of the maximum forces change a lot. The LuGre tyre model shows a clear dependency on a changing friction level. In both characteristics it is clear to see that the longitudinal and cornering stiffness and the magnitude of the maximum force has a strong dependency on the changing friction coefficient. However, it should be noticed that the implementation of the friction level dependency in the LuGre model is not based on any physical behaviour. In agreement with the measurement results the influence on the cornering stiffness is larger than the observed behaviour in the measurements. Finally, from the measurement results it can also be concluded that the composition of the ground surface has a large influence on the tyre behaviour. For example, in figure 6.7b it can be seen that the lateral tyre force describes the same level of steady-state lateral force on rough ice as on snow.

In the figures 6.8, 6.9 and 6.10 the results of combined driving, braking and cornering experiments at different road surfaces and a vertical load of F_z = 5000 N are depicted.

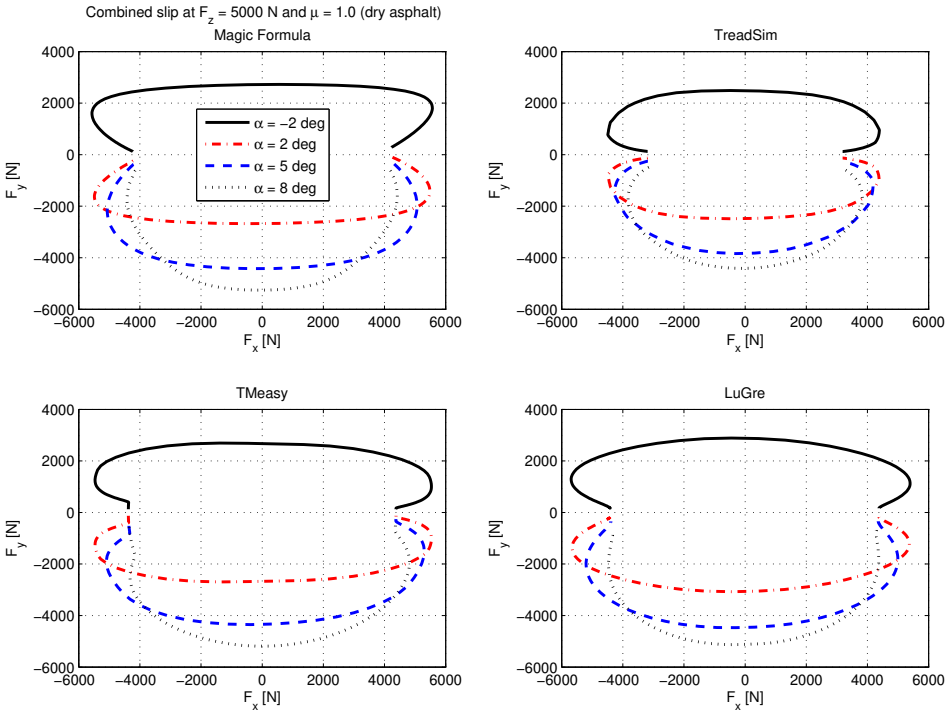

Figure 6.8: Combined driving, braking and cornering on surface corresponding with dry asphalt.

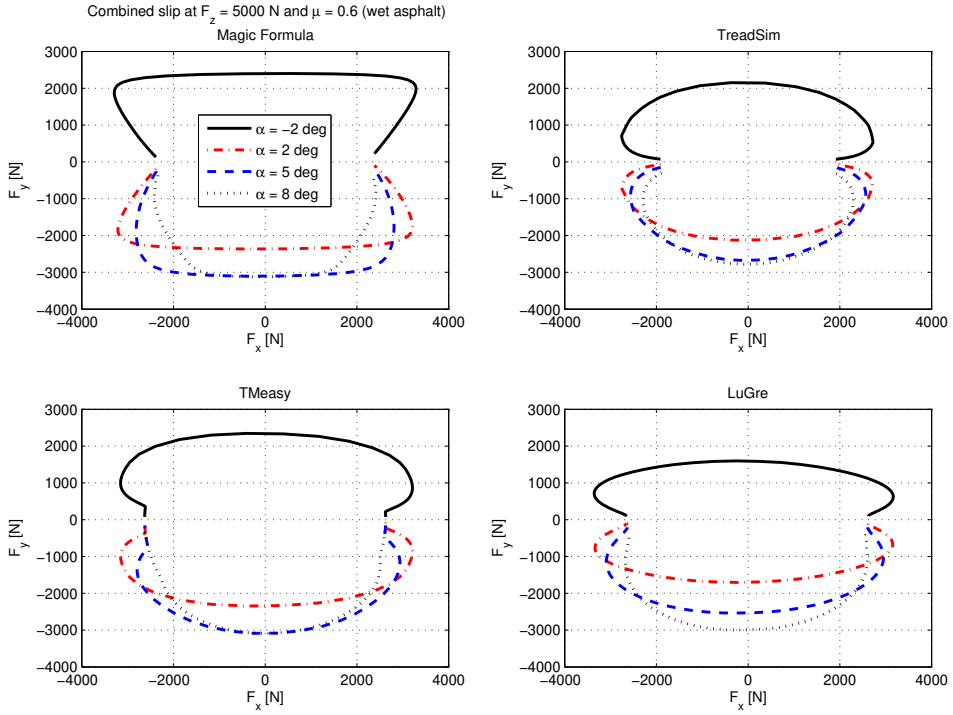

Figure 6.9: Combined driving, braking and cornering on surface corresponding with wet asphalt.

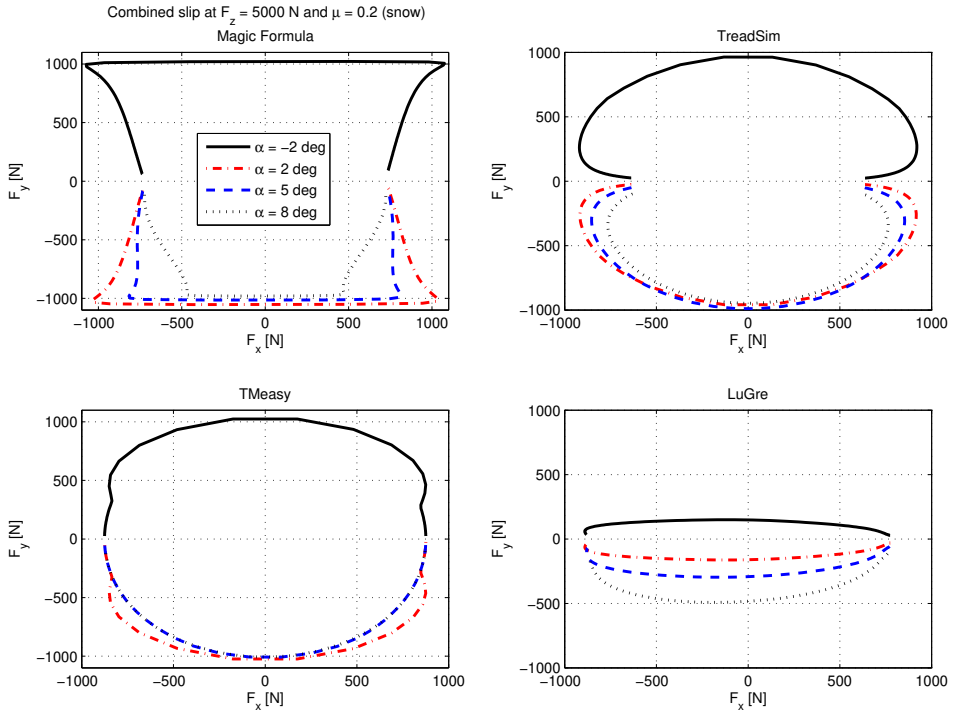

Figure 6.10: Combined driving, braking and cornering on surface corresponding with snow.

From these figures the development of the friction circles for combined driving, braking and cornering at different friction levels can be considered. From the results at dry asphalt it can be concluded that the tyre models show approximately the same tyre behaviour for the combined slip situation. The maximum longitudinal and lateral forces corresponds for the tyre models. When the friction level is changed to a wet surface or even snow, large changes occur in the tyre behaviour between the tyre models. When the situation of combined driving, braking and cornering on snow is considered, it is clear to see that the tyre models respond different on these changes.

The Magic Formula Tyre model shows an unrealistic representation of the tyre behaviour in the combined slip situation on wet asphalt and snow. In these situations so-called friction "squares" occurs. For the TMeasy and the TreadSim tyre model a clear decreasing of the maximum longitudinal and lateral forces can be seen. The LuGre tyre model shows the largest alteration for the combined slip situation on a wet or snow surface. The magnitude of the lateral force is lower at the friction levels corresponding with a wet and snow surface with respect to the other tyre models. Another effect that the LuGre model shows, is the increasing lateral force for an increasing slip angle, caused by the reduced cornering stiffness at lower friction levels.

From the experiments performed at different friction levels it can be concluded that the different tyre models show different tyre behaviour. It is difficult to give a conclusion on which tyre model gives the best approximation of the influence of the friction coefficient on the tyre behaviour. Not a lot of measurement data of measurements performed at snow/ice surfaces are available. However, it can be concluded that modelling the friction dependency in tyre models is difficult and using a simple scaling factor to account for surface differences is not an adequate representation of the real tyre behaviour. Especially the effect of the altering friction levels on the tyre stiffness and temperature is an important factor that influences the tyre behaviour and these effects are not included in any of these tyre models.

6.4 Prospective view on tyre modelling

During the past 20 years, enormous progress has been made in chassis engineering and vehicle driveability. Today's vehicles are significantly safer and at the same time more comfortable than cars in the past. The reasons for this progress can be found in the areas of the various electronic systems and the precise design and tuning by using modern analysis and simulation methods. This results in an increase of product quality and shorter development times. In this context, the significance of modelling and simulation of the tyre behaviour becomes increasingly important. As the link between the vehicle and the road, the tyre ultimately determines the driving characteristics that can be realised and is an important factor for the ride comfort. Due to the constantly increase of computer power tyre modelling will become more important, while modelling is a lot faster and inexpensive than real-time testing. As a result of the increase in computer power, more complex vehicle models can be realised for describing the vehicle behaviour. Therefore, also tyre models are needed that give an accurate approximation of the steady-state force and moment characteristics. With that in mind and the knowledge of the different types of tyre models acquired during this thesis, the following subjects will be treated:

- Classification of the tyre models for a wide range of applications.
- Improvement and extension of tyre measurements and parameterisation.
- Proposal of possible improvements of the existing tyre models.
- Demands with respect to a potential new tyre model.

Classification of tyre models for vehicle dynamic simulations

In the literature of Ammon [2] typical issues of chassis and vehicle dynamics system design are presented and from that the resulting requirements for tyre modelling and simulation are defined. An overview of the fields of application of tyre simulation is given and further outlined here.

Given the great variety of applications, the question arises of how many different tyre models are required in order to cover all the applications. The fields of application that can be thought of are: vehicle dynamics analysis, driving comfort analysis, durability, safety system design, suspension and steering development, etc. Looking at this wide range of applications, an universal tyre model should be accessible as a dynamic three-dimensional force element, cope with contact calculations with a stationary or moving road surface independently and represent the following application conditions realistically [2]:

- wheel loads between 0 and 3 times the reference wheel load.
- frequencies between 0 and 30 Hz (or up to 150 Hz).
- speeds up to +250 km/h.
- longitudinal slip and side slip angle up 25% $\deg^{-1}$.
- camber angle up to 15°.
- road surface unevenness and changing friction coefficient.

Available tyre models are fulfilling these requirements to a higher or lower degree. However, it is quite difficult to evaluate the quality of the results without extensive expert knowledge and experience in tyre simulation. On the basis of the model complexity or model design, three to four model categories can be distinguished in the main. These categories are depicted in figure 6.11.

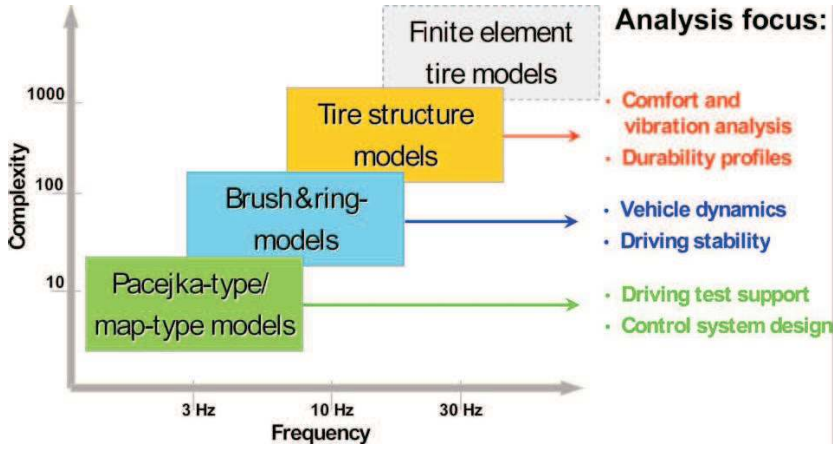

Figure 6.11: Classification of tyre models and main fields of application [2]

It is clear to see that different kind of tyre models are suitable for different fields op application. In this thesis the semi-empirical and physical tyre models are investigated for steady-state vehicle handling analysis. However, these models are also the basis for the Brush and Ring models, as an example, the Magic Formula is the basis of the dynamic tyre model SWIFT, that is used in dynamic analysis. So it is important that the steady-state tyre models gives an accurate description of the tyre forces and moments in changing driving conditions for application in dynamic tyre models. With the increasing computational efficiency the physical tyre models will become more interesting for use in vehicle handling analysis. It is also clear to see that the complexity of Finite Element Models is much larger with respect to the other categories. The use of a FEM-model as a tyre model for vehicle handling analysis is quite difficult, while the computational time will extensively increase due to the complexity of these models. However, the accuracy of a brush model can be improved by including some elements derived from FEM-models, such as the normal pressure distribution and the contact patch deformations. Furthermore, the FEM-models are especially suitable for the investigation of tyre-road noise and stress analysis of the tyre structure.

Improvement and extension of tyre measurements and parameterisation

Tyre models need to be parameterised with measurements performed on special tyre test rigs under reproducible conditions in order to determine the required tyre properties. In this thesis it becomes clear that the structure of the measurement program, see table A.2 in appendix A, provided for the parameterisation of the tyre models, was insufficient to investigate the different extrapolation qualities of the different tyre models. Globally, when sufficient test rigs are available, the following type of measurements should be performed:

- steady-state behaviour
  - steady-state forces and moments
  - vertical stiffness
- dynamics of tyre force generation
  - longitudinal and lateral stiffness experiments
  - transient longitudinal and side slip excitations
- transmission response to road surface excitations
  - enveloping behaviour
  - single obstacle or vertical step excitations
  - durability test excitations
  - measurements of structural stiffness and damping

From this global representation of the different types of measurements, it can be seen that tyre measurements are as complex as tyre modelling. First of all the necessary test rigs need to be available in house, which can be very expensive to have measurement equipment for all these categories. It is important that these measurement are performed with high accuracy, to exclude that procedural preconditioning effects influences the measurements.

The measurement data provided for this thesis was obtained from the TNO Tyre Test Trailer. These measurements are performed with a specific procedure defined by TNO, see appendix A. With this Test Trailer the steady-state forces and moments, transient longitudinal and side slip excitations are usually performed at test tracks. The several stiffness experiments and the enveloping behaviour can be performed at the Flat Plank Tyre Tester, which is available at Eindhoven University of Technology. The following recommendations can be considered:

- Now measurements are usually performed at 60 km/h. Extend the measurement program for a wide range of velocities, so the tyre behaviour at these velocities can be investigated. Subsequently, when this data is available it can be investigated if the tyre models represent accurate tyre behaviour at different velocities.
- Measurements are usually performed at dry asphalt, however, it is important to study the tyre behavior at wet asphalt and even snow and ice surfaces. A normal summer tyre can experience all these kind of situations when mounted under a vehicle. With this type of measurements it is also possible to investigate the dynamic friction properties of the tyre models and if the models represent physical correct behaviour in these circumstances.
- In most tyre models no dependency of the inflation pressure is modelled. It is a very common situation that people forget to inflate the tyres of a vehicle on a regular basis, which results in slightly deflated tyres with respect to the nominal inflation pressure. A changing inflation pressure causes an alteration of the contact patch and it has influence on the forces and stiffnesses of the tyre. So it is important that measurements at different inflation pressures are performed to investigate this behaviour. In the research of I. op het Veld (2007) [27] the inflation pressure dependency is investigated and the Magic Formula Tyre model (i.e. MF-Swift) is extended with the inflation pressure dependency.

- In the physical tyre models many tyre parameters need to be optimised with respect to the measurement data. It is possible that these optimised tyre parameters results in physical incorrect data. Therefore, it would be desirable to obtain the relevant tyre properties directly from the tyre manufacturers. However, this requires generally known and accepted standards for tyre simulation which are not yet available. Thus it is recommended that, especially for the physical tyre models, the relevant tyre properties are measured with the available test rigs.

The measurement data is used to perform the parameterisation of the tyre models. In general, a quantity of 10-100 scalar parameters need to be determined to approximate the relevant tyre properties. In table 6.1 the exact numbers necessary for describing the steady-state characteristics are presented. For the semi-empirical tyre models the description of forces and moments relies also on measured and observed force-slip characteristics. However, in this thesis it was also observed that the physical tyre models (TreadSim and Deur) still have some parameters that need to be optimised with respect to the measurement data. These parameters are physical defined parameters, such as the tread stiffness, carcass stiffness, friction parameters and parameters for the normal pressure distribution. The optimisation of the tyre parameters is performed with numerical optimisation techniques. These techniques minimise the error between the measured and the described forces and moments characteristics. It is possible that the optimised values for the tyre parameters results in physical incorrect data. So it would be desirable to obtain the relevant tyre properties directly from the tyre manufacturer. However, this requires generally known and accepted standards for tyre simulation which are not yet available [2]. So it is recommended that, especially for the physical tyre models, the relevant tyre quantities are measured with the available test rigs and not determined through optimisation.

Possible improvements of the existing models

After the study of the different tyre models it can be remarked that in the existing tyre models various assumptions are usually adopted:

- In semi-empirical tyre models no dependency on changing environmental conditions are included. The tyre parameters are usually derived for one condition, when these tyre models are applied in vehicle dynamic simulations significant differences may occur.
- In the physical tyre models the following assumptions are usually adopted. The friction coefficient is constant over de entire contact patch. The normal pressure distribution is normally approximated by a simplified pressure distribution in longitudinal direction, such as a trapezoid or an inverted boat-shaped distribution. In lateral direction the normal pressure is usually approximated by an uniform distribution. The deformation model of the carcass is assumed to be parabolic or a combination of three components; translational, bending and twisting. And the tyre contact patch is assumed to be rectangular and is not influenced by the presence of either a side force or a camber angle.

To improve the different tyre models studied in this thesis, the following improvements can be considered:

- Magic Formula:
  The Magic Formula gives very accurate descriptions of the steady-state tyre forces and moments characteristics for one exact measurement situation. A disadvantage is the large number of tyre parameters that need to be determined to give this accuracy of the tyre characteristics. The Magic Formula respond bad or not on changing environmental circumstances, such as velocity, friction, inflation pressure, temperature, etc. To include these effects in the Magic Formula, these different effects need to be investigated and then it is possible to extend the Magic Formula with these effects to improve the accuracy.
- TMeasy:
  The TMeasy tyre model is not as accurate as the Magic Formula Tyre model. The model requires less tyre parameters to describe the tyre characteristics. However, the tyre parameters are defined for pure longitudinal and pure lateral tyre characteristics. With these pure slip parameters

also the combined slip situation is described. This results in large errors of the combined slip situation because the optimisation routine only minimises the pure slip characteristic. To improve the model the description of the combined slip situation need to be improved. The TMeasy tyre model is a semi-empirical based tyre model and a dependency on changing environmental circumstances, such as velocity, friction, inflation pressure, etc. is not included. The model can be improved when these effects will be included.

- TreadSim:
  The TreadSim tyre model is thoroughly studied by de Hoogh and already improved at some points. The TreadSim model gives quite large fit errors with respect to the measurement data. To improve the description of the forces and moments the carcass deformation routine could be improved. The TreadSim model showed that the peak friction coefficients are generally too high at higher vertical loads. This could be improved by including an accurate contact patch shape and deformation and a more accurate normal pressure distribution. Studies after the normal pressure distribution and knowledge acquired from FEM-models shows that the inverted boat-shape pressure distribution is a poor approximation. This can be improved by including a finite element carcass model that is able to generate contact patch shapes and pressure distributions. At the moment the important tyre properties of the model are determined with numeric optimisation. It could be considered to validate the TreadSim model by directly measuring the tyre properties.

- LuGre:
  The LuGre tyre model uses the deformation of the bristles and a friction law to describe the forces and moments characteristics. The model built for this thesis is the static distributed tyre model, this is the linearised form that describes the deformation of the bristles over a certain length of the contact patch. The results of the LuGre model gives reasonable fits of the measured forces and moments characteristics. Improvements of the model that can be considered are to improve the contact patch shape and deformation and improving the applied trapezoidal normal pressure distribution. It can be considered to connect the LuGre tyre model to a rigid ring model or a flexible carcass, also to improve the dynamic tyre behaviour. The same recommendation formulated for TreadSim also counts for the LuGre tyre model, that the tyre properties are optimised with a numeric routine. It should be better if these tyre properties were measured directly and implemented in the model. Finally, the model built for this thesis is the 3D brush-type dynamic tyre friction model based on the literature of Deur. In the more recent research of Deur the LuGre model is already extended with tyre effects, such as camber, turn-slip, conicity, plysteer and more. The implementation of these effects should be studied and it has to be considered to implement these effects in the model created for this thesis.

Advantages and disadvantages of the tyre models:

In this study a distinction is made between physical and empirical tyre models. In the next overview a short list of the advantages and disadvantages of the model categories is given:

Advantages empirical models:

- High accuracy in describing the steady-state force and moment characteristics.
- Separate model parameters for every tyre characteristic.
- Result of the separate model parameters, fast parameter identification (fit).

Disadvantages empirical models:

- Difficult to extend the models with new effects, results in an increasing number of model parameters.
- The models have inaccurate extrapolation qualities.

Advantages Physical models:

- Less model parameters defined for describing the steady-state force and moment characteristics.
- The models have better extrapolation results.
- Physical models are more suitable to extend with new effects.

Disadvantages physical models:

- The model parameters have influence on all force and moment characteristics.
- Complexer parameter identification (fit), as a result of the influence of the model parameters on the force and moment characteristics.
- Poor assumptions in the models included to reduce the computational effort, results in larger fit errors.
- To improve the description of the steady-state force and moments characteristics, empirical elements are added in the models.
- The tyre width is not included in the physical models. Normally an uniform pressure distribution is assumed, while an asymmetric pressure distribution occurs under influence of a slip or camber angle.

Demands with respect to a potential new tyre model

As mentioned before, the tyre is the link between the vehicle and the road and ultimately determines the driving characteristics that can be realised and is an important factor for the ride comfort. It is expected that tyre modelling and simulation become more important for the development of vehicles. From this study it can be concluded that the traditional view on tyre modelling, see figure 1.2, is a bit outdated. Extra inputs are necessary to fulfill the high demands on tyre modelling in the future. Therefore, the following recommendations for different elements of a tyre model can be considered:

- It is important that a tyre model in the further is capable of dealing with various operating conditions, such as camber, velocity, inflation pressure, friction, temperature, durability, tyre wear, tyre noise, road condition etc. These effects are mostly nonlinear and difficult to implement in a tyre model. The complexity of the models will increase and these effects will probably causes an increase of the model parameters. Therefore, an extensive study after these types of operating conditions is necessary to get more insight of the tyre behaviour in these circumstances.
- To include the extra inputs in the semi-empirical models, an increase of model parameters is necessary. To extend the brush-type dynamic tyre models with extra operating conditions, the model complexity will increase and parameter identification (fit) becomes more difficult.
- In the current models the input of the road is neglected. It can be considered to define the road roughness as an extra input of a tyre model. A certain classification of the road condition should be defined that is implemented in describing the steady-state forces and moments.
- When an accurate brush-type tyre model is available, this tyre model should be connected with a rigid ring model or even a flexible carcass model to describe the dynamic tyre behaviour up to 100 Hz.
- It can be considered to describe the contact patch shape and deformations due to the appearances of a slip and camber angle, inflation pressure, etc. with elements of a tyre FEM-model. To use a complete tyre FEM-model in vehicle dynamics simulations for describing the steady-state tyre characteristics is too complex. However, if the deformations of the contact patch are described with a FEM-model the accuracy could increase.

- In the brush-type tyre models the normal contact pressure is approximated with an uniform or a non-uniform pressure distribution and assumed not to change in the presence of a slip or camber angle. However, the actual contact pressure distribution is considerably different even under static or free-rolling conditions. The tyre-road interaction during cornering or braking brings about the forward inclination of distribution and the backward shift of the whole contact patch against the steering axis [25]. A necessary improvement is to adapt the normal pressure distribution of the existing tyre models. An accurate normal pressure distribution generated by a FEM-model is depicted in figure (B.4) of Appendix B.
- In the future manufacturers of tyres have to cope with legislation on safety, CO_2 reduction (rolling resistance) and noise (exterior). It will become important that a tyre model in the future is capable of dealing with these kind of situations and can give accurate approximations of the tyre behaviour in these situations.

Chapter 7

Conclusions and recommendations

In this thesis different tyre models are investigated for studying the steady-state vehicle handling behaviour. To give a good description of the steady-state and dynamic behaviour of a vehicle, it is very important that a tyre model is available that gives an accurate description of the tyre forces and moments. The aim of this thesis is to make an overview of the selected existing tyre models that are available in literature. The selected tyre models are studied in detail and compared with each other. Based on the insight obtained by studying the various models, recommendations for an improved tyre handling model are given.

7.1 Conclusions

The following conclusions can be made concerning the different tyre models studied in this thesis.

- From the fit results it can be concluded that the Magic Formula tyre model gives the best approximation of the steady-state tyre characteristics. For both the optimization with and without camber influence, the magnitude of the fit errors is considerably smaller with respect to the other tyre models.
- From the optimization with camber influence included it can be concluded that in general the accuracy of the pure slip characteristics are influenced by a camber angle and the fit errors increases. The optimization routine needs to fit three curves at one vertical load with camber included and therefore the accuracy of the pure slip characteristic will decrease.
- It can be concluded that the physically oriented tyre models can not achieve the same accuracy as the semi-empirical based tyre models at the moment. In the physical tyre models some assumptions are made to decrease the computational effort. For example, the poor approximation of the normal pressure distribution, the rectangular shape of the contact patch, empirical formulae to improve the aligning torque behaviour, etc.

To get more insight in the qualities of the different tyre models two extrapolation situations are studied. The tyre models are studied for different forward velocities and the behaviour for different friction levels. The following conclusions on the velocity dependency can be drawn:

- It is common practice that tyres are measured at one forward velocity, generally at a velocity of 60 km/h. For different velocities hardly any information is available in literature or gathered from measurements. Therefore, it is difficult to get a clear insight in the tyre behaviour at different velocities.
- In the two semi-empirical tyre models, the Magic Formula and TMeasy, no dependency of the velocity is included. A reason that this dependency is not included in the Magic Formula Tyre

model is, the lack of information of the tyre behaviour at different velocities. If a clear dependency of the velocity on the tyre behaviour is proved, this dependency could have been included in the Magic Formula.

- A disadvantage of the semi-empirical tyre models in this situation is, if the models are applied in full vehicle models for vehicle handling analysis. In vehicle dynamic simulations with a changing velocity the output of the tyre forces and moments will not change and significant differences may occur in these situations.

- In comparison with the tyre behaviour observed from the measurement data it can be concluded that the influence of the velocity on the longitudinal and lateral tyre force characteristics of the LuGre tyre model is too large. The described tyre force characteristics of the TreadSim tyre model corresponds better with the observed measurement data.

- In the measurement results and the corresponding lateral force characteristics it is clear to see that the saturated lateral force increases at very low travelling speeds and decreases at high speeds. This phenomenon is investigated in a study of Guo *et al.*. According to [19] this phenomenon arise because the friction coefficient is a function of the sliding speed with a peak value at low sliding speeds.

The following conclusions can be considered for the investigation of the tyre behaviour for different friction levels:

- From the results it can be concluded that the three tyre models (Magic Formula, TMeasy, TreadSim) have a dependency on the friction level included. The tyre characteristics are scaled with a friction scale coefficient and that results in an alteration of the maximum forces. However, the friction level has not influence on the longitudinal and cornering stiffness, this seems not an adequate representation of the real tyre behaviour.

- The LuGre tyre model shows a clear dependency on changing friction levels. In both the longitudinal and lateral force characteristic it is clear to see that the longitudinal and cornering stiffness and the magnitude of the maximum force has a strong dependency on changing friction levels. A remark on this behaviour has to be made, because the implementation of the friction dependency is quite an empirical adaptation and the influence on the force characteristics is large with respect to the measurement results found in literature.

- When the combined slip situation is considered it can be concluded that the Magic Formula Tyre model shows an unrealistic representation of the tyre behaviour in the combined slip situation for low friction levels. In these situation so-called friction "squares" occurs. For the TMeasy and the TreadSim tyre model a clear decreasing of the maximum longitudinal and lateral forces can be seen. The LuGre tyre model shows the largest alteration for the combined slip situation on a wet or snow surface. The magnitude of the lateral force is lower at the friction levels corresponding with a wet and snow surface with respect to the other tyre models. Another effect that the LuGre model shows, is the increasing lateral force for an increasing slip angle, caused by the reduced cornering stiffness at lower friction levels.

- It is difficult to give a conclusion on which tyre model gives the best approximation of the influence of the friction coefficient on the tyre behaviour. Not a lot of measurement data of measurements performed at snow/ice surfaces are available. It can be concluded that modelling the friction dependency in tyre models is difficult and using a simple scaling factor to account for surface differences is not an adequate representation of the real tyre behaviour. Especially the effect of the altering friction levels on the tyre stiffness and temperature is an important factor that influences the tyre behaviour and these effects are not included in any of these tyre models.

In this study two model categories are studied, empirical and physical models. The following conclusions on the advantages and disadvantages can be drawn:

- During the study of the different tyre models it becomes clear that availability of the documentation of the different tyre models is necessary to give a good comparison between the models. The documentation of the TMeasy tyre model is insufficient to create an accurate model, some assumptions had to be made. The documentation of the Magic Formula Tyre model instead is complete to create an accurate model that represents the model very well. The documentation of the physical tyre models is sufficient to create the models. However, it is not described how the model parameters in these models are determined. In this study an optimisation routine is used to determine the different model parameters.
- The advantages of the empirical models are the high accuracy in describing the steady-state characteristics. Separate model parameters are defined for describing the force and moment characteristics. This results in fast parameter identification (fit).
- The disadvantages of the empirical models are the difficulty of extending the models with new operating conditions, while the number of model parameters will increase. And the empirical models have inaccurate extrapolation qualities.
- The advantages of physical models, are the smaller number of model parameters necessary for describing the steady-state force and moments characteristics. The physical models have better extrapolation qualities and are more suitable for extending with new operating conditions.
- The disadvantages of these models, are the influence of the model parameters on all force and moment characteristics. Therefore, a more complex parameter identification (fit) is necessary and that results in lower computational effort. To increase the computational effort, poor assumptions are included, which results in larger fit errors of the steady-state characteristics. To improve the fit results of the models, some empirical elements are included. However, this degrade the models to a more semi-physical behaviour.

7.2 Recommendations

After the study of the tyre models for steady-state vehicle handling analysis described in this thesis, the following recommendations can be considered for further research.

In this thesis it becomes clear that tyre measurements and accurate parameter identification are of great importance in tyre modelling. Therefore, the following recommendations on tyre measurements are given:

- The structure of the measurement program used for parameterisation of the tyre models is insufficient to investigate the tyre behaviour for changing environmental conditions. Extend the measurement program with a wider range of velocities, perform measurements at different road surfaces.
- In recent research the implementation of the inflation pressure dependency is investigated. To validate this behaviour, measurements at different inflation pressures need to be added to the measurement program.
- In the physical tyre models many tyre parameters need to be optimised with respect to the measurement data. It is possible that these optimised tyre parameters results in physical incorrect data. Therefore, it is desirable that the relevant tyre properties are measured with the available test rigs or obtained directly from the tyre manufacturers.

In this thesis different types of tyre models from the fields of semi-empirical and physical based tyre models are investigated. The following recommendations of possible improvements for the different tyre models can be considered:

- The Magic Formula can be improved by including dependency on changing environmental conditions, such as velocity, friction, inflation pressure, temperature, road condition, etc.

- The TMeasy tyre model is not as accurate as the Magic Formula Tyre model, especially for the combined slip situation. To improve the model accuracy, the combined slip approximation need to be improved. The recommendation defined for the Magic Formula is also valid for TMEasy, that the model can be improved by including dependency on environmental effects.
- For the TreadSim and LuGre tyre model the same recommendations are given for improving the model accuracy. In both physical models assumptions are made to increase the computational effort. However, to reach the same accuracy as the semi-empirical tyre models these assumptions need to be improved. The contact patch shape and deformation have to be dependent on the vertical load, inflation pressure, slip angle and camber angle. The simplified normal pressure distribution can be improved by including a finite element carcass model that is able to generate accurate normal pressure distributions. Improve the carcass deformation mode by extending the tyre models with a flexible carcass or elements of finite element models.
- In further research of Deur the LuGre model is already extended with tyre effects, such as camber, turn-slip, conicity, plysteer and more. The implementation of these effects should be studied and it has to be considered to implement these effects in the version built for this thesis. With the implementation of these effect, empirical approaches need to be avoided.
- For all studied tyre models the recommendation is given to replace the current scaling factors to account for surface differences with the implementation of an adequate friction dependency. This friction coefficient should influence the maximum forces and the tyre stiffnesses, the alteration of the tyre temperature is important in this matter.

In the future the traditional view on tyre modelling will not be sufficient to deal with the high demands. The following recommendations for an improved tyre handling model are given:

- In the future a new tyre model for vehicle handling analysis needs to be capable of dealing with various operating conditions, such as velocity, inflation pressure, friction, (ambient) temperature.
- It can be considered to define tyre wear and road roughness as extra inputs of a tyre model. These phenomena have influence on the tyre forces and moments.
- An accurate approximation of the contact patch shape and normal pressure distribution, both dependent on the vertical load, inflation pressure and a slip and camber angle.
- An improved tyre model that accurate describes the steady-state force and moment characteristics, could be connected with a rigid-ring or flexible carcass model for describing the dynamic tyre behaviour up to 100 Hz.
- An improved dynamic tyre handling model should be applicable in large fields of application, such as: Vehicle handling and parking behaviour, ride comfort and noise, influence on the road surface. Subsequently, this tyre handling model can be used in the development of a vehicle, such as: Suspension design, steering-mechanism design, safety system design, powertrain and full vehicle simulations.

Bibliography

[1] http://www.20sim.com/webhelp4/library/iconic-diagrams/mechanical/friction/static-friction-models.htm.

[2] D. Ammon. Vehicle dynamics analysis tasks and related tyre simulation challenges. *Vehicle System Dynamics*, Vol. 43(Supplement):30–47, 2005.

[3] E. Bakker, L. Nyborg, and H.B. Pacejka. Tire modelling for use in vehicle dynamics studies. *SAE Paper*, (No. 870421), 1987.

[4] E. Bakker, H.B. Pacejka, and L. Lidner. A new tire model with an application in vehicle dynamics studies. *SAE Paper*, (No. 890087), 1989.

[5] P. Bayle, J.F. Forissier, and S. Lafon. A new tyre model for vehicle dynamics simulation. *Automotive Technology International*, pages 193–198, 1993.

[6] I.J.M. Besselink. *Lecture notes of the course Vehicle Dynamics 4L150.* 2003.

[7] C. Canadus de Wit, H. Olsson, K.J. Åström, and P. Lischinsky. A new model for control of systems with friction. *IEEE Transactions On Automatic Control*, Vol. 40(No. 3):419–425, march 1995.

[8] C. Canadus de Wit and P. Tsiotras. Dynamic tire friction models for vehicle traction control. *Proc. 38th IEEE Conference on Decision and Control*, pages 3746–3751, 1999.

[9] D. Chou. Dahl friction modelling. Technical report, Massachusetts Institute of Technology, 2004.

[10] J. Deur. Modeling and analysis of longitudinal tire dynamics based on the lugre friction model. *3rd IFAC Workshop Advances in Automotive Control*, pages 101–106, 2001.

[11] J. Deur. Extension of lugre tyre friction model with camber and turn slip effects. Internal report 07/06/04, University of Zagreb, Zagreb, Croatia, 2004.

[12] J. Deur. Extension of lugre tyre friction model with carcass compliance, conicity, and ply-steer effects. Internal report 07/20/04, University of Zagreb, Zagreb, Croatia, 2004.

[13] J. Deur, J. Asgari, and D. Hrovat. Modeling and analysis of longitudinal tire dynamics. FRL Technical report No. SRR-2000-0145, Ford Motor Company, Scientific Research laboratory MD 1170, Dearborn, MI 48121-2053, USA, 2000.

[14] J. Deur, J. Asgari, and D. Hrovat. A dynamic tyre friction model for combined longitudinal and lateral motion. *Proceedings of 2001 ASME International Mechanical Engineering Congress and Exposition*, Vol. 2, 2001.

[15] J. Deur, J. Asgari, and D. Hrovat. A dynamic tyre friction model for combined longitudinal and lateral motion. FRL Technical Report No. SRR-2001-0022, Ford Motor Company, Scientific Research laboratory MD 1170, Dearborn, MI 48121-2053, USA, 2001.

[16] J. Deur, J. Asgari, and D. Hrovat. A 3d brush-type dynamic tire friction model. *Vehicle System Dynamics*, Vol. 42(No. 3):133–173, 2004.

[17] J. Deur, V. Ivanovic, M. Troulis, C. Miano, D. Hrovat, and J. Asgari. Extensions of the lugre tyre friction model related to variable slip speed along the contact patch. *Vehicle System Dynamics*, Vol. 43(supplement):508–524, 2005.

[18] M. Gipser, R. Hofer, and P. Lugner. Dynamical tyre forces response to road unevennesses. *Vehicle Sytem Dynamics Supplement*, Vol. 27:94–108, 1997.

[19] K. Guo, Y. Zhuang, D. Lu, S. Chen, and W. Lin. A study on speed-dependent tyre-road friction and its effect on the force and the moment. *Vehicle System Dynamics*, Vol.43(Supplement):329–340, 2005.

[20] W. Hirschberg, G. Rill, and H. Weinfurter. User-appropriate tyre-modelling for vehicle dynamics in standard and limit situations. *Vehicle Dynamic System*, Vol. 38(No. 2):103–125, 2002.

[21] J. de Hoogh. Implementing inflation pressure and velocity effects into the magic formula tyre model. Master's thesis, Eindhoven University of Technology, 2005.

[22] I. Kageyama and S. Kuwuhara. A study on tire modeling for camber thrust and camber torque. *JSAE Review*, Vol. 23:325–331, 2002.

[23] M. Liukkula. Tyre characterisation on summer and winter surfaces. In *Tire Technology Expo*, pages 1–20. 3rd International Colloqium on Vehicle-Tyre-Road Interaction, 2006.

[24] F. Mancosu. Overview of vert project: prediction of full vehicle behaviour in dangerous situations. Contract number: G3RD-CT-2002-00805 "VERTEC".

[25] N. Miyashita and K. Kabe. A new analytical tire model for cornering simulation. part ii: Cornering and self-aligning torque. *Tire Science and Technology*, Vol.34(No.2):100–118, 2006.

[26] H. Olsson, K.J. Åström, C. Canudas de Wit, M. Gäfvert, and P. Lischinsky. Friction models and friction compensation. *European Journal of Control*, 1998.

[27] I.B.A. op het Veld. *Enhancing the MF-Swift Tyre Model for Inflation Pressure Changes*. Master Thesis's. Eindhoven University of Technology, 2007.

[28] H.B. Pacejka. *Tyre and Vehicle Dynamics*. Butterworth-Heinemann, 2002.

[29] H.B. Pacejka and E. Bakker. The magic formula tyre model. *Supplement Vehicle System Dynamics*, Vol. 21:1–18, 1993.

[30] G. Rill. Vehicle dynamics. Lecture Notes, October 2005.

[31] M. Sjahdanulirwan and Q. Yang. Prediction of tyre-road friction with an inverted-boat shaped pressure distribution. *Vehicle System Dynamics*, Vol. 24(No. 2):145–161, 1995.

[32] A. van Zanten, W.D. Ruf, and A. Lutz. Measurement and simulation of transient tire forces. *SAE paper*, (890640), 1989.

[33] B. Witte and J. Zuurbier. Detection of the friction coefficient in a running vehicle and measurement of tire parameters on different road surfaces. *VDI Berichte*, Vol. 24(No. 12):61–78, 1995.

Appendix A

Sign conventions and measurement data for the reference tyre

In this thesis it is decided to use one general coordinate system to describe the forces and moments. All the forces and moments that are introduced in this thesis are conform the ISO-definitions, which means that the coordinate system is right-handed and the z-axis is perpendicular to and points away from the road surface; the x-axis is parallel to the road surface and point in the driving direction. An overview of the ISO axis system is depicted in figure (A.1).

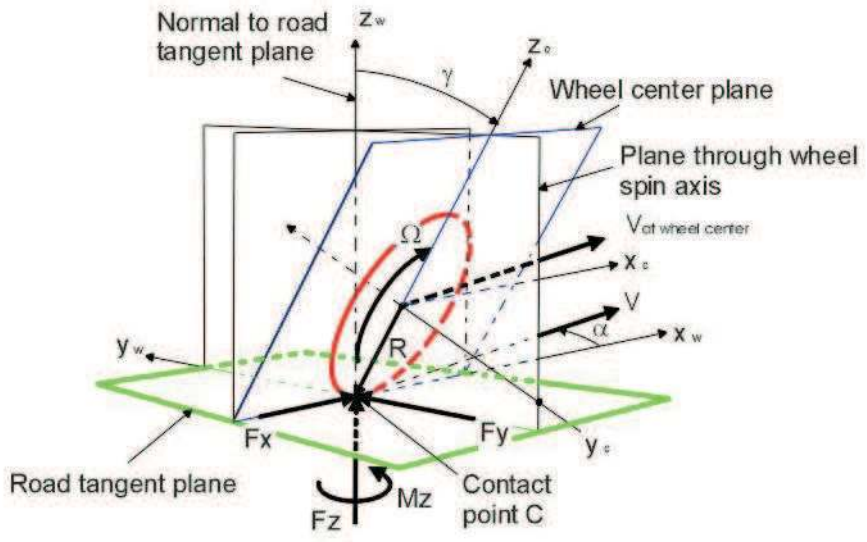

Figure A.1: Overview ISO axis system.

In figure (A.2) an overview of the ISO sign convention, the definition of the slip angles and the influence of a camber angle on the characteristics are depicted.

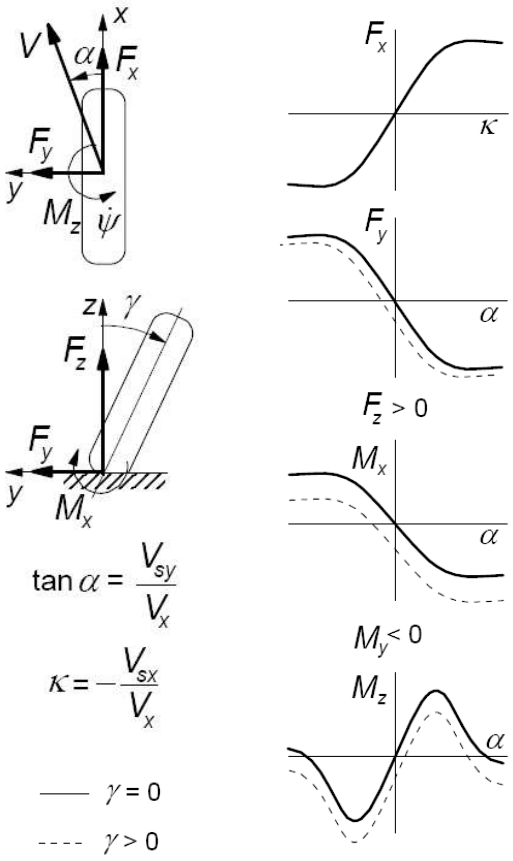

Figure A.2: ISO sign conventions.

To validate the different tyre models, measurement data is made available with pure alpha sweeps, pure kappa sweeps and combined slip measuruments. The measurement file is used for the validation of the different tyre models and to optimise the tyre parameters of the tyre models. The specifications of the tyre used during the measurements are presented in table (A.1).

Continental SportContact 2 225/50/R17:

Rim diameter = 0.432 m
Rim width = 0.191 m
Inflation pressure = 2.2 bar
Unloaded radius = 0.331 m
Tyre width = 0.225 m
V_x = 60 km/h

Table A.1: Tyre data Continental SportContact 2.

The measurement file exist of the following performed measurements defined in table (A.2):

	α [deg]	κ [-]	γ [deg]
Pure alpha sweeps	-12 to 12	0	-5, 0, 5
Pure kappa sweeps	0	0 to -0.9	-5, 0, 5
Combined slip	-2, 2, 5, 8	0 to -0.9	-5, 0, 5

Table A.2: Overview measurements.

Appendix B

Different approach for describing contact pressure

A different semi physical tyre model, is the BRIT model (Brush and Ring Tyre Model) developed by M. Gipser. BRIT is a so called brush model, some principal features and properties of this model, described in [18], are:

- rigid ring-shell for the tyre belt connected with spring-damper-elements to the wheel rim.
- geometrical algorithm for the calculation of the tyre contact area by road surface profile and tyre belt (ring-shell) position.
- approximation of quasi-static deformation of tyre patch due to contact forces and moments.
- assumption of normal stress distribution in the tyre patch taking into account the rolling resistance.
- detailed modelling of the tyre patch by tread stripes consisting of discrete, massless tread blocks with tangential stiffness and damping (dynamic tread model).
- calculation of lateral and longitudinal forces by tread block displacements.

The basic description of the normal stress distribution in the patch by monomial functions (a particular kind of polynomial having just one term) did not allow to take into account the effects of the value of the tyre normal force and the local road surface curvature with respect to the character of these distributions functions.
The essential qualitative characteristics of the stress distribution for the two mentioned influences are:

- stress distribution in lateral direction: With increasing normal force and decreasing curvature κ ($\kappa < 0$) corresponds to a test rig with the test tyre on the outside of the driven drum) the stresses in the tread shoulder increase relatively to those in the longitudinal center line of the patch.
- stress distribution in longitudinal direction: For a relatively small normal force this distribution shows a maximum in the center of the patch. With increasing normal force and decreasing curvature this one is maximum is replaced by two increasing maxima that shift more and more to the edges of the patch. In the middle of the patch a minimum is created.

In the paper the details of the BRIT model are not described, only the basic idea of the changes to the model are mentioned. In the paper some references are made to variables used in the model, it is not sure how these are calculated, therefore some assumptions are made with respect to these parameters.

The following standardised quantities are defined:

$$\bar{x} = \frac{x}{L(y)/2}; \qquad \bar{y} = \frac{y}{b/2}; \qquad \bar{F} = \frac{F_{K,z}}{F_N}; \qquad \bar{\kappa} = \kappa \cdot r_G \tag{B.1}$$

The variable κ represents the curvature of the surface contour in the longitudinal x-direction. Because the measurement data used in this project is measured at a flat road, the parameter κ is assumed to be zero.
By several optimisation procedures the following characteristic quantities are determined:

$$\begin{aligned}
\upsilon &= -1 + (0.65 \cdot \bar{F}^2) \cdot (1 - 0.65 \cdot \bar{\kappa}) && \text{(B.2)}\\
k(\bar{y}) &= k_0 - (k_0 - 1) \cdot \bar{y}^2 && \text{(B.3)}\\
k_0 &= 1 + [0.9 - 0.645 \cdot (\bar{\kappa} + 0.381)^2] \cdot \bar{F}^2 && \text{(B.4)}\\
a(\bar{y}) &= a_0 - (a_0 - a_{00}) \cdot \bar{y}^2 && \text{(B.5)}\\
a_0 &= 1 + 0.7 \cdot e^{1.31 \cdot \bar{\kappa}} \cdot \bar{F} && \text{(B.6)}\\
a_{00} &= a_0(\bar{\kappa} = 0) = 1 + 0.7 \cdot \bar{F} && \text{(B.7)}
\end{aligned}$$

Summing up, the complete description for the normal stress distribution in the patch can be described by:

$$\begin{aligned}
p(x,y) = \max \Bigg[& 0, p(0,0) \cdot \left(1 + \upsilon(\bar{F}, \bar{\kappa}) \cdot |\bar{y}|^4\right) \cdot \frac{L(y)}{L_{max}} \cdot \\
& \left(1 - |\bar{x}|^{a(\bar{y},\bar{F},\bar{\kappa})}\right) \cdot \left(1 + k(\bar{y}, \bar{F}, \bar{\kappa}) \cdot |\bar{x}|^{a(\bar{y},\bar{F},\bar{\kappa})}\right) \Bigg]
\end{aligned} \tag{B.8}$$

In the equations described above, several parameters are used and the notation of the specific quantities are:

x	position in longitudinal direction of the patch, $-\frac{L(y)}{2} \leq x \leq \frac{L(y)}{2}$
y	position in lateral direction of the patch, $-\frac{b}{2} \leq y \leq \frac{b}{2}$
b	patch-width
$L(y)$	length of tread stripe
L_{max}	reference length of patch
$p(x,y)$	normal pressure in the patch
$F_{K,z}$	normal contact force
F_N	nominal tyre load (characteristic quantity of type of tyre)
κ	road surface curvature in longitudinal direction
r_G	maximum geometric tyre radius

In the following overview the normal stress distributions for three different vertical loads are depicted. In figure B.3 a strange behaviour occurs. Large pressures at both sides of the contact area arise. This seems not not to be an adequate representation of an accurate normal pressure distribution.

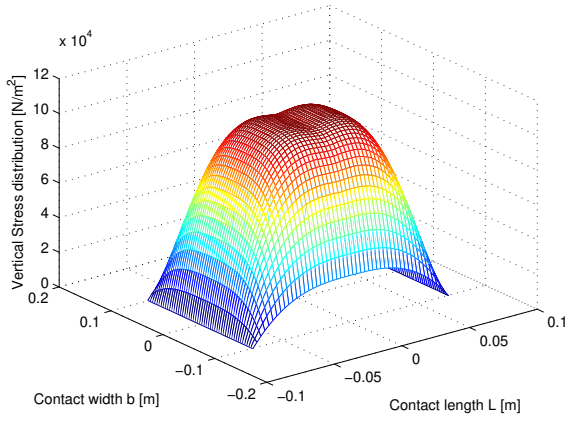

Figure B.1: Calculated normal stress distribution in the contact patch at Fz=3000.

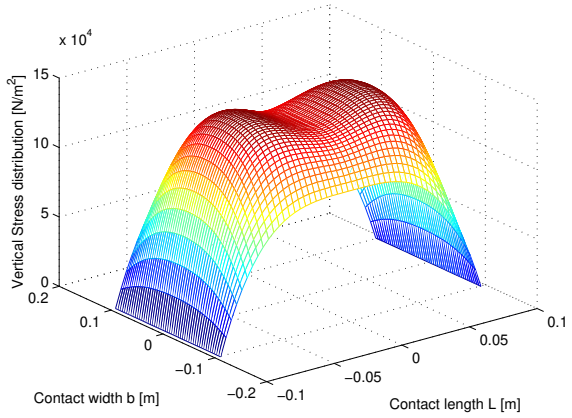

Figure B.2: Calculated normal stress distribution in the contact patch at Fz=5000 N.

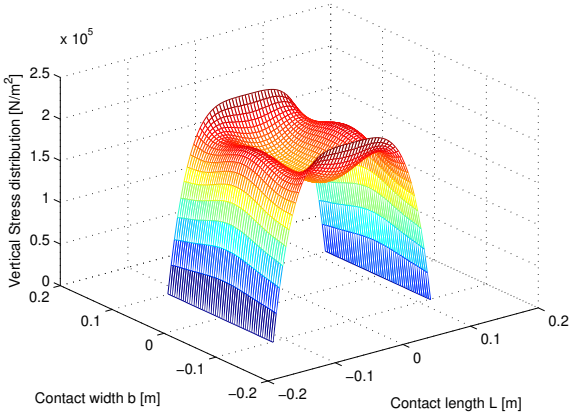

Figure B.3: Calculated normal stress distribution in the contact patch at Fz=7000 N.

In several projects at Eindhoven University of Technology studies are performed after the tyre/road friction modelling and tyre/road noise and vibration modelling. These projects use a FEM-based modelling approach for loaded rolling tyres. In figure (B.4) an example is given of the normal pressure distribution of an inflated tyre and loaded with a force of 2750 N modelled in the FEM program Abaqus. In this figure it is clear to see that with an increasing normal force the normal pressures in the tread shoulder increases. At this normal force a minimum normal pressure at the centre of the contact patch exist, in longitudinal direction two increasing maxima shift more and more to the edges of the contact patch. From these results it can be concluded that the different approaches of the tyre models studied in this thesis have an unrealistic approximation of the normal pressure distribution.

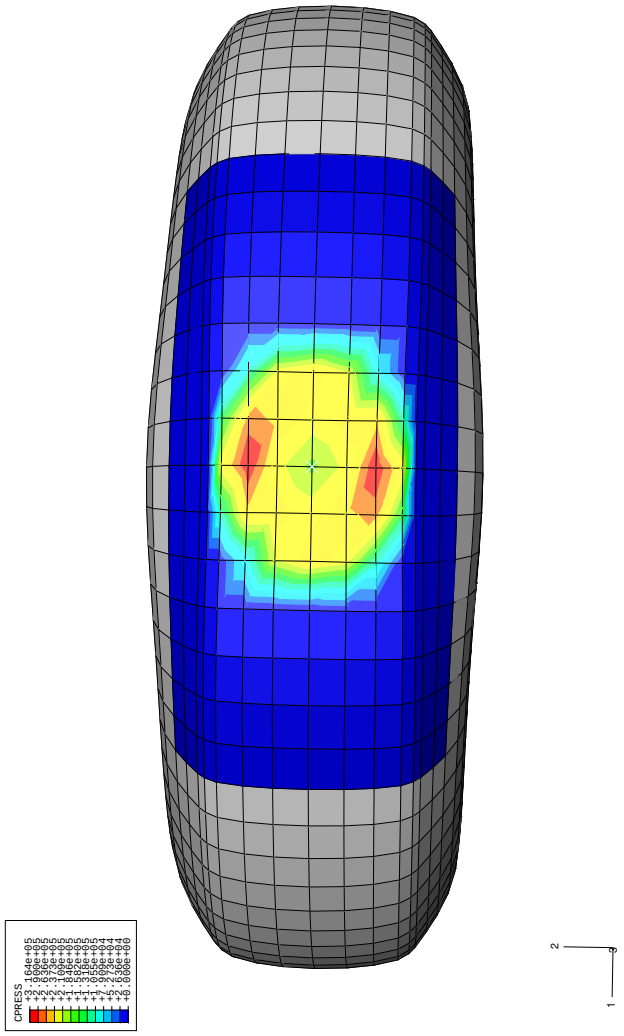

Figure B.4: Normal pressure distribution of a FEM model of a tyre.

Appendix C

Explanation friction law's

In chapter 5 where the dynamic tyre friction model is presented, different friction effects are mentioned. In this appendix the different friction effects will be explained in more detail.

Coulomb friction

Static friction phenomena only have a static dependency on velocity. The first static friction model was the classic model of friction of Leonardo Da Vinci: friction force is proportional to load, opposes the direction of motion and is independent of contact area. Coulomb (1785) further developed this model and the friction phenomena described by the model became known as Coulomb friction. The model is given in the figure below.

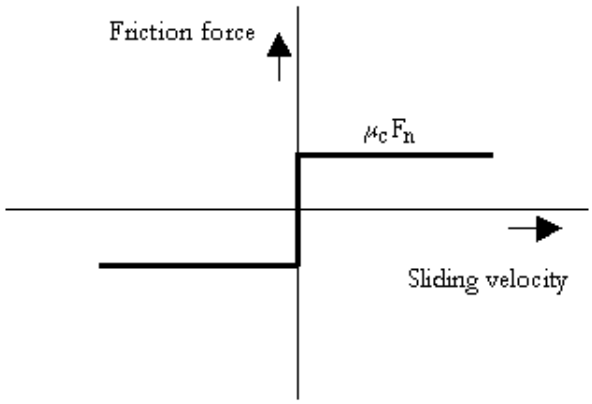

Figure C.1: The Coulomb friction model [1].

The Coulomb friction model is, because of its simplicity, often used. In many textbooks is is also referred to as dynamic friction and μ_c described as the dynamic friction coefficient.

Static friction

Morin (1833) introduced the idea of static friction: friction force opposes the direction of motion when the sliding velocity is zero.

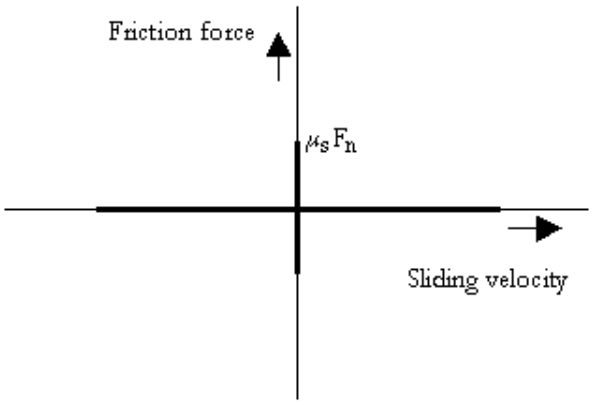

Figure C.2: The Static friction model [1].

The static friction force is equal to the tensile forces until a maximum or minimum is reached.

Viscous friction

Reynolds (1866) developed expressions for the friction force caused by the viscosity of lubricants. The term viscous friction is used for this friction phenomenon.

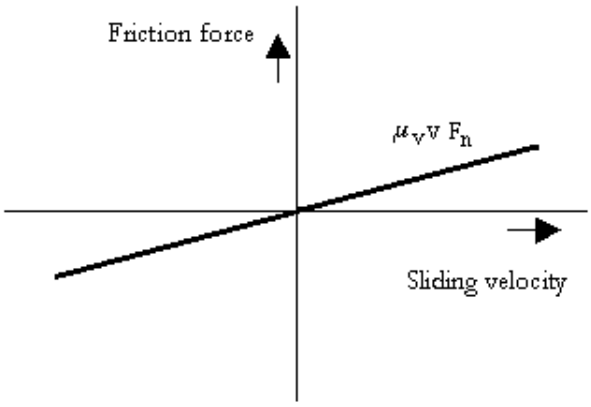

Figure C.3: The Viscous friction model [1].

Coulomb plus viscous friction

The viscous friction combined with the Coulomb friction gave the model given in the figure below.

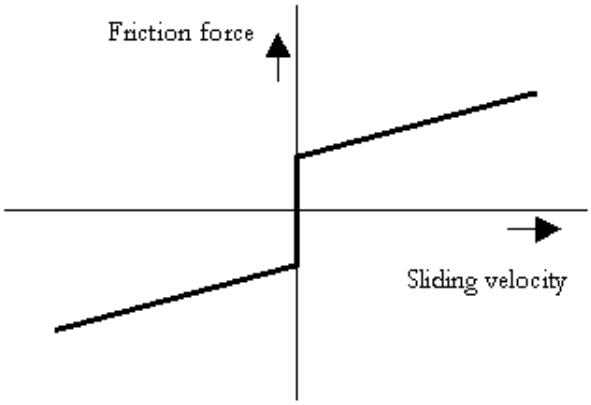

Figure C.4: The Coulomb plus viscous friction model [1].

Static plus Coulomb plus viscous friction

When static friction is added, a friction model appears that is commonly used in engineering: the static plus Coulomb plus viscous friction model. This model is depicted in the figure below.

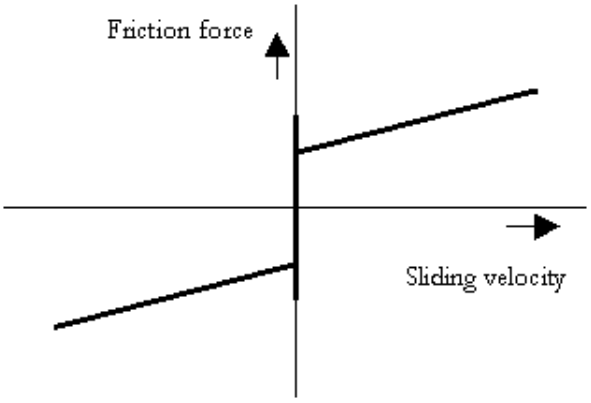

Figure C.5: The Static, Coulomb plus viscous friction model [1].

Static plus Coulomb plus viscous plus Stribeck friction

Stribeck (1902) observed that for low velocities, the friction force is decreasing continuously with increasing velocities and not in a discontinuous matter as described above. This phenomenon of a decreasing friction at low, increasing velocities is called the Stribeck friction or effect. The model including static, Coulomb, viscous and Stribeck friction is given below.

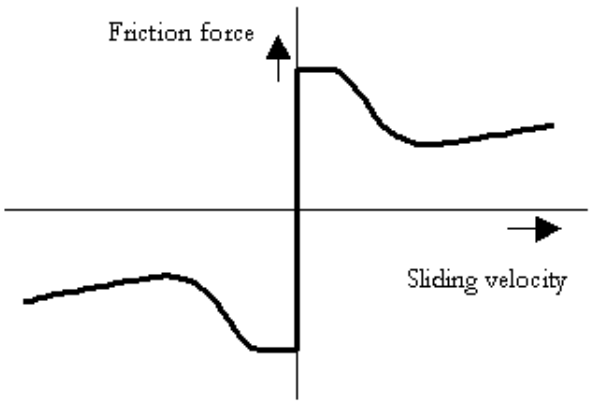

Figure C.6: The Static, Coulomb, viscous plus Stribeck friction model [1].

The Dahl model

In 1968 P.R. Dahl proposed an alternative to the Coulomb friction model. While observing the behavior of ball bearings, he noted that very small amplitude input forces were reacted against by small elastic restoring forces. From this observation, he developed his theory of solid friction in which he describes friction as the macroscopic result of quantum mechanical bonds between two contact surfaces. Intermolecular bonds keep the surfaces together, but shearing or tensile forces cause them to break. This rupture behavior is demonstrated more familiarly in material deformation tests, and Dahl found that stress-strain behavior serves as a good analogy for the continuous friction force-displacement relationship.

Dahl likens the transition from static to kinetic friction to that of elastic to plastic deformation in ductile materials. The quantum mechanical bonds at a surface are strong enough at low tensile loads that the behavior is elastic and spring-like. Hence, upon relaxation of the load, the bonds return to their original, unstressed state. If the load is larger, the bonds experience permanent displacement analogous to plastic deformation, and if the load is then decreased, the bonds will not return to exactly their previous state. Therefore, the bonds experience hysteresis similar to that found in plastic material deformation. If the load is eventually increased beyond the strength of the bonds, the bond will break. This limit is analogous to the rupture stress of a ductile material or the ultimate tensile stress of a brittle one.

A commonly-used analogy to convey this idea is the bristle model; initially, an applied load will not move the intersection point of the bristle to the surface but merely deform the bristles elastically. If the load is removed, the bristles will return to their original positions. However, when the load exceeds that of only bristle deformation, the entire brush moves. The stiffness of the bristle is equivalent to the elasticity of the contact surfaces, and the non-linear behavior at the tip of the bristle is the point of interest [9].

The starting point for Dahl's model is the stress-strain curve in classical solid mechanics, see figure C.7. When subject to stress the friction force increases gradually until rupture occurs. Dahl modeled the stress-strain curve by a differential equation. Let x be the displacement, F the friction force, and F_c the Coulomb friction force. Then Dahl's model has the form

$$\frac{dF}{dx} = \sigma \left(1 - \frac{F}{F_c} sgnv\right)^{\alpha} \tag{C.1}$$

where σ is the stiffness coefficient and α is a parameter that determines the shape of the stress-strain curve. The value $\alpha = 1$ is most commonly used [26]. Higher values will give a stress strain curve with a sharper bend. The friction force $|F|$ will never be larger than F_c if its initial value is such that $|F(0) < F_c|$.

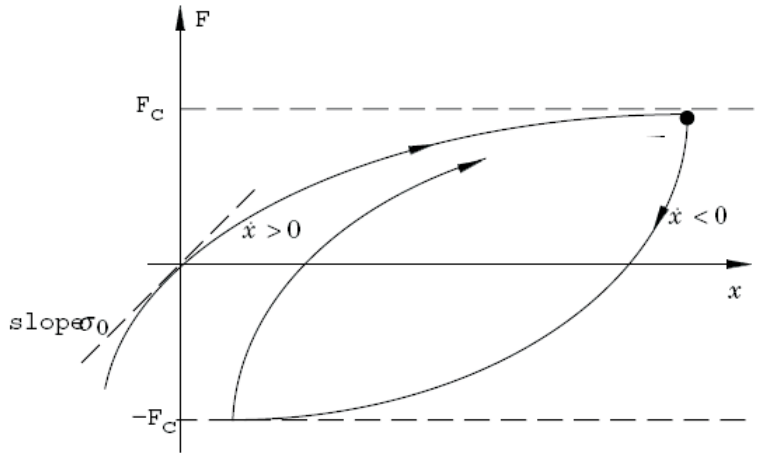

Figure C.7: Friction force as a function of displacement for Dahl's model [26].

Notice that in this model the friction force is only a function of the displacement and the sign of the velocity. This implies that the friction force is only position dependent. This so called rate independence is an important property of the model. It makes it possible to use the theory of hysteresis operators.

To obtain a time domain model Dahl observed that

$$\frac{dF}{dt} = \frac{dF}{dx}\frac{dx}{dt} = \frac{dF}{dx}v = \sigma\left(1 - \frac{F}{F_c}sgnv\right)^{\alpha} v \tag{C.2}$$

Implementation of friction models in a tyre model

In figure C.8 an overview of different static and dynamic friction effects is depicted. These friction effects were mentioned in the chapter where the dynamic tyre friction model of Deur is presented and the implementation in a tyre model is described in detail here.

Friction is usually described by the static friction curve shown in figure C.8a. This curve includes the following static friction effects: Coulomb or dry friction, viscous friction, Stribeck friction at low relative speeds, and stiction in the zero-speed region.

The static friction model from figure C.8a cannot be implemented as a simulation model, because friction is not uniquely defined at zero speed. This can be physically correct described by the presliding displacement curve in figure C.8b. This curve corresponds to the hysteric stress-strain curve which describes the process of elastic and plastic horizontal deformation of the bristle (or of the asperity contacts for a sliding or rolling bearing). It implies that there is some varying relative displacement x_r between the contacting surfaces (in the case of a brush model, between the base point and tip), before the real sliding occurs.

There are two other dynamic friction effects known from tribology experiments. According to the variable breakaway force effect, see figure C.8c, the breakaway force decreases from the maximum stiction F_S to the Coulomb friction force F_C as the rate of change of applied force (i.e., the rate of change of stiction) increases. This means that the Stribeck effect becomes less emphasised for more abrupt stick-to-slip transitions. According to the frictional lag effect, figure C.8d, the low-speed friction response with respect to periodic change of relative speed closes a hysteretic loop around the static friction curve. The loop is wider for higher frequencies of relative speed.

The main weakness of the Dahl model previous described and depicted in figure C.7 is that it does not include the breakaway friction drop described by the Stribeck effect (figure C.8a). This weakness is avoided by approximating the hysteric presliding displacement curve in figure C.8a with a straight line (see figure C.9), and saturating stiction to the speed dependent sliding friction force $g(v_r)$ defined in (5.5). This leads to the following dynamic friction model:

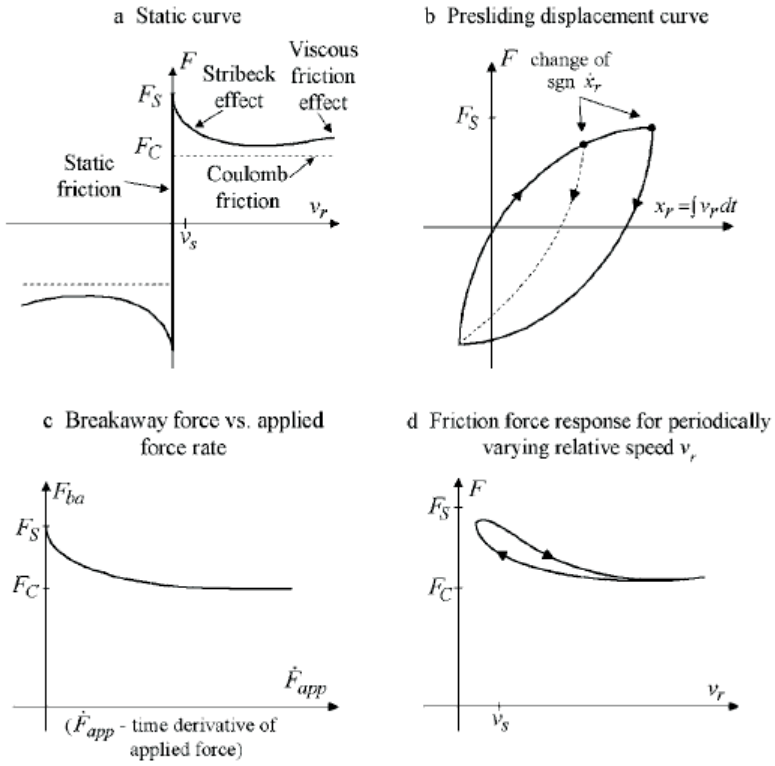

Figure C.8: Illustration of different static (a) and dynamic (b-d) friction effects [16].

$$\frac{dz}{dt} = v_r \tag{C.3}$$

$$F = \sigma_0 sat\left(z, \frac{g(v_r)}{\sigma_0}\right) \tag{C.4}$$

Here, the friction state variable z corresponds to the horizontal bristle deflection, and sat is the saturation function (note that the correct saturation implementation assumes that z is saturated in the state equation (C.3) to avoid integrator windup.

The main weaknesses of the friction model (C.3,C.4) are inaccurate presliding displacement curve (linear bristle spring is assumed), and incompact mathematical form. These weaknesses are avoided in an extension of the Dahl model with the Stribeck effect, as proposes in [7] and known as the LuGre friction model and presented in chapter 5. The constant Coulomb friction force F_C in the Dahl model (C.2) is simply replaced by the speed dependent sliding friction function $g(v_r)$, see (5.5) [16].

Subsequently, the LuGre friction model is extended for the use in a dynamic tyre friction model, as described in chapter 5.

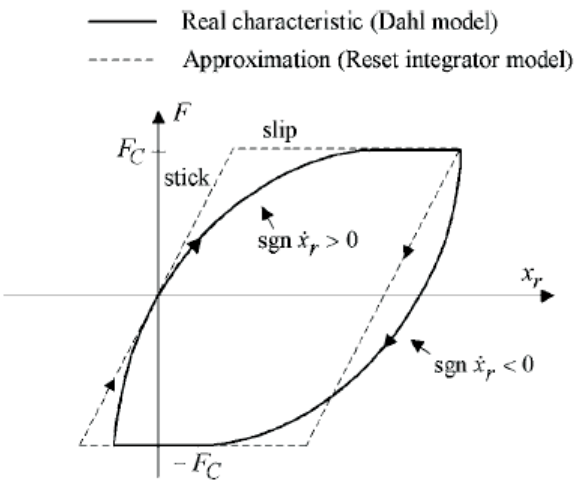

Figure C.9: Friction versus displacement curve ($F_s = F_c$) [16].